Aus dem Nationalen Zentrum für Strahlenforschung in der Onkologie – OncoRay
Direktorin: Prof. Dr. Mechthild Krause

Variable Relative Biological Effectiveness in Proton Treatment Planning: Assessment, Harmonisation and Mitigation

D i s s e r t a t i o n s s c h r i f t

zur Erlangung des akademischen Grades
Doctor rerum medicinalium (Dr. rer. medic.)
vorgelegt
der Medizinischen Fakultät Carl Gustav Carus
der Technischen Universität Dresden
von

M.Sc. Christian Hahn
aus Essen

Dresden 2022

1. Gutachter: Prof. Dr. Wolfgang Enghardt

2. Gutachter: Prof. Dr. Kristian Smeland Ytre-Hauge

Tag der mündlichen Prüfung: 29. Juni 2023

gez.: .....

Prof. Dr. Christian Richter

Vorsitzender der Promotionskommission

Abstract

Protons are more effective in cell killing than photons. However, the clinically applied constant proton relative biological effectiveness (RBE) neglects emerging clinical evidence for RBE variability driven by the linear energy transfer (LET). This thesis aims to safely account for RBE variability in proton treatment plans to mitigate potential side effects. First, an elevated risk for RBE induced overdosage was found in brain tumour patients. However, this could not be mitigated systematically by clinical planning strategies. Second, a multicentric European study revealed that centre-specific non-standardised LET calculations differed substantially. A harmonised LET definition was proposed which reduced the inter-centre variability to a clinically acceptable level and allows for future consistent outcome reporting. Finally, four strategies to include RBE variability in treatment plan optimisation were applied to brain tumour patients, which considerably reduced the estimated risk for necrosis and blindness. Of these, LET optimisation in high dose regions may be suited for clinical practice to further enhance patient safety in view of a variable RBE.

Kurzfassung

Protonen töten Zellen wirksamer ab als Photonen. Die klinisch verwendete konstante relative biologische Wirksamkeit (RBW) für Protonen vernachlässigt jedoch erste klinische Evidenz einer RBW-Variabilität, die vom linearen Energietransfer (LET) abhängt. Diese Arbeit trägt dazu bei, die RBW-Variabilität in Protonen-Bestrahlungsplänen zu berücksichtigen, um potenzielle Nebenwirkungen zu vermindern. Zuerst wurde ein erhöhtes Risiko für RBW-induzierte Nebenwirkungen bei Hirntumorpatienten festgestellt. Dies konnte jedoch nicht systematisch durch klinische Planungsstrategien reduziert werden. Zweitens ergab eine multizentrische europäische Studie, dass die zentrums-spezifischen, nicht standardisierten LET-Berechnungen erheblich voneinander abweichen. Eine harmonisierte LET-Definition wurde vorgeschlagen und reduzierte die Variabilität zwischen den Zentren auf ein klinisch akzeptables Niveau, was künftig eine einheitliche Dokumentation des Therapieergebnisses ermöglicht. Abschließend wurden vier Strategien zur RBW-Reduktion in der Planoptimierung bei Hirntumorpatienten angewandt, die das Risiko für Nekrose und Erblindung erheblich reduzierten. LET-Optimierung in Hochdosisregionen erscheint besonders geeignet, um die Sicherheit der Patientenbehandlung künftig weiter zu verbessern.

Contents

List of Figures

List of Tables

List of Acronyms and Abbreviations

$D_{1.1}$	absorbed dose weighted with RBE of 1.1
D_{RBE}	absorbed dose weighted with a variable RBE
BGopt	biological effectiveness guided optimisation
CI	conformity index
CSDA	continuous slowing down approximation
CT	computed tomography
CTV	clinical target volume
DDopt	dirty dose optimisation
DECT	dual-energy computed tomography
DICOM	Digital Imaging and Communications in Medicine
DNA	deoxyribonucleic acid
DOSEopt	constant RBE-weighted dose optimisation
DRBEopt	variable RBE-weighted dose optimisation
DS	double scattering
DSB	double-strand break
DVH	dose-volume histogram
GATE	GEANT4 Application for Emission Tomography
GUI	graphical user interface
HI	homogeneity index
HLUT	Hounsfield Unit look-up table
HU	Hounsfield Unit
IMPT	intensity-modulated proton therapy
LET	linear energy transfer
$\mathrm{LET_d}$	dose-averaged linear energy transfer
$\mathrm{LET_t}$	track-averaged linear energy transfer
LETopt	$\mathrm{LET_d}$ optimisation
LQ	linear-quadratic

MC	Monte Carlo
MCO	multi-criteria optimisation
MCS	multiple Coulomb scattering
MFO	multi-field optimisation
MRI	magnetic resonance imaging
MU	monitor units
NTCP	normal tissue complication probability
OAR	organ at risk
PBS	pencil beam scanning
PTV	planning target volume
PVR	periventricular region
RBE	relative biological effectiveness
RIBI	radiation-induced brain injury
ROI	region of interest
SECT	single-energy computed tomography
SFO	single-field optimisation
SIB	simultaneous integrated boost
SOBP	spread-out Bragg peak
SPR	stopping-power ratio
TEopt	track-end optimisation
TOPAS	Tool for Particle Simulation
TPS	treatment planning system
UPTD	University Proton Therapy Dresden
voxel	volume element
WPE	The West German Proton Therapy Centre Essen

1 Introduction

Radiotherapy is one of the three pillars in the treatment of cancer, which comprises 19 million cases annually and a mortality rate of almost 50 % worldwide (Baskar et al., 2012; Ferlay et al., 2021). The primary aim of radiotherapy is to eliminate all tumour cells through the deposition of dose, i.e. energy per mass, to the target volume while sparing surrounding healthy tissue (Holthusen, 1936). This would allow for high tumour control while limiting the probability for side effects.

Radiotherapy can be delivered by different modalities, such as photons or charged particles. Protons, as charged particles, deposit most of their dose at the end of their track which can be placed in tumour tissue. Their finite and controllable range and the corresponding inverse depth dose profile translate into highly conformal tumour irradiation and greater normal tissue sparing as compared to conventionally used photons. Accordingly, proton therapy is applied to reduce the dose burden and therewith the long term side-effects in patients with high life expectancy (Thomas & Timmermann, 2020). Proton therapy also provides a treatment option to further increase local tumour control in vicinity of dose-limiting organs at risk (OARs), particularly where photon therapy may fail (Ares et al., 2009; Fossati et al., 2016). In recent years, the potential of protons to elevate the therapeutic window led to a rapid increase in operating proton therapy centres worldwide (Particle Therapy Co-operatice Group, 2022), despite their high costs for construction and operation (Durante et al., 2017). However, proton treatment planning and delivery still relies on the long-term clinical experience on suitable OAR tolerance doses and tumour prescription doses acquired with photons since proton-specific outcome data is scarce (Karger et al., 2021). This is due to the fact that only about 1 % of radiotherapy patients are treated with protons currently (Mohan, 2022). However, dose levels for tumour control and OAR sparing from photon therapy cannot be transferred directly to proton therapy due to the higher biological effectiveness per unit absorbed dose for the latter.

The dose conversion into biological effect underlies substantial uncertainties and was investigated in this thesis. In clinical treatment planning and delivery, protons are considered

10 % more biologically effective than photons under all circumstances (De Luca, 2007; Paganetti et al., 2019). The constant relative biological effectiveness (RBE) was derived for the centre of the treatment field, which covers the tumour volume and ensures tumour control (Paganetti et al., 2002). However, this simplistic constant RBE model neglects broad preclinical evidence that RBE increases, among other factors, with the ionisation density of particles (Paganetti, 2014). The ionisation density can be characterised by the linear energy transfer (LET) which varies throughout the treatment field. The LET, and thus RBE, is expected to be particularly high at the treatment field edges (Lühr et al., 2018), which must be placed in healthy tissue due to mandatory safety margins in proton therapy (Tommasino & Durante, 2015). The use of a constant RBE was recently challenged by emerging clinical data, showing that radiation-induced side effects correlate with LET suggesting the clinical relevance of a variable RBE (Underwood et al., 2022).

Currently, proton therapy centres indirectly account for the uncertainty and risk of RBE induced side effects by applying restrictions in treatment planning such as considering special beam arrangements, preventing beams from stopping in OARs or using additional treatment fields (Heuchel et al., 2022; Sørensen et al., 2021). However, the benefit of these mitigation strategies can hardly be quantified, since LET and variable RBE visualisation tools are not available in clinical treatment planning system (TPS). Consequently, centres independently started to develop methods to inform their clinicians on treatment plan safety in view of RBE variability and to provide additional information for proton treatment planning (Toma-Dasu et al., 2020). As opposed to absorbed dose, LET and variable RBE calculations are not yet standardised (Hahn et al., 2022c; Kalholm et al., 2021), which may translate in inconsistencies in clinical decision making and complicate the transferability of future patient outcome reporting from one proton therapy centre to another.

This thesis aims towards safely considering a variable proton RBE in clinical practice. First, LET and variable RBE distributions for clinical treatment plans were quantified and the potential of clinical mitigation strategies was assessed, also in view of setup and range uncertainties (chapter 3). Second, a multi-centric study was conducted to assess the status and comparability of LET calculations and RBE modelling at eight European proton therapy centres (chapter 4). Finally, novel treatment plan optimisation approaches beyond absorbed dose were introduced and compared to actively mitigate RBE variability in selected OARs (chapter 5). Thereby, this work contributes to an active and consistent consideration of RBE variability in proton therapy to further enhance patient safety.

2 Theoretical background

The use of accelerated protons to treat deep-seated tumours was proposed by Wilson (1946). First proton treatments began in 1954 (Lawrence, 1957). Currently, over 100 proton therapy centres are under operation, 30 more are under construction and more than 280 000 patients have been treated with protons until 2022 (Particle Therapy Co-operatice Group, 2022). The rationale for proton therapy over conventional radiotherapy with photons is their favourable depth-dose distribution with lower doses in healthy tissue while delivering high dose to the tumour volume (Figure 2.1). The differences in physical interactions with the medium, i.e. the patient, also translate into differences in the biological effect, which will be presented in this chapter.

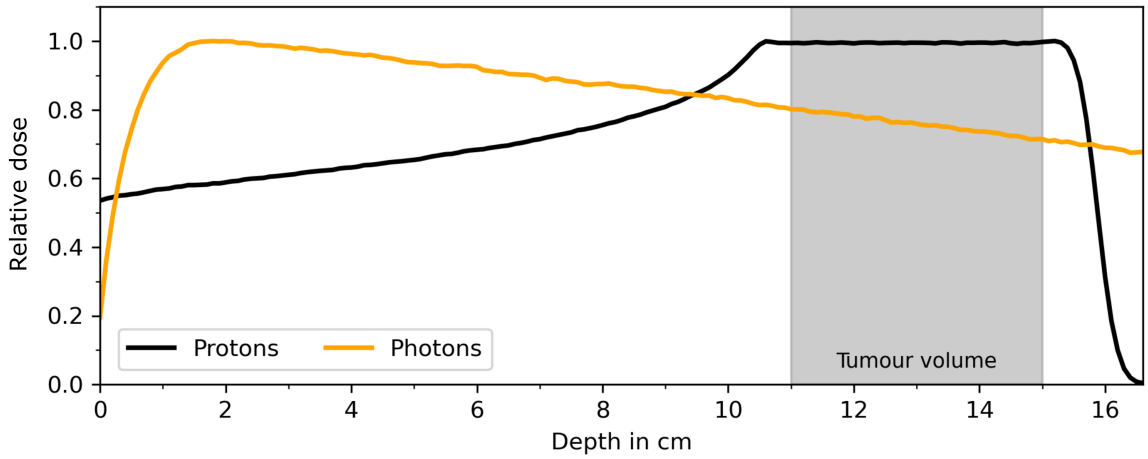

Figure 2.1: Relative depth dose distributions in water for 6 MV photons and a spread-out Bragg peak of protons with energies between 120 MeV to 150 MeV. Data courtesy of Lena Heuchel, TU Dortmund.

2.1 Proton interactions with matter

In radiotherapy, protons are accelerated up to 250 MeV to allow for the irradiation of tumours in water-equivalent depths of more than 30 cm. In the continuous slowing down approximation (CSDA), protons with initial energy E_0 lose their energy continuously along their tracks, so that the range R of a proton beam in the patient can be described as (Berger et al., 1993):

$$R = \int_{E_0}^{0} -\frac{1}{\mathrm{d}E/\mathrm{d}l}\mathrm{d}E = \int_{0}^{E_0} \frac{1}{S}\mathrm{d}E \quad , \tag{2.1}$$

where the mean energy loss $\mathrm{d}E$ by a charged particle of given type and energy per unit path length $\mathrm{d}l$ is given by the (total) material-specific stopping power S and energy loss fluctuations are neglected. S can be divided in three independent components (Seltzer et al., 2011):

$$S = S_{\mathrm{el}} + S_{\mathrm{nuc}} + S_{\mathrm{rad}} \quad , \tag{2.2}$$

with the electronic stopping power S_{el}, nuclear stopping power S_{nuc} and radiative stopping power S_{rad}, respectively. Protons in the therapeutic energy range mainly undergo inelastic Coulomb scattering with the atomic electrons of the target material (Figure 2.2), i.e. the patient, while the energy loss contributions through radiative and nuclear interactions are negligible (Newhauser & Zhang, 2015) .

The incident protons lose small fractions of their energy in frequent electronic interactions with the target electrons, in which the angular deflection of the former is minimal (Berger et al., 1993). For therapeutic proton energies, S_{el} can be approximated by the Bethe-Bloch formula without correction factors (Berger et al., 1993; Bethe, 1930):

$$S_{\mathrm{el}} = k_0 \frac{z^2}{\beta^2} \eta L(\beta) \approx k_0 \frac{z^2}{\beta^2} \eta \left[\ln\left(2m_e c^2 \frac{\beta^2}{1-\beta^2} \right) - \beta^2 - \ln I \right] \quad , \tag{2.3}$$

where the electronic energy loss of a particle beam per unit path length is determined by the projectiles charge z (for protons $z = 1$) and velocity β in units of the speed of light in vacuum c and the material properties of the target with electron density η and the mean excitation energy I of electrons with mass m_e. $L(\beta)$ is the material stopping number function and k_0 a constant with 5.1 × 10^{-25} MeV cm^2. Towards the end of range, the proton

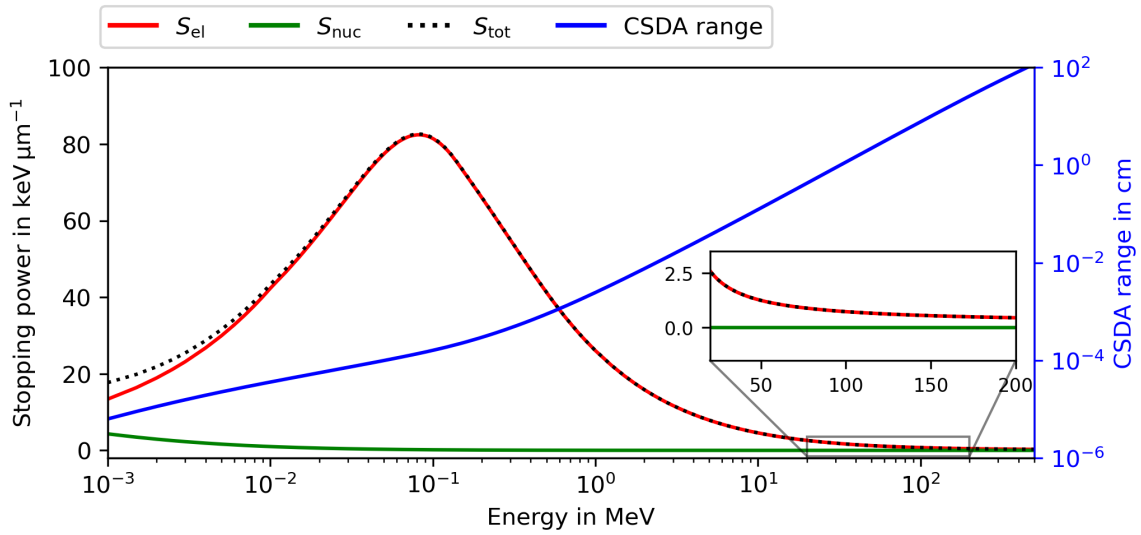

Figure 2.2: Contributions of electronic (S_{el}) and nuclear (S_{nuc}) stopping power to the total stopping power (S_{tot}) as a function of proton energy in liquid water and the corresponding range using the continuous slowing down approximation (CSDA). Data was retrieved from the National Institute of Standards and Technology (Berger et al., 2017). Note that radiative stopping power is not shown as its contribution to S_{tot} is negligible in proton therapy. Adapted from (Newhauser & Zhang, 2015).

energy-loss rate increases since the protons transfer more momentum to the electrons with decreasing velocity β (Gottschalk, 2011). For proton treatment planning and range prediction, the material-specific stopping power relative to the one of water is used typically (Wohlfahrt & Richter, 2020):

$$\mathrm{SPR} = \frac{S}{S_{\mathrm{water}}} = \hat{\eta}\,\frac{\ln\left(2m_e c^2 \dfrac{\beta^2}{1-\beta^2}\right) - \beta^2 - \ln I}{\ln\left(2m_e c^2 \dfrac{\beta^2}{1-\beta^2}\right) - \beta^2 - \ln I_{\mathrm{water}}}\,, \tag{2.4}$$

where $\hat{\eta}$ is the electron density relative to that of water.

The LET describes the mean energy transferred to electrons by a charged particle with charge z and energy E_p per unit path length in electronic interactions (Seltzer et al., 2011). The maximum energy transferred to a target electron can be approximated by $E_p/500$ and is for a therapeutic proton beam in the order of 0.5 MeV, which corresponds to an approximate electron range of 2 mm in liquid water (Newhauser & Zhang, 2015). Smaller energy transfers in the order of $\approx$ 100 eV are, however, most probable (Pimblott & LaVerne, 2007). Thus, the deposited energy is closely concentrated around a proton track ($\approx$ µm) making

the LET a measure for ionisation density. Considering only energy transfers below a defined energy cut-off Δ, i.e. omitting the high-energy tail, is expressed as the restricted LET (Seltzer et al., 2011):

$$\mathrm{LET}_{\Delta} = S_{\mathrm{el}} - \frac{\mathrm{d}E_{\mathrm{ke},\Delta}}{\mathrm{d}l} \quad , \tag{2.5}$$

where $\mathrm{d}E_{\mathrm{ke},\Delta}$ is the mean sum of kinetic energy of electrons greater than Δ. In contrast, including the contribution of all secondary electrons ($\Delta \to \infty$) results in the unrestricted LET, which equals S_{el}, and is simply denoted as LET from here on.

The produced electrons deposit their energy in the surrounding tissue and thereby inflict damage to the primary target of radiotherapy, the deoxyribonucleic acid (DNA) in the cell nucleus. The mean energy $\mathrm{d}E$ imparted by ionising radiation to matter of mass $\mathrm{d}m$ is described by the absorbed dose D (Seltzer et al., 2011):

$$D = \frac{\mathrm{d}E}{\mathrm{d}m} = \frac{S}{\rho}\Phi \quad , \tag{2.6}$$

where S is the stopping power, ρ the density of the material and Φ is the particle fluence during a given exposure or treatment (Gottschalk, 2011). In radiotherapy, the dose is used as a surrogate to predict biological effects in tumour and in normal tissue (Holthusen, 1936). Therefore, treatment plan optimisation and evaluation is based on dose. At the end of proton range, S increases rapidly which leads to the characteristic sharp dose maximum for a broad monoenergetic proton beam, called Bragg peak, followed by a steep dose fall-off. The superposition of multiple Bragg peaks with different intensities and ranges allow to homogeneously irradiate the tumour volume (Figure 2.3).

Radiotherapy is typically delivered with total doses D of about 50 Gy to 70 Gy in 2 Gy fractions to a target volume of 10^3 cm^3 (Gottschalk, 2011), which requires approximately 10^{11} protons per Gy (Schellhammer, 2019). Additionally, every quasi-monoenergetic proton beam features an initial energy spread and the proton interactions with the target underlie statistical fluctuations leading to energy straggling. The proton beam also produces secondary protons, neutrons, photons and heavier target fragments via non-elastic nuclear reactions with the target medium. While the LET is defined unambiguously for a given particle type and energy, the presence of different particle types of different energies create an LET distribution in every point of the voxelated patient geometry. The average of an LET spectrum of different particles and energies can be derived with the track-averaged linear

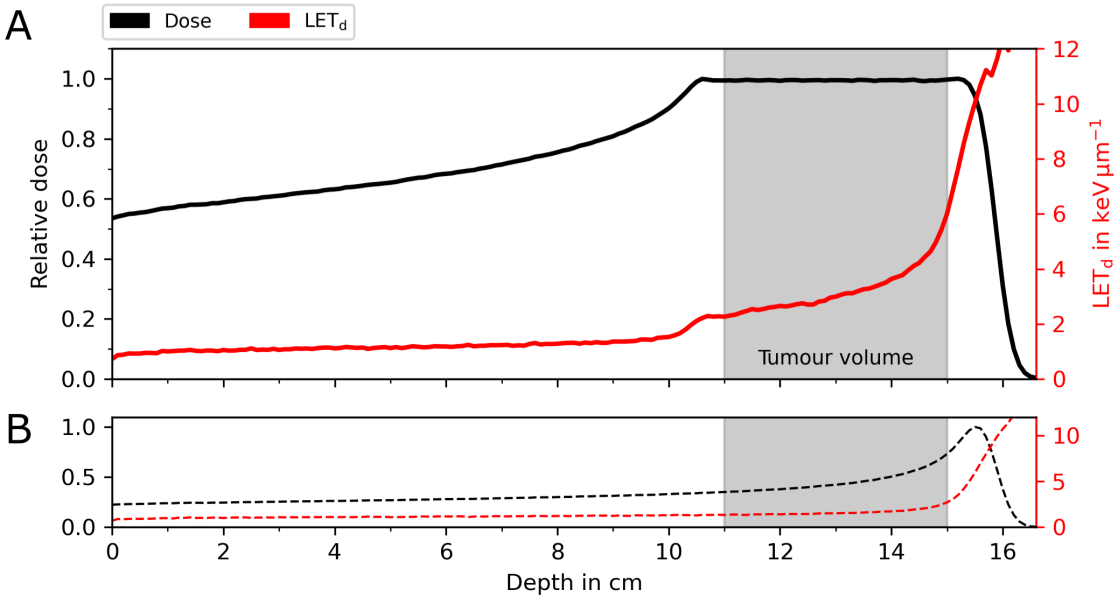

Figure 2.3: Relative depth dose (black) distribution and corresponding proton dose-averaged linear energy transfer (LET$_d$, red) for **A** a spread-out Bragg-peak (SOBP, solid line) and **B** one pristine Bragg-peak with 150 MeV (dashed line). Multiple pristine Bragg-peaks with different energies and intensities are superimposed to build the SOBP.

energy transfer (LET$_t$) (Guan et al., 2015):

$$\mathrm{LET_t} = \frac{\sum_z \int_0^\infty \Phi(E,x) S_{\mathrm{el}}(E) \mathrm{d}E}{\sum_z \int_0^\infty \Phi(E,x) \mathrm{d}E} \quad , \tag{2.7}$$

where $S_{\mathrm{el}}(E)$ is the material-dependent electronic stopping power of particles with charge z and kinetic energy E and $\Phi(E,x)$ is their fluence at location x. Alternatively, the average value of S_{el} can be weighted with the particles contributions to the local linear energy transfer and thus absorbed dose, by using the dose-averaged linear energy transfer (LET$_d$):

$$\mathrm{LET_d} = \frac{\sum_z \int_0^\infty \Phi(E,x) S_{\mathrm{el}}^2(E) \mathrm{d}E}{\sum_z \int_0^\infty \Phi(E,x) S_{\mathrm{el}}(E) \mathrm{d}E} \quad . \tag{2.8}$$

From here on, averaged LET will be written simply as LET throughout this thesis, if not stated otherwise. In summary, the absorbed dose can be considered as radiation quantity as it is proportional to the number of particles. In contrast, the LET describes the energy

deposition pattern around an individual particle track and is thus a measure for radiation quality. The combination of both these physical factors determines the fate of a cell after irradiation.

2.2 Biological effect of radiation

The outcome of radiotherapy greatly depends on the inactivation of irradiated cells. The primary aim is to inactivate tumour cells by inducing damage to their DNA thereby preventing tumour growth and metastatic dissemination (Baumann et al., 2016).

2.2.1 Linear-quadratic model

Clonogenic cell survival *in-vitro* is the most studied endpoint to assess the biological effect of radiation. The biological effect of a radiation type can be determined by quantifying the cell survival in a cell-dish after being irradiated with a homogeneous absorbed dose (Karger et al., 2021; Paganetti et al., 2019). The survival fraction SF of cells after exposure to n fractions of single doses d of radiation can be described by the linear-quadratic (LQ) model (Kellerer & Rossi, 1972) for clinically relevant fraction doses:

$$SF(d) = e^{-n(\alpha d + \beta d^2)} \quad , \tag{2.9}$$

where α describes complex and lethal double strand breaks (DSBs) from a single particle track with multiple energy transfers in proximity to each other, which is proportional to the absorbed dose d. The probability of two energy depositions close to each other is thought to increase with increasing ionisation density. Protons and other particles with high ionisation density, and thus high LET, deposit their energy predominantly through these lethal events. Low LET radiation, such as photons, is considered sparsely ionising, which causes ionisation and excitation that is more spread out throughout the cells nucleus. The combination of sublethal but unrepaired cell damage can, however, induce DSBs which is described by β and proportional to d^2. Both these constants are derived by a fit to experimental data.

The ratio α/β describes the shape of the survival curve and therefore the radiosensitivity and repair capacity of the irradiated tissue. Tumour tissue typically features high α/β ($\approx$ 10 Gy) indicating low repair capacity and thus low fractionation sensitivity. In contrast, the low

α/β of healthy ($\approx 2\,\mathrm{Gy}$) tissue enables better repair and thus lower cell death between two successive fractions.

The fractionated radiotherapy delivery enhances the therapeutic window. Treatment schedules with $1.8-2\,\mathrm{Gy}$ per fraction, once a day and five times a week are called normofractionated (Baumann & Gregoire, 2009). Higher and lower fraction doses are termed hypo- and hyperfractionation, respectively (Baumann & Gregoire, 2009). The biological effect of fractionation schedules other than normofractionated treatment can be derived by conversion to equivalent doses given in 2 Gy fractions (EQD_2) with:

$$EQD_2 = D\frac{\alpha/\beta + d}{\alpha/\beta + 2\,\mathrm{Gy}} \quad , \tag{2.10}$$

where the total dose D is the product of dose per fraction d and number of fractions n.

However, it is not solely the dose that determines the fraction of surviving cells after irradiation. Protons, being charged particles, feature different energy deposition characteristics on a microscopic scale compared to the conventionally used photons. Their higher LET induces more initial and remaining DSBs, more complex chromosome aberrations and thus more lethal lesions, which lead to a higher fraction of inactivated cells than photons for the same absorbed dose (Paganetti, 2011b). Importantly, the proton LET changes with energy due to the protons energy loss when traversing the medium, whereas the photon LET is assumed to be low ($\approx 0.5\,\mathrm{keV\,\mu m^{-1}}$) and constant.

2.2.2 Relative biological effectiveness

The concept of RBE was introduced to transfer the longstanding empirical clinical experience with photons to radiotherapy with ions (Karger et al., 2021). This concerns both suitable levels for tumour prescription dose and tolerance doses to healthy tissue. The RBE is expressed by the quotient of the doses required by two types of radiation for the same biological effect:

$$\mathrm{RBE} = \left.\frac{D_{\mathrm{ref}}}{D_{\mathrm{test}}}\right|_{\text{same biological effect}} \quad , \tag{2.11}$$

where D_{ref} and D_{test} are the administered doses of the reference radiation type and the test radiation type. The RBE helps to predict the effectiveness of protons (D_{test}) in the tumour and normal tissues based on photon data (D_{ref}). For clinical practice, protons are assumed

to be 10 % more biologically effective than photons under all circumstances which results in a constant RBE of 1.1 (De Luca, 2007; Paganetti et al., 2019). It is thus recommended to distinguish the absorbed dose from the RBE-weighted dose, which is defined as the product of absorbed dose and RBE, by using the unit Gy(RBE) for the latter (De Luca, 2007). The clinically used constant RBE was deduced as an average value of measured RBE values *in-vivo* in the early days of proton therapy and adopted clinically as a conservative value for tumour control (Paganetti et al., 2019). This reflects a simplification since the RBE, by definition, depends on the considered endpoint itself.

It is known from *in-vitro* experiments that RBE depends both on physical and biological parameters and is therefore not a constant (Paganetti, 2014; Paganetti et al., 2019). The comparison of dose-response curves for different radiation types irradiating the same cell type enables the systematic assessment of physical parameters on RBE. Likewise, irradiating cells of different biological properties with the same radiation type reveals biological RBE dependencies. The RBE of protons depends on the LET, dose, endpoint, track-structure around an ion-track and tissue-type (Paganetti, 2014). Since RBE is defined as the ratio of photon fraction dose d_{x} and proton fraction dose d_{p} for the same biological effect, i.e. cell survival, rearranging and solving equation (2.9) for d_x/d_p expresses variable RBE per volume element (voxel) i as a function of proton parameters with index p and photon parameters with index x as:

$$\mathrm{RBE}_i = \frac{1}{2d_{\mathrm{p},i}}\left[\sqrt{\left(\frac{\alpha}{\beta}\right)_{\mathrm{x}}^2 + 4d_{\mathrm{p},i}\,\mathrm{RBE}_{\max}\left(\frac{\alpha}{\beta}\right)_{\mathrm{x}} + 4d_{\mathrm{p},i}^2\,\mathrm{RBE}_{\min}^2} - \left(\frac{\alpha}{\beta}\right)_{\mathrm{x}}\right] \tag{2.12}$$

with:

$$\begin{aligned}\mathrm{RBE}_{\max}(d_{\mathrm{p}} \to \infty) &= \frac{\alpha_{\mathrm{p}}}{\alpha_{\mathrm{x}}} \\ \mathrm{RBE}_{\min}(d_{\mathrm{p}} \to 0) &= \sqrt{\frac{\beta_{\mathrm{p}}}{\beta_{\mathrm{x}}}}\ ,\end{aligned} \tag{2.13}$$

where α and β represent the intrinsic cell radiosensitivity and $\mathrm{RBE}_{\min}$ to $\mathrm{RBE}_{\max}$ spans the range of RBE values in the limits of very low and high proton fraction doses d_{p}, respectively.

This led to the development of LQ-based variable RBE models, that were derived from the comparison of *in-vitro* cell survival after proton and photon irradiation and were summarised

Table 2.1: Model parameters c_j and function dependencies for selected empirical variable relative biological effectiveness (RBE) models. $\mathrm{RBE}_{\mathrm{max}}$ and $\mathrm{RBE}_{\mathrm{min}}$ describe RBE in the limits of high and low doses.

Authors	$\mathbf{RBE}_{\mathbf{max}}$		$\mathbf{RBE}_{\mathbf{min}}$		
	c_0	c_1	c_2	c_3	$f(\mathrm{LET}_i)$
Carabe et al. (2012)	0.843	0.414	1.09	0.016	$\mathrm{LET_i}(\alpha/\beta)_{\mathrm{x},i}^{-1}$
Wedenberg et al. (2013)	1.000	0.434	1.00	0.00	–
McNamara et al. (2015)	0.990	0.356	1.10	-0.00387	$\mathrm{LET_i}(\alpha/\beta)_{\mathrm{x},i}^{-0.5}$
Mairani et al. (2017)	1.000	0.377	1.00	0.00	–
Rørvik et al. (2017)	1.000	0.645	1.00	0.00	–

LET_i: voxelwise averaged LET.

by Rørvik et al. (2018). Accordingly, these models are based on fits of $\mathrm{RBE}_{\mathrm{max}}$ and $\mathrm{RBE}_{\mathrm{min}}$ to *in-vitro* experiments as functions of LET and (α/β). However, each individual variable RBE model is based solely on a subset of all available *in-vitro* data covering different ranges of LET values and cell lines with different (α/β) (Rørvik et al., 2018).

Based on an extensive review, proton RBE should increase with increasing dose-averaged linear energy transfer ($\mathrm{LET_d}$) and decreasing absorbed dose per fraction and α/β, respectively (Paganetti, 2014). Furthermore, the LET-RBE relationship for clinically relevant LET values below 30 keV µm^{-1}, i.e. below the overkill effect (Jones, 2015), was found to be best described by a linear relationship (Mairani et al., 2017). Table 2.1 summarises the published RBE models that satisfy these criteria, for which $\mathrm{RBE}_{\mathrm{max}}$ and $\mathrm{RBE}_{\mathrm{min}}$ can be described as:

$$\begin{aligned} \mathrm{RBE}_{\mathrm{max},i} &= c_0 + c_1 \frac{\mathrm{LET}_i}{(\alpha/\beta)_{\mathrm{x},i}} \\ \mathrm{RBE}_{\mathrm{min},i} &= c_2 + c_3 f(\mathrm{LET_i}) \quad , \end{aligned} \tag{2.14}$$

with model-specific fitting parameters c_j. Therefore, RBE in in voxel i can be described based on the corresponding averaged LET and cell intrinsic radiosensitivity to photon reference irradiation, which is typically retrieved from the literature.

The parameters in Table 2.1 can thus be used for voxelwise variable RBE calculations in patient treatment plans. Intrinsically, this assumes that all cells in voxel i feature the same radiosensitivities and are exposed to the same absorbed dose and LET (Paganetti, 2022). Using the RBE models in Table 2.1, high RBE values will particularly occur in cells or voxels with lower $(\alpha/\beta)_{\mathrm{x}}$.

RBE models can be broadly divided into empirical models (see Table 2.1) and mechanistical models (Flint et al., 2022). The latter offer insights into the underlying mechanics of how an individual particle track may interact with the cell. The most commonly applied mechanistic models are the local effect model (Scholz et al., 1997) and the microdosimetric kinetic model (Hawkins, 1996), which are both in clinical use for heavy ion therapy where few ion tracks traverse a cell per unit dose. However, mechanistic models require cell-line specific parameters such as the radius of the cell nucleus which are rarely known. This limits their use and complicates the comparison of their performance against the empirical models (Flint et al., 2022). Instead, empirical models simply describe the trends observed in experiments without giving further insights on the mechanics of cell damage (Flint et al., 2022). As many individual tracks traverse a cell or a voxel in proton therapy (Paganetti, 2005), it is considered a reasonable simplification to use LET as a measure for radiation quality on voxel level, which enables the use of empirical RBE models.

It is clear from numerous *in-vitro* experimental data (Paganetti, 2014) and initial *in-vivo* data (Saager et al., 2018), that proton RBE varies as a function of dose per fraction, LET, tissue type and endpoint. Yet, it is under debate whether the RBE for clonogenic survival *in-vitro* translates to clinically relevant endpoints such as patient toxicity where volume effects may play an important role (Paganetti et al., 2019; Sørensen et al., 2021; Wagenaar, 2022). Emerging studies showed clinical evidence of RBE variability in proton therapy (Bahn et al., 2020; Eulitz et al., 2019b; Ödén et al., 2020; Peeler et al., 2016; Underwood et al., 2018; Wang et al., 2020). A recent systematic review concluded that clinical RBE variability remains overall statistically weak at present, which may be caused by a multitude of factors: the lack of large prospective datasets, differences in statistical methods and the inclusion or exclusion of confounding clinical factors and patient-specific radiosensitivities (Underwood et al., 2022). The reported RBE variability and their unresolved clinical impact already affect patient treatment by applying indirect measures to account for the potentially elevated RBE at the end of range (Sørensen et al., 2021). By doing so, this may influence clinical outcomes as fewer RBE related adverse events were reported than would have been expected based on preclinical studies (Heuchel et al., 2022). In todays clinical practice, an RBE of 1.1 is used (Paganetti et al., 2019).

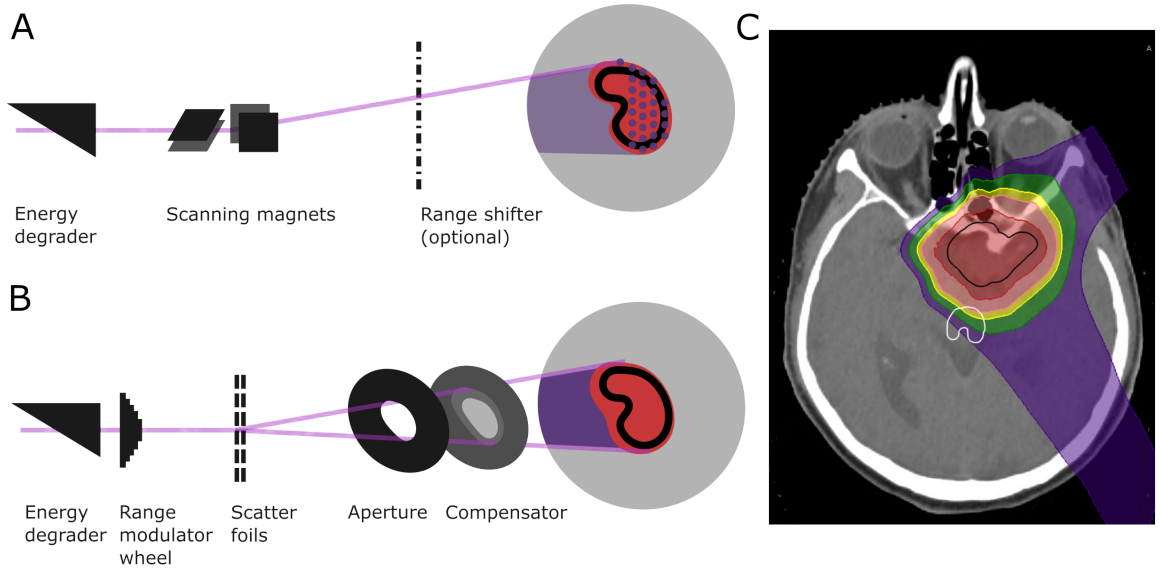

Figure 2.4: Delivery techniques in proton therapy: **A** Pencil beam scanning, **B** double scattering and **C** a dose distribution on an axial computed tomography slice with high doses to the tumour volume (black), while sparing the healthy brainstem (white), is exemplarily shown for a patient case. Adapted from Dutz (2020).

2.3 Proton beam delivery and field formation

Proton therapy facilities require an accelerator that can produce protons of up to 230 MeV. In a cyclotron, protons are accelerated to the maximum energy and are then slowed down to the required energy by inserting energy degraders in the beam path (Mohan, 2022). The accelerated protons are then guided to the patient treatment room under influence of quadrupole and dipole magnets, which focus and steer the pencil beam shaped proton beam. The treatment head at the end of the beam line, the so-called nozzle, then points towards the patient targeting the tumour volume to be irradiated. The treatment head is either fixed (fixed beam line) or may rotate around the patient (gantry). However, the narrow proton beam must be shaped laterally and longitudinally to conform with the target volume while sparing normal tissue simultaneously. The beam widening adaptation can be realised with pencil beam scanning (PBS) or double scattering (DS), which is schematically illustrated in Figure 2.4.

PBS proton therapy was first delivered over 20 years ago (Lomax et al., 2001) and is currently the most advanced form of planning and delivering proton therapy (Lomax et al., 2004; Mohan, 2022). The longitudinal treatment field shaping is realised by adapting the

beam energy, whereas the lateral shape is determined by magnetically steering the pencil beam to laterally conform with the tumour volume. The treatment is delivered in layers, beginning with the highest energy, where each layer consists of many spots with the same energy. Each spot reflects the position of proton Bragg peaks for a quasi-monoenergetic proton pencil beam of Gaussian-shaped lateral distribution and with given intensity and thus fluence, which is proportional to the monitor units (MU) (Flanz, 2011). The pencil beam is steered from one spot to another using two sets of dipole magnets perpendicular to the beam. After delivery of all spots to a given energy layer, the energy is reduced and the process is repeated. A range shifter may be used for water-equivalent ranges below 4.1 cm to 7.7 cm, as the typical minimum beam energy is typically between 70 MeV to 100 MeV (Mohan, 2022). Therefore, PBS allows for conformal proximal, distal and lateral treatment field adjustment which increases tumour coverage and spares healthy tissue compared to standard photon therapy. No patient-specific beam shaping devices are thus needed in PBS. However, additional lateral collimation systems may further reduce the lateral penumbra of each spot and thereby improve lateral conformality (Bäumer et al., 2021; Hyer et al., 2014a, 2014b). The energies for each proton spot are a result of the plan optimisation process (Mohan, 2022).

For DS, a rotating modulation wheel and scattering foils are used to spread-out the treatment field longitudinally and laterally (Mohan, 2022). Additionally, the field is laterally conformed to the patient-specific target volume through brass apertures. The longitudinal treatment field shape is then customised to the distal edge of the target volume by means of a range compensator made from polymethyl methacrylate. Thereby, DS does not allow for shaping the treatment field proximal to the target volume. Both the aperture and range compensator must be milled for each treatment field and patient individually. The presence of beam shaping devices in the beam path also results in higher neutron production in DS. However, as DS can be delivered much faster than PBS, it is still used for the treatment of moving tumours in proton therapy.

2.4 Treatment planning

Radiotherapy treatment planning and delivery requires patient imaging information to localise the tumour, delineations to define the target volume and OARs for plan optimisation,

information on the planned dose distribution and finally the machine parameters to deliver dose to the patient. The Digital Imaging and Communications in Medicine (DICOM) standard allows to unambiguously store these patient-specific information and transfer them between different softwares and manufacturers in dedicated DICOM radiotherapy objects during the radiotherapy workflow. In the following, the plan optimisation and evaluation process will be described and what information is to be stored in DICOM objects.

2.4.1 Patient modelling and structure definition

In radiotherapy, an X-ray based planning computed tomography (CT) scan is acquired to determine the anatomy of the patient prior to beam delivery. On this scan, and sometimes using auxiliary information from other imaging modalities, the visible tumour volume(s) and OARs are delineated by the radiation oncologist (Engelsman, 2011). The visible tumour volume is expanded to account for possible microscopic spread of the tumour. The resulting expanded volume is called clinical target volume (CTV) and represents the target volume of interest in proton treatment planning. The radiation oncologists also provide a prescription dose, which is the dose to be delivered in a certain number of fractions to the target to achieve the desired tumour control. Prescription doses and the expansion from visible tumour volume to CTV are based on clinical experience. Uncertainties in the target location and beam delivery will be discussed in chapter 2.5. The delineations for the target volumes and OARs are stored in the DICOM RT Structure Set. The DICOM CT image stores the three-dimensional voxelised patient geometry and the Hounsfield Units (HUs).

The CT is used in treatment planning as a virtual representation of the patient at the time of beam delivery (Engelsman, 2011). The patient is thus represented by CT voxels which are the smallest image information available for treatment planning. Each voxel contains photon attenuation coefficients relative to those in water, called HUs. Therefore, it requires a conversion from HU to electron density and proton stopping power (ratios) to use the CT scan in proton treatment planning (Schneider et al., 1996; Schneider et al., 2000). HU and stopping-power ratio (SPR) are linearly dependent on the electron density for human tissues (Newhauser & Zhang, 2015). This allows to use a so-called Hounsfield Unit look-up table (HLUT) for voxelwise SPR prediction by HU conversion to either SPR directly or to mass density followed by a conversion to material composition and then SPR, as done in some TPS (Wohlfahrt & Richter, 2020).

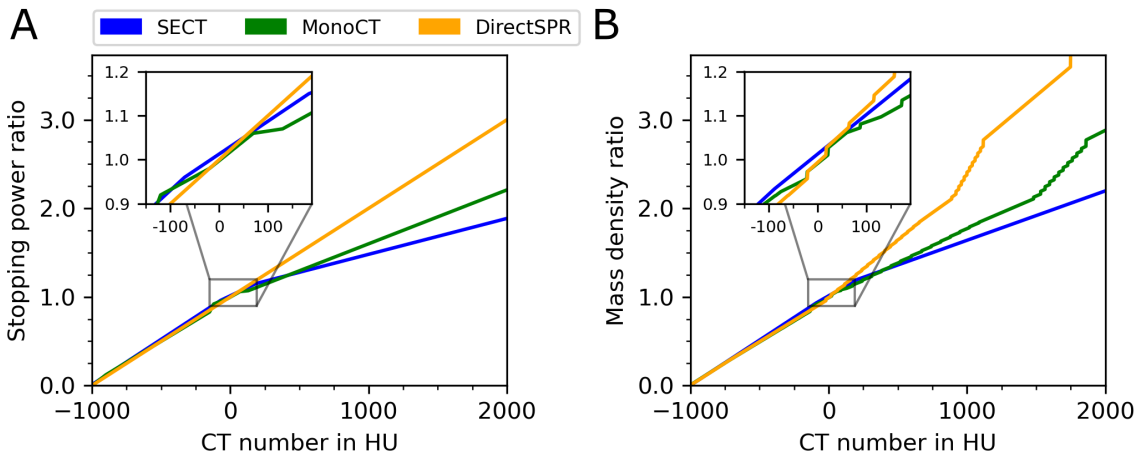

Figure 2.5: Conversion from computed tomography (CT) numbers **A** into stopping power ratio (SPR) or **B** into mass density ratio for different patient image datasets: single-energy CT (SECT), dual-energy CT based pseudo-monoenergetic CT (MonoCT) and direct SPR prediction (DirectSPR). Adapted from Peters et al. (2022).

Different approaches may be used to derive SPR (Figure 2.5). Single-energy computed tomography (SECT) applies a heuristic conversion from CT numbers to SPR. Based on dual-energy computed tomography (DECT), it is possible to create MonoCT images, which is similar to an idealised SECT images obtained with a monochromatic X-ray beam (Peters, 2021). Alternatively, SPR can be predicted directly from DECT and in principle does not require a HLUT. For Monte Carlo (MC) dose calculation, the mass density and material composition of the tissues are additionally required to calculate the corresponding cross sections for particle interactions (Schneider et al., 2000). HLUT are CT-scanner and thus centre-specific as they depend on the experimental setup used for calibration as well as the scan and image reconstruction parameters applied (Peters, 2021).

2.4.2 Treatment plan optimisation

Proton treatment planning optimises the absorbed dose weighted with a constant RBE of 1.1. Treatment planning aims at high doses in the target volume to achieve tumour control while optimally sparing dose to normal tissues to minimise side-effects. OAR tolerance doses stem from the initial review on photon data from Emami et al. (1991) that were updated and refined by Marks et al. (2010). Furthermore, initial consensus-based tolerance doses are available for proton therapy (Lambrecht et al., 2018) and are continuously updated by proton therapy centres according to their centre-specific practice.

Treatment plan optimisation is then based on these tolerance and prescription doses. A clinically acceptable treatment plan to be delivered to the patient must feature a dose distribution that adheres to these clinical goals. In PBS proton therapy, plan optimisation is an inverse process. First, the treatment planner formulates the clinical goals for each patient individually that must be respected by defining so-called objective functions (Unkelbach & Paganetti, 2018). Subsequently, the TPS iteratively adjusts the energy, fluence and lateral position of all spots to find the dose distribution that fulfils the formulated objectives.

An objective function θ can be defined for each structure of interest s as a function of the distribution d, where a minimal $\theta_s(d)$ indicates an optimal dose distribution in the structure. The optimisation problem can thus be expressed as:

$$\begin{aligned} \underset{x}{\text{minimise}} \quad & \theta_s(d) \\ \text{subject to} \quad & d_i = \sum_j x_j \cdot D_{ij} \\ & x_j \geq 0 \ , \end{aligned} \tag{2.15}$$

where d_i is the dose in voxel i of structure s, x_j is the spot weight of pencil beam j and D_{ij} is the dose contribution of pencil beam j to voxel i. The lower and upper limits of the spot weights x are proportional to the proton fluence and depend on the minimum and maximum beam current of the accelerator as well as the lower limit of the beam monitoring to detect very small current (Mohan, 2022). Thus, x_j is beamline- and centre-specific.

For instance, a quadratic penalty function is defined for OARs that aims to minimise the volume receiving doses above the maximum allowable dose $D^{\max}$ by reducing the d_i (Trofimov, 2011):

$$\theta_s(d) = \sum_{i \in s} H(d_i - D^{\max})(d_i - D^{\max})^2 \ , \tag{2.16}$$

where $H(d)$ is the Heaviside function being 1 for $d_i - D^{\max} > 0$ and 0 otherwise. Note that the formulated dose levels $D^{\max}$ for OARs must not necessarily match the clinical goals as it is desirable to minimise the dose even below the tolerance dose. For tumour volumes, $D^{\max}$ may be replaced with the minimum allowable dose $D^{\min}$ and one may consider two objectives to the target volume with $D^{\max}$ and $D^{\min}$ to keep the dose close to prescription. Accordingly, the patient-specific optimisation includes multiple structures of interest, so that the entire optimisation problem to be minimised becomes:

$$\underset{x}{\text{minimise}} \;\; F(d) = \sum_s \omega_s \theta_s(d), \; x_j \geq 0 \;\; , \tag{2.17}$$

where $F(d)$ is the composite objective function and ω_s is the weight of the structure-wise objective function θ_s. Balancing ω_s between different structures allows for prioritising competing structure-wise objectives over one another, as they may also be mutually exclusive, to achieve a high overall treatment plan quality. Objectives which must not be compromised are called constraints.

The treatment plan optimisation is handled by a TPS due to the large number of individual pencil beams to be optimised (Nill et al., 2004; Oelfke & Bortfeld, 2001). Finding the optimal dose distribution requires not only many iterations of the optimising algorithm searching for the best set of delivery parameters for the optimisation problem at hand. Instead, the treatment planner may adapt the incident treatment field angles, reformulate objective functions and adapt their weights throughout the planning process to refine the optimisation problem and thereby the desired dose distribution. For the same patient, different treatment planners may thus achieve different results due to differences in the formulation of the optimisation problem, different softwares used as TPS and different machine parameter limits of the clinical system. In modern TPS, MC algorithms can be used for the optimisation of spot weights and position as well for the final dose calculation (Ruangchan et al., 2020). The machine parameters such as treatment field angles, patient specific beam shaping devices as well as spot energies, lateral positions and intensities are stored to DICOM RT Plan. The voxelised dose distribution is stored as DICOM RT dose.

State-of-the-art proton therapy is typically planned and delivered with two to four treatment fields (Heuchel et al., 2022), such that the dose contributions of multiple treatment fields to a single voxel can be optimised simultaneously with PBS (Lomax, 1999). Since every proton spot can be optimised individually, the intensity of the spots can be varied even within a single treatment field. Single-field optimisation (SFO) aims for a homogeneous dose distribution within each treatment field of the treatment plan, thereby reducing the differences of spot-wise intensities within an energy layer. The result of SFO thus is that a treatment field delivers almost the same dose to each voxel of the target volume. This may result in treatment plans less sensitive to delivery and positioning uncertainties but at the expense of degrees of freedom in plan optimisation and therefore decreased normal tissue sparing (Anand & Bues, 2022). Alternatively, multi-field optimisation (MFO) allows to

fully modulate the intensity of proton spots for each field individually, resulting in inhomogeneous field-wise dose distributions (Lomax et al., 2001). The spots of all treatment fields are then optimised together to achieve a homogeneous summed dose distribution. PBS is thus also referred to as intensity-modulated proton therapy (IMPT). Intensity-modulation, in both SFO and MFO, allows to plan and deliver a higher dose to parts of the target volume - the boost volume. It is therefore possible to create different dose levels in the target volume delivered in the same treatment session in each field. The concept of delivering multiple dose levels to the tumour volume simultaneously is hereafter referred to as simultaneous integrated boost (SIB). Intensity-modulation allows for optimising LET and other quantities beyond dose (Deng et al., 2021), but none of these novel optimisation approaches is used in clinical routine yet.

2.4.3 Treatment plan evaluation

The evaluation of the calculated dose distributions represents a fundamental part in treatment planning, since it unravels and quantifies the quality of a treatment plan to be delivered to the patient. The three-dimensional dose distribution is visualised with lines of the same dose, isodoses, to evaluate target volume coverage as well as sparing of OARs. Dose volume histograms (DVHs) are the current standard for the evaluation of the three-dimensional dose distribution (Hernandez et al., 2020). The dose distribution in the patient is visualised in voxels, each of which contains information on the local absorbed dose. Dose and volume information for a given region of interest (ROI), i.e. the tumour volume or healthy organ, are retrieved and their cumulative sum builds the DVH. The cumulative DVH thus contains information on the relative volume of a ROI receiving doses above a specified dose level (Figure 2.6).

Clinical goals to be met for acceptable tumour control and normal tissue sparing are then formulated based on single DVH parameters. $D_{x\%}$ reflects the minimum dose that is received by x % of a structure. $V_{x\,\mathrm{Gy(RBE)}}$ describes the volume V of a structure that receives dose of at least x Gy(RBE). The odds for a certain toxicity are assumed to be reasonably low for OARs receiving a dose below the formulated DVH threshold (Lambrecht et al., 2018). For serially structured organs, the dose to small volumes is particularly important, so that relevant DVH parameters are $D_{1\%}$ and $D_{2\%}$. For organs with parallel structures, volume parameters are used. For tumour volumes, the minimum dose is particularly relevant

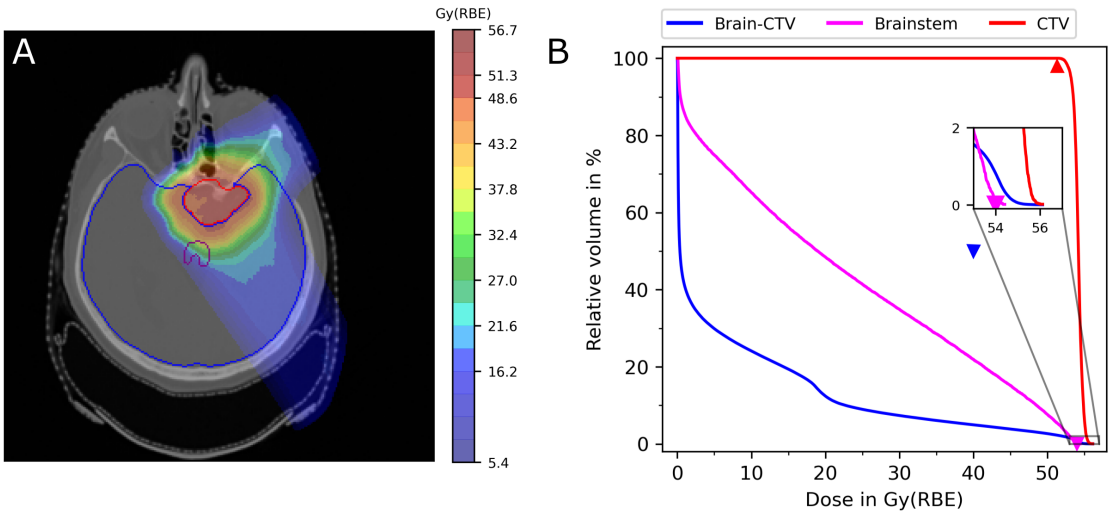

Figure 2.6: A Overlay of the dose distribution on the patient computed tomography scan for the clinical target volume (CTV), brainstem and CTV-free brain tissue. **B** The resulting cumulative dose-volume histogram. Clinical dose-volume goals are depicted as triangles. Triangles pointing down and up reflect maximum tolerance doses in healthy tissue and minimum dose to the tumour volume, respectively. The position of the triangles reflect the clinical dose-volume goals.

to ensure tumour control, such that $D_{95\%}$ and $D_{98\%}$ are used for instance.

Besides DVH parameters characterising the dose distribution within a structure, a high quality treatment plan features high conformity to the tumour volume, thereby also limiting unnecessary dose exposure of healthy tissue. Conformity is described by the conformity index (CI):

$$\mathrm{CI} = \frac{V_{\mathrm{RI}}}{V_{\mathrm{target}}} \quad , \tag{2.18}$$

where V_{RI} is the reference isodose volume, such as the volume encompassed by the 98 % isodose line, and V_{target} is the volume of the target to be treated (Feuvret et al., 2006). A CI of 1 reflects ideal conformity, but does not ensure a spatial overlap of high dose and target volume. Thus, the homogeneity index (HI) may be used in addition to characterise the dose in the target explicitly:

$$\mathrm{HI} = \frac{D_{\mathrm{max}} - D_{\mathrm{min}}}{D_{\mathrm{mean}}} \quad , \tag{2.19}$$

with D_{max}, D_{min} and D_{mean} being the maximum, minimum and mean doses to the ROI, respectively. Instead of using the point maximum and minimum in dose reporting, it is rec-

ommended, in particular for intensity-modulated radiotherapy, to use the dose to a small volume, e.g. 1 % or 2 %, instead (De Luca et al., 2010).

A single DVH metric might not fully reflect the dose-response relationship (Lambrecht et al., 2018). Therefore, models to explicitly calculate the sigmoid-shaped tumour control probability and normal tissue complication probability (NTCP) after radiotherapy were developed based on DVH information. Numerous NTCP models are available for organ-specific endpoints but they are rarely considered clinically (Bentzen et al., 2010).

The functional structure of an OAR can be considered in NTCP calculations by using the relative seriality (RS) model (Källman et al., 1992). The parameter s describes the extent of seriality in an organ as the ratio of serial subunits to all subunits. Serially-structured organs are modelled with s equal to 1, whereas s approaches 0 for organs with a parallel structure. NTCP after irradiation of an organ with i voxels can then be expressed as:

$$\begin{aligned} \mathrm{NTCP}_{\mathrm{RS}} &= \left[1 - \prod_{i=1}^{n} \left(1 - P(D_i)^s\right)^{v_i}\right]^{1/s} \\ \text{with } P(D_i) &= 2^{-\exp\left[e\gamma\left(1-\frac{D_i}{TD_{50}}\right)\right]}, \end{aligned} \tag{2.20}$$

where $P(D_i)$ is the probability that no cell survives in voxel i with relative volume v_i and seriality s after irradiation with the total dose D_i calculated with Poisson statistics. TD_{50} and γ describe the position and slope of the dose-response curve, respectively. Alternatively to the RS model, Lyman-Kutcher-Burman models can be used to be predict endpoint-specific NTCP under consideration of the tissue structure (Kutcher & Burman, 1989). There, the inhomogeneous dose distribution in an organ is reduced to a uniform one using the generalised equivalent uniform dose that would cause the same probability of a side effect (Niemierko, 1997). Both models can include a dose-modifying factor to include clinical factors in prediction (Defraene et al., 2012).

In the relative seriality model and the LKB model, each voxel of an OAR is considered to equally contribute to the side effect in question. In contrast, multivariate logistic regression models allow for assigning different radiosensitivities within one OAR, including information on patient comorbidities and risk factors and combining the contribution of dose in different OAR for the same endpoint, e.g. the involvement of many muscles in the head and neck region in swallowing and therefore dysphagia (Ebert et al., 2021). In multivariate logistic regression, NTCP is given by:

$$\begin{aligned} \mathrm{NTCP}_{\mathrm{MLR}} &= \frac{1}{1+e^{-g(x)}} \\ \text{with } g(x) &= \beta_0 + \sum_{m=1}^{\mathrm{M}} \beta_m x_m \ , \end{aligned} \tag{2.21}$$

where β_0 is a constant and β_m is the regression coefficient for the predictor x_m.

NTCP models can aid the comparison of two treatment plans, i.e. photons and protons, as is done clinically in the model-based approach (Langendijk et al., 2013). Therefore, NTCP models can be used for prospective and retrospective treatment plan analyses. In this thesis, plan quality is thus defined by target homogeneity and conformity and adherence to OAR tolerance doses or NTCP.

2.5 Proton therapy uncertainties and mitigation strategies

IMPT techniques are more sensitive to uncertainties than other radiotherapy techniques including uncertainties in range, setup, anatomic changes, dose calculation and biological effect (Zhang et al., 2021). These physical and biological uncertainties in proton therapy render the dose distribution on the planning CT an imperfect representation of the dose administered to the patient (Goitein, 1985). From here on, the dose displayed on the planning CT is referred to as nominal dose, i.e. without accounting for uncertainties.

Uncertainties in predicting the absorbed dose distribution to the patient are summarised as physics uncertainties and result mainly from an imperfect patient model and patient motion during and between fractions (Unkelbach & Paganetti, 2018). Biological uncertainties arise from the simplified constant RBE that neglects the RBE dependence on LET and α/β and are mainly expected at the end of proton range (Figure 2.3). Uncertainties in fluence delivery to the patient are not described as they would have been detected during machine quality assurance prior to treatment (Paganetti, 2012; Unkelbach et al., 2018). Likewise, uncertainties in dose calculations are negligible when using MC codes for particle transport with a sufficient number of incident particles, as the remaining uncertainty in range prediction even in inhomogeneities is in the order of 0.1 % (Paganetti, 2011a, 2012). The mitigation of uncertainties can be divided into two steps: Minimising their presence and their impact, followed by including their remainder in plan optimisation. Since the impact of both range and RBE uncertainties is expected at the end of range, their impact on the

treatment plan is generally also partly considered in finding suitable patient-specific beam angles.

2.5.1 Clinical mitigation strategies

The finite proton range increases the importance for suitable beam angle selection in proton therapy and, if done properly, reduces the impact of physical and biological uncertainties on the treatment plan (Engelsman, 2011). The remaining uncertainty can be handled through treatment plan optimisation strategies.

Placing the incident field directions perpendicular to the patient surface avoids skimming of the treatment field as well as the impact of patient misalignment translating into range deviations (Anand & Bues, 2022). The avoidance of inhomogeneities and sharp density gradients reduces the impact of range uncertainties. Avoiding organs with day-to-day anatomical or organ filling variations in the beam path reduces the risk of range degradation (Unkelbach & Paganetti, 2018). Biological uncertainties can be mitigated by choosing wide opening angles between incident fields to prevent a superposition of multiple distal field edges with potentially elevated LET at the end of range. For beams inevitably stopping in front of an OAR, a lower field weight is often considered (Heuchel et al., 2022; Sørensen et al., 2021). The magnitude of setup uncertainties is further reduced through patient immobilisation devices ensuring rigid and reproducible patient positioning over the whole course of the fractionated treatment as well as daily position verification through image guidance (Lowe et al., 2016; Paganetti, 2012). The following mitigation strategies thus include the remaining physical and biological uncertainties. A treatment plan is considered robust if the perturbation of the nominal dose distribution through different sources of uncertainties remains within acceptable limits (Ödén, 2019). Plan robustness may be achieved through different strategies.

In radiotherapy, physical uncertainties are commonly handled through using additional safety margins. Treatment planning is then based on a planning target volume (PTV) which is typically derived by (entity-specific) isotropic expansion of the CTV taking into account uncertainties arising during beam delivery (Fredriksson et al., 2011). However, safety margins in proton therapy are not isotropic as the typically considered uncertainty in beam direction of 3.5 % of the beam range (Paganetti, 2012; Taasti et al., 2018) exceeds that in lateral beam direction due to setup uncertainties, particularly in deep-seated tumours. This

led to the invention of a beam-specific PTV with larger margins in beam direction (Park et al., 2012).

Robust optimisation

Robust optimisation allows to explicitly include physical uncertainty scenarios into the plan optimisation process instead of optimising solely for the nominal scenario on the planning CT. Physical uncertainties can be modelled by uncertainties in the dose influence matrix (Unkelbach et al., 2018):

$$d_i^k = \sum_j x_j \cdot D_{ij}^k \quad , \tag{2.22}$$

where D_{ij}^k is the uncertain dose contribution of pencil beam j to voxel i in scenario k.

Robust optimisation approaches can be categorised in minimax approaches and stochastic approaches (Unkelbach et al., 2018). Minimax approaches assign the same importance weight to all discrete error scenarios k and optimise the plan quality for the worst case error considered:

$$\underset{x}{\text{minimise}} \ \max_k \left[\theta_s\left(d^k\right)\right] \quad , \tag{2.23}$$

where θ_s is the objective function for structure s. Different types of worst-case optimisation exist. Assuming that each voxel i is independently affected by the uncertainty results in the voxelwise worst-case optimisation (Pflugfelder et al., 2008):

$$\underset{x}{\text{minimise}} \ \sum_s \omega_s \sum_{i \in s} \max_k \left[\theta_i\left(d_i^k\right)\right] \quad , \tag{2.24}$$

where ω_s is the relative importance factor. This is equivalent to minimising the worst-case dose distribution over all uncertainty scenarios k simultaneously. Including that all voxel doses to be penalised should stem from the same uncertainty scenario, but individual objectives may be affected by different error scenarios results in the objective-wise worst-case optimisation (Chen et al., 2012):

$$\underset{x}{\text{minimise}} \ \sum_s \omega_s \max_k \left[\theta_s\left(d_s^k\right)\right] \quad , \tag{2.25}$$

which was developed particularly for multi-criteria optimisation. Lastly, the composite worst-

case optimisation is defined as (Fredriksson et al., 2011):

$$\underset{x}{\text{minimise}} \ \max_{k} \sum_{s} \left[\omega_s \theta_s \left(d_s^k \right) \right] \quad , \tag{2.26}$$

where the maximum of the composite objective function over all uncertainty scenarios, organs and objectives is minimised. Alternatively, each error scenario may be assigned a probability to allow for prioritising more likely scenarios over extreme cases (Unkelbach et al., 2009):

$$\underset{x}{\text{minimise}} \ \sum_{k} p_k \theta_s \left(d_s^k \right) \quad , \tag{2.27}$$

where p_k is the weight for uncertainty scenario k and results in the optimisation of the expected plan quality through stochastic programming. Overall, none of the worst-case optimisations systematically outperformed the others although the generated dose distribution depends on the strategy used (Fredriksson & Bokrantz, 2014). Accordingly, clinically used TPS in proton therapy feature different implementations of robust optimisation: RayStation (RaySearch Laboratories AB, Stockholm, Sweden) implemented the composite worst-case method, Pinnacle (Philips Radiation Oncology Systems, Fitchburg, USA) uses the probabilistic approach and Eclipse (Varian Medical Systems, Palo Alto, USA) considers the voxelwise worst-case method (Unkelbach & Paganetti, 2018). Robust optimisation almost exclusively considers range and setup uncertainties (Unkelbach & Paganetti, 2018). Range and setup uncertainties are included in the robust optimisation framework of clinical TPS by up- or down-scaling the mass density or applying rigid shifts to the planning CT (Paganetti et al., 2021; Zhang et al., 2021).

Robustness evaluation

Regardless whether PTV-based, minimax or probabilistic optimisation were used, the plan robustness can be assessed after plan optimisation (Hernandez et al., 2020). Robustness evaluation is based on recalculating with the nominal treatment field information (spot positions, intensities etc.) the perturbed doses on multiple error scenarios. A DVH is determined for each error scenario and all DVH are subsequently grouped as DVH band which only displays the minimum and maximum DVH parameters over all error scenarios as a measure for plan robustness (Trofimov et al., 2012). As a quantitative measure for robustness, the

band width at critical points in the DVH, i.e. dose-volume parameters, is typically used (Mohan, 2022). Here, it may be too restrictive to request the adherence to clinical dose-volume goals in all error scenarios, since clinically used prescription and tolerance doses were derived solely from the nominal scenario on the planning CT (Hernandez et al., 2020). Thus, it should be aimed to fulfil the clinical goals in 90 % of error scenarios (Korevaar et al., 2019).

2.5.2 Optimisation approaches beyond absorbed dose

A biological robust treatment plan features a dose distribution that avoids tumour underdosage and normal tissue overdosage when accounting for RBE variability. This can be realised by using *in-vitro* based variable RBE models or by using RBE driving factors, such as the LET. The latter can be used as surrogate since, for a given dose per fraction and α/β, RBE increases steadily and almost linearly with LET values in the clinically relevant range (Mairani et al., 2017).

In principle, the treatment plan optimisation can be extended to account for variable RBE weighted dose, as described by Unkelbach and Paganetti (2018). In brief, this can be done by evaluating the objective function θ for biological dose b, i.e. absorbed dose times a variable RBE or its driving factors, rather than for absorbed dose d only, so that the optimisation problem becomes:

$$\begin{aligned} \underset{x}{\text{minimise}} \quad & \theta(b) \\ \text{subject to} \quad & b_i = d_i \cdot \mathrm{RBE}_i(c, L_i, (\alpha/\beta)_{\mathrm{x},i}) \\ & L_i = \frac{1}{d_i} \sum_j L_{ij} D_{ij} x_j \quad , \end{aligned} \tag{2.28}$$

where L_{ij} is the voxelwise averaged LET in voxel i for the dose contribution of pencil beam j, as introduced in equation (2.15). L_i is the LET in voxel i averaged over all pencil beams and c are the variable RBE model specific parameters and $(\alpha/\beta)_{\mathrm{x}}$ the tissue radiosensitivity (Unkelbach & Paganetti, 2018).

This has led to the development of optimisation approaches beyond the conventionally used absorbed dose (Deng et al., 2021). Strategies were presented for the optimisation of LET (An et al., 2017; Cao et al., 2017; Giantsoudi et al., 2013; Liu et al., 2020; Unkelbach et al., 2016), stopping protons (Traneus & Ödén, 2019) or variable RBE (Henjum et al., 2021; Sánchez-Parcerisa et al., 2019). As an alternative to optimising RBE itself, it was

suggested to minimise the variation in RBE through optimisation, which resulted in more biologically robust treatment plans (Bai et al., 2019).

However, optimisation beyond dose is not used in clinical practice. It remains unclear on how to define robustness against RBE uncertainties and the many available models are subject to large uncertainties (Unkelbach et al., 2018), which prevents their clinical consideration given the statistically weak evidence for clinical RBE variability. More importantly, neither the robustness evaluation against biological uncertainties, i.e. recalculating LET and RBE for treatment plans, nor their optimisation is available in clinical TPS. Recently, it was recommended to acquire more clinical data on RBE variability as well as to assess the potential for harm and benefits with optimisation strategies beyond absorbed dose (Paganetti et al., 2021). This urges proton therapy centres to develop methods for LET and RBE visualisation as well as safe and effective optimisation strategies.

3 Variable biological effectiveness in PBS treatment plans

Clinical evidence for a variable RBE in proton therapy emerged in the last years. The RBE uncertainty already affects patient treatment in proton therapy (Sørensen et al., 2021). European proton therapy institutions indirectly account for RBE uncertainties through clinically available measures, such as preventing beams from stopping in front of OARs, avoiding small opening angles between treatment fields, extending the distal field edge beyond an OAR and reducing the relative weight of critical incident angles (Heuchel et al., 2022). Similarly, a decrease in intensity-modulation through SFO was hypothesised to mitigate LET and thus RBE variability (Faught et al., 2022). However, LET and RBE recalculation tools are not available in clinical TPS yet which complicates quantifying the potential benefit of applying these measures (Sørensen et al., 2021). Accordingly, tools to visualise LET and RBE for clinical treatment plans were demanded by proton therapy institutions (Heuchel et al., 2022; Sørensen et al., 2021). These tools would allow to continuously inform clinicians on treatment plan safety in view of a variable RBE, to assess the benefit of clinically applied mitigation strategies and to further investigate the clinical relevance of RBE variability.

In this chapter, a framework to recalculate and visualise LET and RBE for PBS treatment plans is presented (section 3.1). Over the course of this thesis, this framework was implemented at University Proton Therapy Dresden (UPTD) and The West German Proton Therapy Centre Essen (WPE). Both these proton therapy institutions use RayStation as their clinical and research TPS and have similar proton therapy systems installed (Table 3.1). The recalculation framework was used to investigate LET and variable RBE distributions in clinical treatment plans at UPTD and WPE, which will be presented in individual sections. Firstly, the impact of intensity modulation and range uncertainties on LET and biological effectiveness was assessed for six patients treated at UPTD (section 3.2). Secondly, for patients with suspected radiation-induced toxicity after PBS proton therapy, the framework provides treatment plan information beyond absorbed dose to further investigate

Table 3.1: Proton therapy system specifications for pencil beam scanning (PBS) treatment mode at University Proton Therapy Dresden (UPTD) and The West German Proton Therapy Centre Essen (WPE). Adapted from Bäumer et al. (2017).

Technical parameter	UPTD	WPE
Proton therapy system	ProteusPlus	ProteusPlus
Cyclotron type	Isochronous	Isochronous
Nozzle type	Universal	Dedicated
Minimum/maximum proton energy in MeV	100.0, 227.0	70.0, 227.0
Isocentre spot FWHM in mm at 100 MeV, 227 MeV	8.9, 19.0	6.6, 13.4
Treatment planning system, clinical and research	RayStation	RayStation

FWHM: Full width at half maximum.

the role of RBE variability. This will be presented for one exemplary patient case treated at UPTD in section 3.3. Thirdly, the assessment of the potential benefit of using three over two treatment fields to mitigate RBE induced dose burden to healthy tissue at the end of proton range is presented for nine brain tumour patients treated at WPE (section 3.4). All individual studies in this chapter were approved by the respective local ethics committee or covered by the ethics approval of prospective registry trials (EK365072019, DRKS00004384, DRKS00005363). Parts of this chapter were presented at conferences (Hahn et al., 2019; Hahn et al., 2021b) and have been published (Hahn et al., 2020).

3.1 LET and RBE recalculations of proton treatment plans with RayStation

In this thesis, the TPS RayStation was used for PBS treatment plan optimisation, final dose calculation and LET recalculations. Both treatment plan optimisation and calculation were done using the MC method throughout this manuscript. Both LET and variable RBE recalculations of PBS treatment plans were embedded in the respective research version of RayStation by using the MC scoring extensions of the dose engine. The scoring extensions were available since research version 6. Over the course of this thesis, the research version 6 (v5.99.50) and version 9 (v8.99.30) were used.

3.1.1 Monte Carlo dose engine

The MC dose engine implemented in RayStation transports particles in geometries with a rectilinear grid of voxels. The transport grid coincides with the dose reporting grid.

Each voxel is characterised by its mass density, elemental composition and mean excitation energy. The RayStation MC code employs a specific material assignment approach with a set of predefined core materials with known elemental composition and mean excitation energy (RaySearch Laboratories AB, 2016). First, voxelwise HUs from CT scans are converted in mass density with a scanner-specific calibration curve. Second, the voxel mass density is used to assign material properties to this voxel by interpolating between two of the predefined core materials with similar mass density.

The RayStation MC code transports primary and secondary protons with a class II transport method. Energy loss and nuclear absorption are computed for every voxel traversal due to their immediate impact on the protons kinetic energy and the voxel material composition. Based on the Bethe-Bloch equation without shell and density correction, the ionisation energy loss is calculated for each voxel traversal by integrating the stopping power in the local density and medium. Non-elastic nuclear interactions and elastic scattering of protons on nuclei are included (RaySearch Laboratories AB, 2016). The maximum step length for ionisation energy loss integration and nuclear absorption is limited to an water-equivalent path length of 4 mm.

In contrast, multiple Coulomb scattering (MCS) and energy straggling are not considered voxelwise but using the random hinge method (Fernández-Varea et al., 1993). Each hinge consists of two straight legs, connected at the hinge point, and each leg may extend over multiple voxels. The deflection angle due to MCS is drawn from a probability distribution described by the Goudsmit-Saunderson theory (Goudsmit & Saunderson, 1940a, 1940b). For each hinge, the proton energy spread due to energy loss straggling is modelled as a Gaussian distribution. The proton is then transported in a sequence of random hinges until it reaches the default energy threshold of 30.7 MeV corresponding to residual water-equivalent proton range of 1 cm. Below this threshold, MCS and energy loss straggling are neglected for protons. Deuteron and alpha particle transport is modelled by the continuous slowing down approximation, where nuclear absorption, MCS and energy straggling are neglected. Protons, deuterons and alpha particles are tracked until their residual energy reaches 1 MeV per nucleon and then absorbed locally. Heavier secondaries, neutrons and photons were not transported but absorbed locally. δ-electron production is neglected in dose calculation, i.e. they are absorbed locally, since the maximum electron range in water produced by a 200 MeV proton beam is typically within commonly used voxelsizes of 2 mm (RaySearch Laboratories AB, 2016).

The MC dose engine reports absorbed dose to water by scaling the deposited energy with the water to local medium dependent mass stopping power ratio. The statistical error per voxel in dose calculation is estimated as the dose variance of the dose per voxel over twelve independent batches. A single statistical error is then reported per beam as the average one standard deviation over all voxels receiving dose of 50 % of the beams maximum dose.

3.1.2 Monte Carlo scoring extensions

The particle transport in MC simulations is based on macroscopic interaction cross sections, i.e. interaction probabilities, per unit distance (Paganetti, 2011a). Therefore, MC dose engines can be extended to provide voxelwise averaged LET distributions (Giovannini et al., 2016). In this thesis, dedicated research versions of RayStation (v5.99.50, v8.99.30) were used to provide extra scoring output of the MC dose engine through their implemented MC scoring extensions.

The LET per particle is calculated as the mean energy loss per unit path length for the specific simulation step s_n, using the electronic stopping power S_{el} weighted with the electronic energy loss ϵ_{s_n} (Ödén, 2019). The voxelwise $\mathrm{LET_d}$ is derived by summing the product of S_{el} and electronic energy loss for all particles with atomic charge z traversing voxel i divided by their sum of electronic energy loss ϵ_{s_n} and the voxel density ρ:

$$\mathrm{LET}_{\mathrm{d,i}} = \frac{\rho_{\mathrm{water}}}{\rho_{\mathrm{material},i}} \frac{\sum_{z}^{Z} \sum_{n=1}^{N} w_{n,z} \sum_{s_n=1}^{S_n} \epsilon_{s_n} S_{\mathrm{el}}(E_{s_n}, z, i)}{\sum_{z}^{Z} \sum_{n=1}^{N} w_{n,z} \sum_{s_n=1}^{S_n} \epsilon_{s_n}} \quad , \tag{3.1}$$

where N is the total number of events in voxel i, S_n is the number of steps performed to transport the particle with atomic charge Z through voxel i for event n, $w_{n,z}$ is the statistical weight of the particle with charge z, $S_{\mathrm{el}}(E_{s_n}, z, i)$ and ϵ_{s_n} are the electronic stopping power S_{el} for particle type z with energy E_{s_n} in voxel i and the electronic energy loss at simulation step s_n for event n, respectively.

Thus, the voxelwise $\mathrm{LET_d}$ is reported as unrestricted dose-averaged LET to material normalised to unit density tissue in this thesis. The applied $\mathrm{LET_d}$ calculation method corresponds to method C from Cortés-Giraldo and Carabe (2015), which was found to be

independent from the voxelsize and the energy cut for secondary electrons.

For ions with energies of 16 – 250 AMeV where LET changes moderately with kinetic energy (Figure 2.2), the mean particle energy between pre- and post-step points was used to determine S_{el} in the voxel material at simulation step s_n. Below these energies, which corresponds to a maximum proton range of about 3 mm in water, a dedicated track-end stepper sets in to account for the rapid change of S_{el} over a voxel at the end of proton range. S_{el} is sampled at up to 90 logarithmic energy loss steps down to 0.02 MeV and derived analytically for lower energies until the ion transport is terminated.

Variable RBE and thus absorbed dose weighted with a variable RBE (D_{RBE}) were determined voxelwise by considering physical parameters from the patients treatment plan and biological information from the patient anatomy, respectively. Voxelwise RBE calculations were implemented with multiple LET-driven phenomenological variable RBE models, that differ in their model parameters (Table 2.1).

Various LET and RBE scoring options can be selected in RayStation by formulating an user control string. Exemplary scoring option strings for LET scoring and LET-driven, $\alpha/\beta_{\mathrm{x}}$ dependent RBE-models are summarised in Table 3.2. For simplicity, $\alpha/\beta_{\mathrm{x}}$ will be abbreviated with α/β from here on.

Multiple quantities can be recalculated at once by concatenating the strings of all desired option strings without blank spaces. After writing the scoring options to the beam set comment, the final proton dose must be (re-)computed with the MC dose engine to produce all selected auxiliary data and save them to binary files outside of RayStation. Each auxiliary file corresponds to one three-dimensional LET or RBE distribution scored on the dose grid and can then be manually imported and displayed in RayStation. The unrestricted $\mathrm{LET_d}$ for protons in material normalised to unit density water is used as input parameter for all featured RBE models. Additional RBE models were availbale that are independent of α/β (Jones, 2015; Wilkens & Oelfke, 2003), include higher than linear LET dependence (Peeler et al., 2016; Rørvik et al., 2017) or both (Chen & Ahmad, 2012). Mechanistic RBE models (Carlson et al., 2008; Stewart et al., 2015) were also available but not used in this thesis.

3.1.3 Graphical user interface

Over the course of this thesis, Uber (2018) and Sobolewski (2021) designed a graphical user interface (GUI) to simplify and speed up the recalculations. The GUI was implemented

Table 3.2: Scoring option strings in the RayStation research version to calculate distributions of linear energy transfer (LET) and variable relative biological effectiveness (RBE) for models including tissue radiosensitivity α/β. The string must be formatted as `/MCOPT=optionstringwithoutspaces` and can be set in the edit plan dialog in RayStation.

Scoring option string `/MCOPT=...`	**Description**
LET options	
`F2`	LET_d for all protons
`F21`	LET_d per ion type for protons, deuterons and alphas
`F22(doselevel)[cGy]`	LET_d for all protons in voxels above fixed doses
`F23(doselevel)[cGy]`	LET_d for all protons in voxels above fixed doses
`F3`	LET_t for all protons
`F31`	LET_t per ion type for protons, deuterons and alphas
RBE options	
`K5`	RBE(-weighted dose) by Wedenberg et al. (2013)
`K6`	RBE(-weighted dose) by Carabe et al. (2012)
`K9`	RBE(-weighted dose) by McNamara et al. (2015)
Set ROI-specific $(\alpha/\beta)_x$	
`P1(alphaX, betaX)`	set $(\alpha/\beta)_x$ in Gy inside external contour
`P1j(alphaX,betaX, ROIname)`	overwrite $(\alpha/\beta)_x$ in specified ROI name for $j = 1, .., 3$

LET_d: Dose-averaged linear energy transfer. LET_t: Track-averaged linear energy transfer. ROI: Region of interest.

at WPE and UPTD in RayStation research version 9, running on the central processing unit. Clinical treatment plans must be exported to the research version to use the scoring extensions, as they are not embedded in the clinical version. For the recalculation, all selected treatment plans are copied to avoid changes to the original clinical treatment plan, the MU of every beam are divided by 1.1 to derive the absorbed dose. Selected scoring option strings are written to the beam set comment, the beam set dose is invalidated via script to allow for final dose calculation with the MC dose engine, the final dose calculation is performed scoring the selected LET and RBE options in parallel, the externally saved binary file is written to DICOM format and imported in RayStation via script.

Default scoring options

The GUI was tailored to two different user-groups: clinicians and researchers. Clinical personnel requires time-efficient and unambiguous recalculations of treatment plans. For this purpose, the default window does not require a user-defined specification on which averaged LET definition or RBE model to consider (Figure 3.1A). Instead, the default LET definition and variable RBE model were discussed and agreed on with the clinical staff before

implementation. Default LET and RBE options with adaptable α/β for tumour and normal tissue, respectively, are then recalculated on the dose grid and with the MC uncertainty specified in the original clinical treatment plan. In consultation with the clinical personnel, the RBE model from Wedenberg et al. (2013) was implemented as default model to allow for a straightforward variable RBE recalculation of clinical treatment plans at UPTD and WPE. It fulfils the postulated functional dependencies that RBE should increase with increasing LET and decreasing α/β (Paganetti, 2014) and was built on multiple cell-lines covering the clinically relevant α/β range of 2 – 20 Gy (Paganetti, 2022). Furthermore, its model parameters were found to be not significantly different when fitted to an enlarged *in-vitro* dataset (Tian et al., 2022) and its variable RBE-weighted dose predictions lay around the average when compared to other RBE models (Rørvik et al., 2018). Additionally, the RBE model from Wedenberg et al. (2013) was recently found to be consistent with a clinically derived RBE model in brain tissue (Bahn et al., 2020). This matches the anatomical site for which LET and RBE recalculations were most frequently considered at UPTD and WPE, in line with practice at European proton therapy centres (Heuchel et al., 2022).

Firstly, the medical physicist uses the default graphical user interface for LET and RBE recalculations (Figure 3.1A). This is straightforward by setting α/β for the tumour volume and normal tissue and all healthy tissue are assigned the same α/β in this workflow. The script automatically calls the scoring extensions to calculate the proton dose-averaged linear energy transfer (LET_d) and variable RBE-weighted dose (D_RBE) using the RBE model from Wedenberg et al. (2013), i.e. `/MCOPT=F2K5P1(2,1)P11(10,1,CTVlow)`. LET_d and D_RBE are provided in DICOM format and can be displayed as additional treatment plan information, after export from the research version, to the clinical treatment plan in the clinical TPS.

Advanced scoring settings

Secondly, advanced settings are available in the GUI to allow for the isolation and systematic analysis of influencing variables in RBE predictions in mono-centric studies (Figure 3.1B). This includes the model itself, the choice of α/β and the influence of the averaging technique and secondary particles considered in LET scoring. In the advanced settings, the user may set multiple α/β values to different ROIs, select multiple RBE-models from the literature (Table 2.1) and different LET definitions, whereas the latter was not added to the GUI. These settings allow to score quantities that are used as input-parameters in other

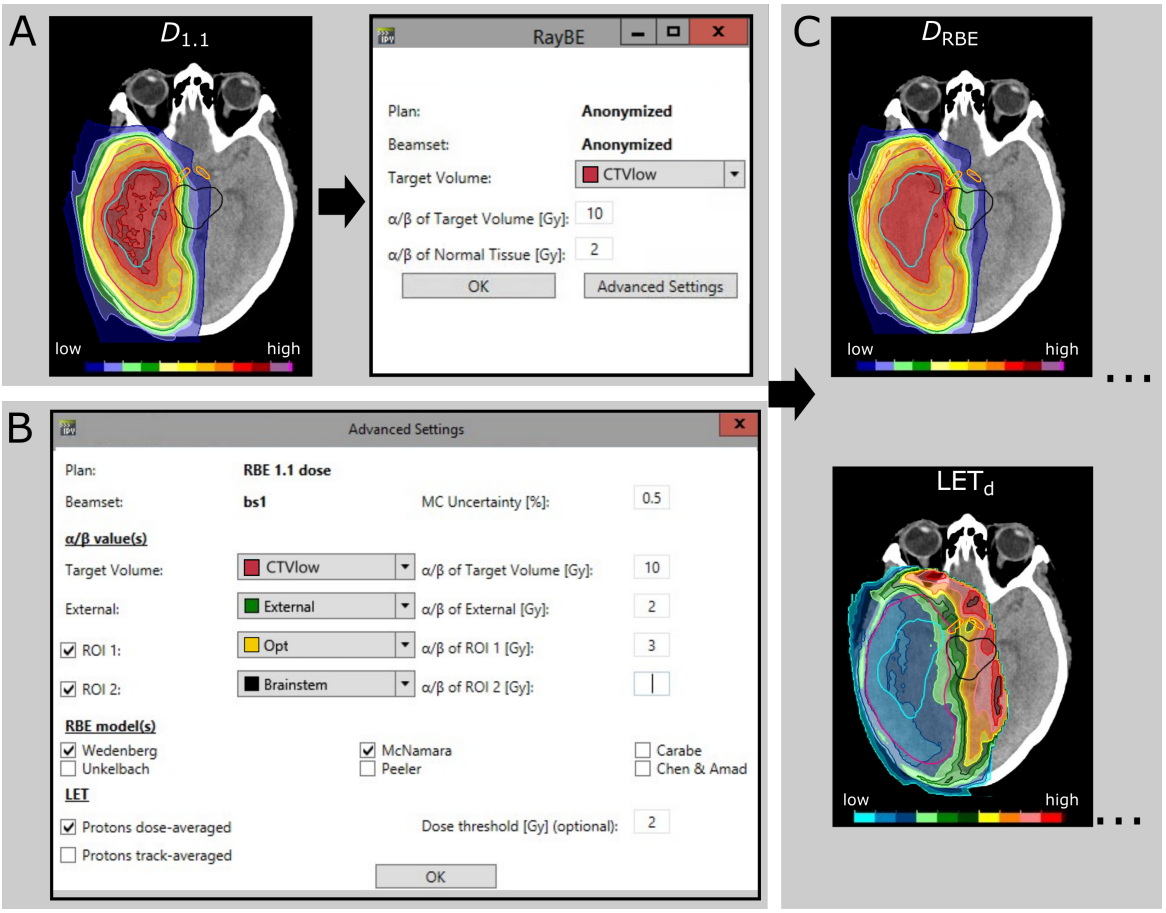

Figure 3.1: Visualisation of the framework and workflow for recalculation of proton pencil beam scanning treatment plans with the research version of RayStation. **A** The graphical user interface (GUI) with the default options on which relative biological effectiveness (RBE) model to score. **B** The advanced setting GUI that allows to further specify the RBE models and its input tissue radiosensitivities. **C** The scored quantities are displayed in the treatment planning system. Abbreviations: absorbed dose weighted with RBE of 1.1 ($D_{1.1}$), absorbed dose weighted with a variable RBE (D_{RBE}), dose-averaged linear energy transfer (LET_d).

RBE and NTCP models. In addition, physical quantities can be stored in this way to later investigate their correlation with radiation-induced toxicity in patients to build and test new models.

3.2 LET assessment and the role of range uncertainties

The MC scoring extensions were used to quantify LET distributions in robust dose-optimised PBS proton treatment plans for different anatomical sites. Image and contour data sets were retrieved for two brain tumour cases, two head and neck tumour cases

Table 3.3: Patient and treatment planning information to quantify the role of range uncertainties on dose-averaged linear energy transfer (LET_d) and relative biological effectiveness (RBE). Simultaneous integrated boost (SIB) was used to deliver the prescription doses to the clinical target volumes (CTV) with two dose levels.

Case	Diagnosis	Prescribed dose in Gy(RBE)		Fx	Treatment field angles (gantry, couch) in °		
		CTV_{high}	CTV_{low}		Field 1	Field 2	Field 3
1	Brain	60	50	30	210, 10	310, 10	–
2	Brain	60	50	30	180, 0	290, 15	–
3	H & N	70	57	33	0, 0	60, 330	300,30
4	H & N	70	57	33	110, 345	240, 20	350,0
5	Prostate	60	48	20	90, 0	270, 0	–
6	Prostate	60	48	20	90, 0	270, 0	–

Fx: Number of fractions. H & N: Head and neck.

and two prostate tumour cases, respectively. The patients from UPTD were randomly selected for each entity. New robust-dose optimised treatment plans were created to allow for assessing the role of intensity modulation, i.e. SFO and MFO, on the LET and RBE distributions. Additionally the role of range uncertainties on LET and RBE distributions was quantified.

3.2.1 Patient cohort and treatment plan creation

For retrospective treatment planning, patients with head and neck cancer received a 120 kVp SECT scan, which was converted into SPR based on the clinical HLUT (Wohlfahrt et al., 2017). For brain and prostate cancer patients, an 80 kVp/140 kVp DECT scan was acquired and SPR datasets were generated with the DirectSPR approach (Wohlfahrt et al., 2018). The respective SPR datasets were imported and used in the TPS RayStation (v5.99.50) using a refined HLUT (Wohlfahrt et al., 2020). Patient and treatment planning information for all six patients are summarised in Table 3.3.

The clinical contours and beam model from the UPTD were used for treatment planning in PBS delivery mode and with the SIB technique. For each patient, two robust optimised treatment plans were generated using SFO and MFO, respectively, since the steepness of the dose and LET_d gradients may be influenced by the degree of intensity modulation. For each patient, gantry and couch angle, dose prescription and fractionation were identical for the respective SFO and MFO plan (Table 3.3). Robust optimisation considered 21 uncertainty scenarios consisting of combinations of range errors of 3.5 % + 2 mm and a setup

Table 3.4: Clinically used dose-volume histogram parameters at the University Proton Therapy Dresden (UPTD).

Organ at risk	Parameter	Clinical goal	Reference
Head, H & N[1]			
Brainstem	$D_{\max}$	54 Gy(RBE)	Mayo et al. (2010b)
Brainstem, surface	$V_{60\mathrm{Gy(RBE)}}$	1 cm^3	Lambrecht et al. (2018)
Optical nerves, chiasm	$D_{\max}$	54 Gy(RBE)	Mayo et al. (2010a)
Lenses	$D_{\max}$	6 Gy(RBE)	
Innear ear	D_{mean}	45 – 60 Gy(RBE)	Jereczek-Fossa et al. (2002)
Remaining brain	D_{mean}	40 Gy(RBE)	Lawrence et al. (2010)
Lacrimal glands	$D_{\max}$	40 – 45 Gy(RBE)	Gordon et al. (1995)
Parotid glands	D_{median}	26 Gy(RBE)	
Spinal cord	$D_{\max}$	45 – 60 Gy(RBE)	
Prostate[2]			
Rectum	$V_{60\,\mathrm{Gy(RBE)}}$	3 %	Dearnaley et al. (2016)
	$V_{57\,\mathrm{Gy(RBE)}}$	15 %	
	$V_{40.8\,\mathrm{Gy(RBE)}}$	60 %	
Bladder	$V_{48.6\,\mathrm{Gy(RBE)}}$	25 %	Dearnaley et al. (2016)
	$V_{40.8\,\mathrm{Gy(RBE)}}$	50 %	
Bowel	$V_{40.8\,\mathrm{Gy(RBE)}}$	17 cm^3	Dearnaley et al. (2016)

D: Dose. H & N: Head and neck. V: Volume. [1] for normalfractionated schedules.
[2] for hypofractionated schedules.

uncertainty of 2 mm (3 mm) for brain and prostate (head and neck) cases. Robust objectives were set to target volumes, optical apparatus, brainstem, spinal cord, parotid glands, rectum and bladder and robust optimisation used the minimax approach (Fredriksson et al., 2011). Treatment plans were optimised to comply with the institution-specific clinical goals for OAR sparing (Table 3.4) and kept doses below the threshold doses as low as reasonably achievable (Bentzen et al., 2010). A statistical MC uncertainty of 0.3 % was used for the final dose calculation. For all patients, each SFO and MFO treatment plan was individually approved by two experienced radiation oncologists according to in-house clinical guidelines.

3.2.2 Simulation of range deviations

Range deviations covering the typical range uncertainty interval of ±3.5 % (Taasti et al., 2018) were simulated by voxelwise SPR scaling. Only the range within the patient was considered as uncertain since the water equivalent thickness of the range shifter was known from measurements (7.38 cm). The SPR scaling $\mathrm{SPR}_{\mathrm{scaled}}$ required to obtain the desired range shift RS of ±3.5 % relative to the nominal treatment plan with $\mathrm{SPR}_{\mathrm{nom}}$ was calculated

as:

$$\mathrm{SPR}_{\mathrm{scaled}} = \frac{\mathrm{SPR}_{\mathrm{nom}}}{1 + \mathrm{RS}} \quad . \tag{3.2}$$

A downscaling of SPR results in longer proton range, which will be from here on referred to as overshoot. Shorter ranges, achieved by upscaling the SPR, will be referred to as undershoot. The nominal scenario did not undergo SPR scaling and is thus the nominal range shown on the planning SPR map. The scaling procedure was validated with simulations of monoenergetic proton beams in a homogeneous water phantom using scaled SPR-maps for different RS scenarios and found to be within the voxelsize of 1 mm. The same gantry and couch angles, isocentre position, energy layers, spot positions and spot weights as for the approved treatment plan on the nominal scenario (SFO, MFO) were used to recalculate the dose and $\mathrm{LET_d}$ distributions on the respective SPR maps for each range scenario and optimisation strategy. In total, dose and $\mathrm{LET_d}$ distributions of 36 treatment plans were simulated and evaluated and cover three range scenarios per patient with two optimisation strategies (SFO, MFO) per scenario and a total of six patients.

3.2.3 Treatment plan recalculation settings

Voxelwise $\mathrm{LET_d}$ scoring included primary and secondary protons, alpha particles and deuterons. This $\mathrm{LET_d}$ definition was used as input parameter for the RBE model from Wedenberg et al. (2013) with entity-specific α/β values for tumours of the brain (Qi et al., 2006), head and neck (Stuschke & Thames, 1999) and prostate (Dasu & Toma-Dasu, 2012). To assess the range of RBE values in radioresistant and radiosensitive tumours for a given set of doses and $\mathrm{LET_d}$ values and to investigate the impact of α/β on RBE, generic α/β values of 2 Gy and 10 Gy were additionally used (Giovannini et al., 2016; Grün et al., 2013). This allows for comparing the impact of uncertainties in α/β on RBE with the range uncertainty induced $\mathrm{LET_d}$ variability in the target volume. For RBE estimations in normal tissues, a generic α/β of 2 Gy was considered in all structures. To evaluate the impact of $\mathrm{LET_d}$ and range uncertainties on a voxel-by-voxel basis and for a clinical endpoint in brain tumour patients, a radiation response model for late radiation-induced brain injury was applied (Eulitz et al., 2019b). The logistic regression response model was built on image changes after proton radiotherapy constituting radiation necrosis and predicts the voxel-wise probability P_{IC} to develop an image change as a function of absorbed dose and

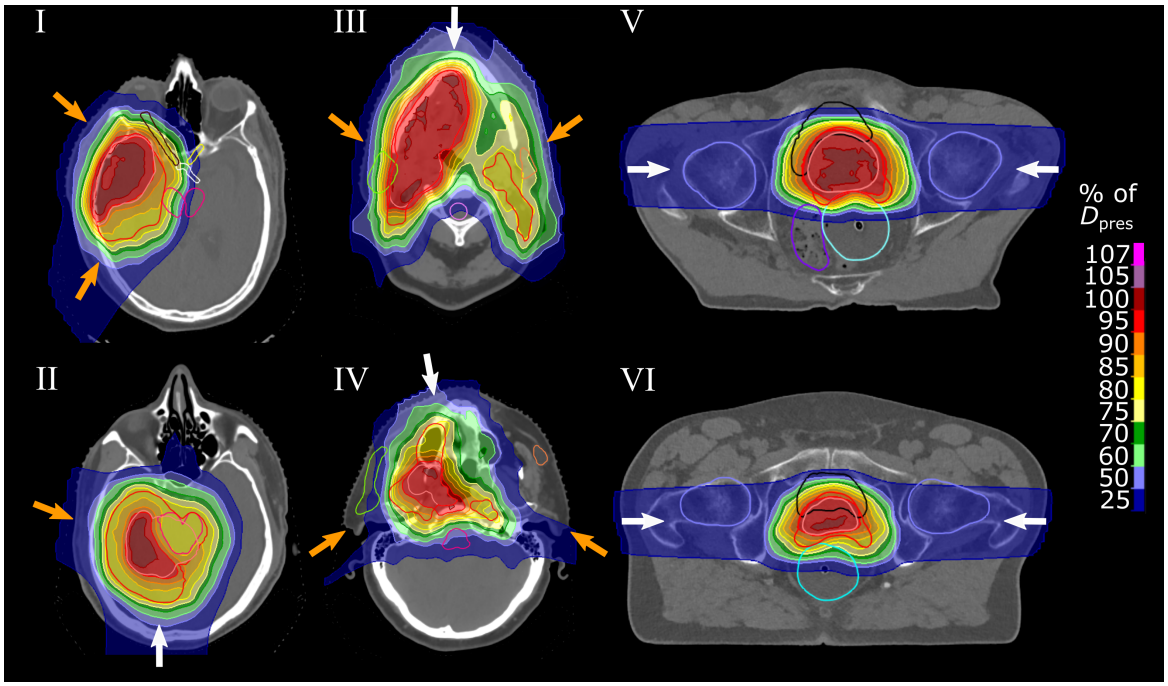

Figure 3.2: Axial dose distributions of nominal multi-field optimised treatment plans for patients with primary tumour of the brain (I, II), head and neck (III, IV) or prostate (V, VI). Coplanar (white) and non-coplanar (orange) treatment field directions are shown as arrows. Clinical target volumes (CTV) for both dose levels (CTV_{low}: dark red, CTV_{high}: light red) as well as organs at risk (Brainstem: magenta, Chiasm: white, Optical nerves: yellow (left) and brown (right), Parotid glands: orange (left) and light green (right), Rectum: light blue, Bladder: black, Femoral heads: violet) are displayed. Isodose lines are displayed relative to their prescribed dose D_{pres}. Adapted from Hahn et al. (2020).

absorbed dose times LET_d with model parameters β_0, β_1 and β_2 of –8.6808, 0.0083 Gy^{-1} and 0.0211 µm Gy^{-1} keV^{-1}, respectively (Eulitz et al., 2019b).

3.2.4 Resulting impact of range deviations

All nominal MFO and SFO treatment plans fulfilled the clinical dose-volume goals at UPTD and were thus clinically approved. MFO featured an increased normal tissue dose sparing as well as inhomogeneous single field dose distributions compared to SFO. Nominal MFO dose and LET_d distributions for all patients are presented in Figures 3.2 and 3.4.

The optimisation strategy had a negligible impact on LET_d distributions in CTVs and OARs. Voxelwise differences in the CTVs between SFO and MFO were on average (standard deviation) 0.1 ± 0.1 keV µm^{-1}. Likewise, the 95 % confidence intervals of LET_d distributions in the CTVs overlapped between SFO and MFO (Figure 3.3). The degree of intensity modulation also had a minor impact on LET_d distributions in OARs as it neither substan-

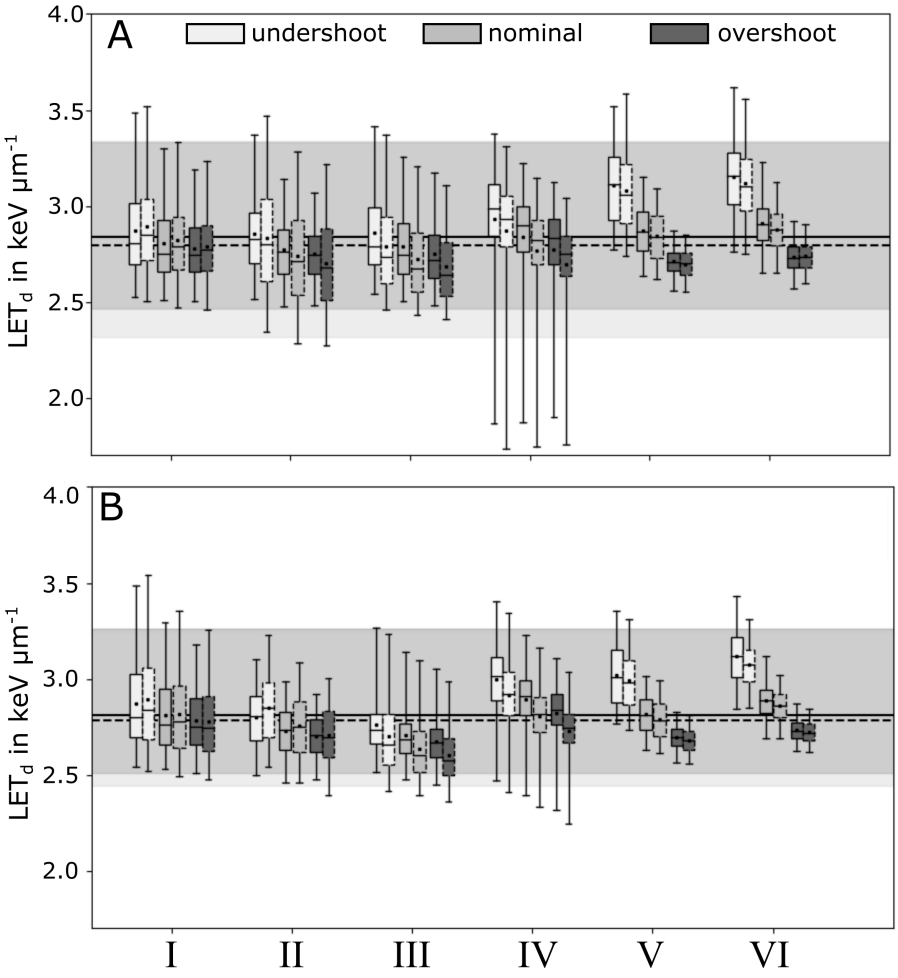

Figure 3.3: Dose-averaged linear energy transfer (LET_d) distributions in the **A** clinical target volume (CTV_{low}) and **B** CTV boost volume (CTV_{high}) for all three range scenarios and each patient (I-VI) using single-field (SFO, dashed lines) or multi-field optimisation (MFO, solid lines). Horizontal lines display the arithmetic mean of LET_d calculated over all patients with 95% confidence interval for SFO (light gray area) and MFO (dark gray area). Adapted from Hahn et al. (2020).

tially altered the absolute LET_d values and their value range within an OAR nor influenced the systematic effect of range deviations in OARs. The impact of optimisation strategy was highest, though still small, in OARs with small volumes or those located in the low-dose region. Thus, the following results are presented only for MFO treatment plans if not stated otherwise.

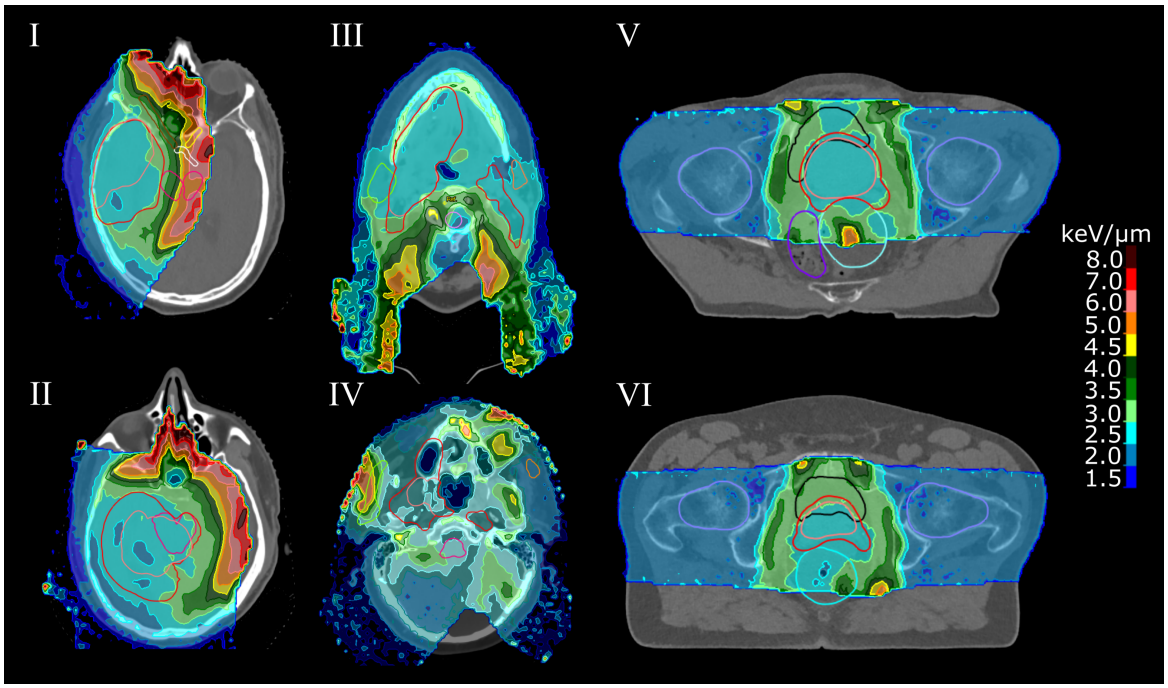

Figure 3.4: Dose-averaged linear energy transfer (LET_d) distributions for voxels with an absorbed dose above 1 Gy of nominal multi-field optimised treatment plans for patients with primary tumour of the brain (I, II), head and neck (III, IV) or prostate (V, VI). Clinical target volumes (CTV) for both dose levels (CTV_{low}: dark red, CTV_{high}: light red) as well as organs at risk (Brainstem: magenta, Chiasm: white, Optical nerves: yellow (left) and brown (right), Parotid glands: orange (left) and light green (right), Rectum: light blue, Bladder: black, Femoral heads: violet) are displayed. Adapted from Hahn et al. (2020).

Quantification in clinical target volumes

LET_d distributions in the CTVs were homogeneous and robust against range deviations (Figures 3.3, 3.4). LET_d homogeneity in the CTVs was characterised by the similarity of near-minimum and near-maximum LET_d which did not differ much from the average LET_d therein. LET_d values in the CTVs were comparable for all entities and the overall 95 % confidence interval of both optimisation strategies covered LET_d values from 2.3 keV µm^{-1} to 3.3 keV µm^{-1}. For the CTVs, absolute LET_d values and LET_d homogeneity increased for smaller targets in beam direction, i.e. beam modulation width, and were thus highest for the prostate cases. For all entities, a range undershoot resulted in a systematic increase in LET_d inhomogeneity within the CTVs, while an overshoot had the opposite effect. The maximum differences in arithmetic mean of LET_d in the CTV due to range deviations were found for prostate cases with differences smaller than 0.5 keV µm^{-1} (Figure 3.3).

The observed 95 % confidence interval of 2.3 – 3.3 keV µm^{-1} in all CTVs translated, as-

Table 3.5: Variation in relative biological effectiveness (RBE) estimates in the clinical target volume (CTV) due to variations in dose-averaged linear energy transfer (LET_d) induced by range deviations. For each tumour entity, the 95% confidence interval (CI) of the LET_d distributions and a homogeneous target dose equivalent to the prescribed average absorbed dose and entity specific α/β were considered. Additionally, for all patients, an absorbed dose per fraction of 1.82 Gy, representative for normofractionation, and generic α/β of either 2 or 10 Gy were assumed to estimate RBE intervals. ΔLET_d and ΔRBE represent the width of CIs.

Entity (α/β)	**Target volume**	**Dose** in Gy	**LET_d** in keV µm^{-1}		**RBE** in a.u.	
			ΔLET_d	95 % CI	ΔRBE	95 % CI
Brain (10 Gy)	CTV_{low}	1.52	1.1	2.3 – 3.4	0.03	1.08 – 1.11
	CTV_{high}	1.82	0.8	2.5 – 3.3	0.02	1.08 – 1.10
H & N (10.5 Gy)	CTV_{low}	1.57	1.2	2.1 – 3.3	0.04	1.06 – 1.10
	CTV_{high}	1.93	0.8	2.4 – 3.2	0.03	1.07 – 1.10
Prostate (1.5 Gy)	CTV_{low}	2.18	0.8	2.6 – 3.4	0.05	1.18 – 1.23
	CTV_{high}	2.73	0.7	2.6 – 3.3	0.04	1.15 – 1.19
All entities (2 Gy)	CTV_{low}	1.82	1.0	2.3 – 3.3	0.07	1.17 – 1.24
	CTV_{high}	1.82	0.9	2.4 – 3.3	0.05	1.18 – 1.23
All entities (10 Gy)	CTV_{low}	1.82	1.0	2.3 – 3.3	0.03	1.07 – 1.10
	CTV_{high}	1.82	0.9	2.4 – 3.3	0.02	1.08 – 1.10

H & N: Head and neck.

suming a generic α/β of 2 Gy (or 10 Gy) and a constant absorbed dose per fraction, into a modelled variable RBE range of 1.17 – 1.24 (or 1.07 – 1.10) (Table 3.5). Using the entity-specific α/β values in the target volumes, range deviations induced LET_d variations resulted in RBE variations of less than 0.05 for all considered dose levels and entities. For a given dose level and LET_d, uncertainties in α/β translated into RBE variations exceeding 0.10 in the CTVs (Table 3.5).

Quantification in organs at risk

LET_d distributions in the OARs were inhomogeneous (Figure 3.5) and showed higher LET_d values compared to the CTVs (Figure 3.3). LET_d values in OARs were particularly elevated when the OAR was located in the lateral or distal penumbra of at least one treatment field. Accordingly, the highest LET_d values were found in the brain cases where both protons from both treatment fields stopped in vicinity of at least one OAR. This field arrangement resulted in LET_d distributions exceeding 7 keV µm^{-1} in healthy brain tissue, the brainstem and the optical apparatus. Similarly, elevated LET_d values of 4.5 keV µm^{-1} were observed

within the rectum and bladder of the prostate cases where both treatment fields were placed orthogonally to these OARs. LET_d values exceeded 4.0 keV µm^{-1} in the healthy brain of both head and neck cases. Similar LET_d values were in the parotid glands, left optic nerve and brainstem of patient IV, which was less systematical as in the brain and prostate cases. Highest LET_d values occurred in voxels of negligible dose in all entities, i.e. in the left optic nerve of patient II, the healthy brain of patient IV and the bulbus of patient V, respectively (Figure 3.5).

Range deviations had a greater impact on OARs than CTVs. Range deviations systematically altered LET_d distributions in OARs when each individual treatment field of the treatment plan ended laterally or distally to the respective OARs. Then, within SFO and MFO, median LET_d increased with shorter beam ranges. This was observed in the right optic nerve and chiasm for patient I, the brainstem of patient II as well as the rectum, bladder and bulbus for patients V and VI, respectively (Figure 3.5). Range deviations caused differences in median LET_d of up to 3.0 keV µm^{-1} and were highest within the brain cases, particularly for the right optic nerve of patient II. Additionally for the brain cases, the heterogeneity of LET_d distributions within the respective OAR increased since the sharp distal LET_d gradient was essentially pulled back into the OAR by range deviations. The highest 95 % confidence interval was found with 2.5 – 7.4 keV µm^{-1} in both brain tumour cases. Overall, the impact of range deviations on LET_d was less conclusive in head and neck cases where three treatment fields were used and the treatment fields passed through more anatomical heterogeneities.

The observed LET_d distributions in OARs for brain patients translated in highly inhomogeneous RBE distributions with a higher sensitivity to range deviations compared to the CTV (Figure 3.6). In brain tumour cases, the RBE in all investigated OARs exceeded 1.27 and the upper limit of the RBE 95 % confidence interval was larger than 2.0 in all OARs, except for the right optic nerve in brain case I and the chiasm in brain case II (Figure 3.6).

The highest probability for image changes was observed in areas where the lateral and distal edges of both treatment fields coincided. This is shown exemplary in Figure 3.7, where the highest voxelwise risk was predicted in healthy brain tissue receiving high absorbed dose and elevated LET_d close to the optical apparatus and the brainstem (Figure 3.7). Although the absolute risk depended on the range scenario investigated, the highest probability for image changes was consistently predicted at the end of beam range in all range scenarios, which remained below 2.1 % for both brain tumour patients.

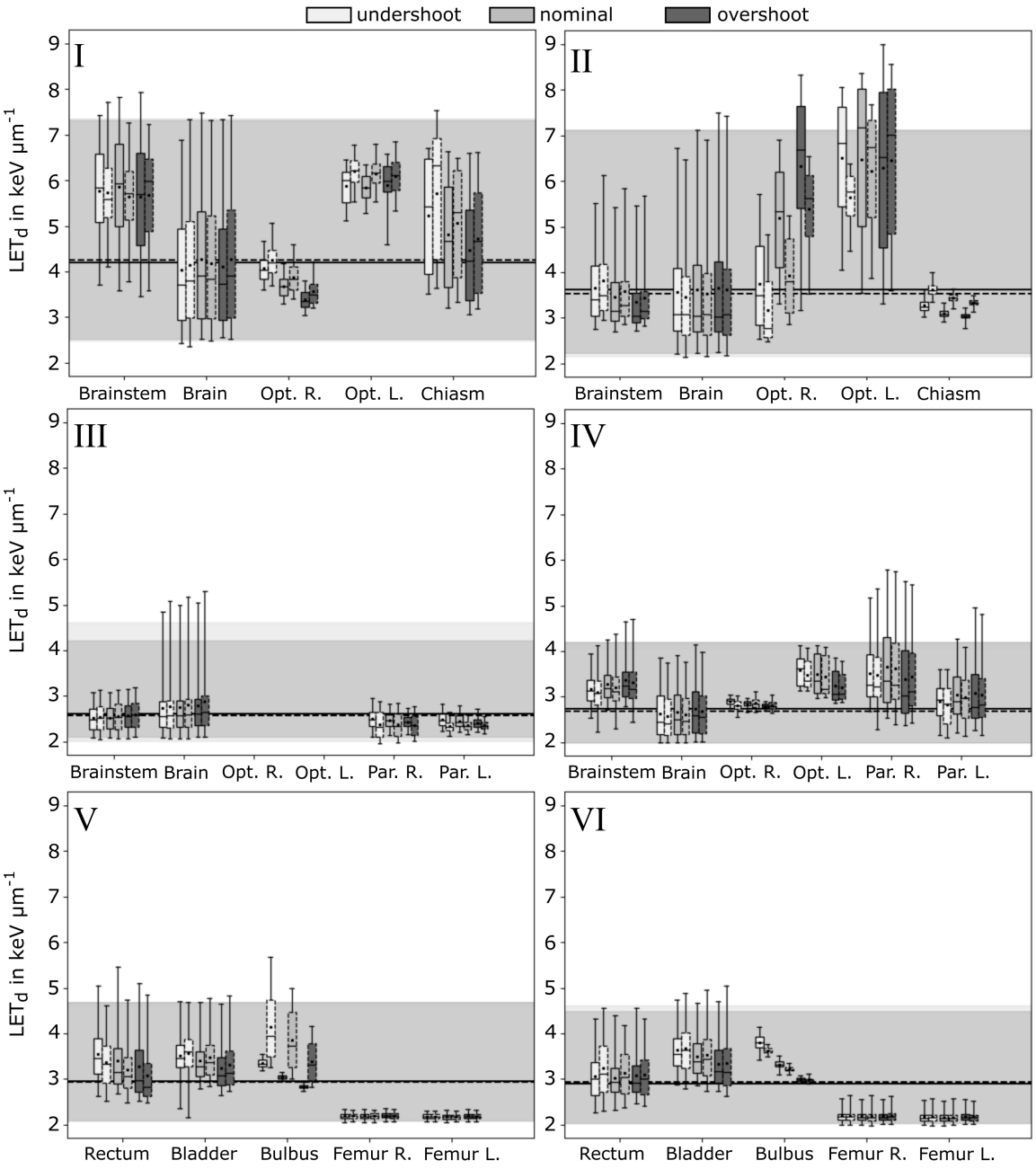

Figure 3.5: Dose-averaged linear energy transfer (LET_d) distributions in the organs at risk (OAR) for each patient (I-VI) using single-field (SFO, dashed lines) or multi-field optimisation (MFO, solid lines). Horizontal lines display the arithmetic mean of LET_d calculated over all displayed OARs of a patient with 95% confidence interval for SFO (light gray area) and MFO (dark gray). Abbreviations: Opt.: Optical Nerve, Par.: Parotid gland, R.: Right, L.: Left. Adapted from Hahn et al. (2020).

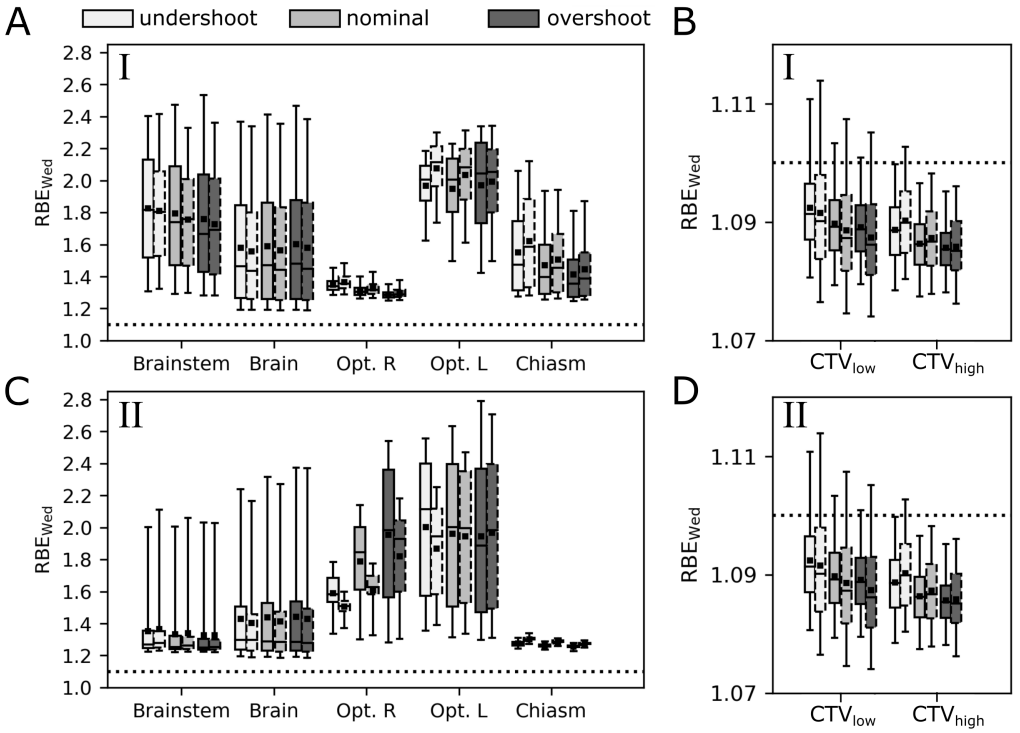

Figure 3.6: Relative biological effectiveness (RBE) distributions **A, C** in organs at risk (left column, α/β of 2 Gy) and **B, D** clinical target volumes (CTV, right column, α/β of 10 Gy) of brain-tumour patients (I) and (II) using the Wedenberg (Wed) RBE model. Multi-field optimisation (MFO) is presented in solid lines, single-field optimisation (SFO) is shown in dashed lines for all range scenarios. All three range scenarios (undershoot, nominal, overshoot) are displayed. Horizontal dotted lines display the clinically used constant RBE of 1.1. Note the different y-axis. Abbreviations: Opt.: Optical Nerve, R.: Right, L.: Left. Adapted from Hahn et al. (2020).

3.3 Patient recalculations in case of side effects

At UPTD, recalculations of clinically delivered treatment plans are performed to further investigate the role of RBE variability in radiation-induced toxicity in addition to other clinical factors. Treatment plans are recalculated on a case by case basis and primarily for brain tumour patients.

Signal abnormalities in the brain on patient follow-up magnetic resonance imaging (MRI) are contoured by experienced radiation oncologists and neuro-radiologists. Patient treatment plan recalculations are carried out by medical physicists. To provide this data with the highest accuracy available, the developed LET recalculation framework was coupled with available methodologies for accurate range prediction and image registration. This is particularly important as treatment plan information and follow-up images stem from differ-

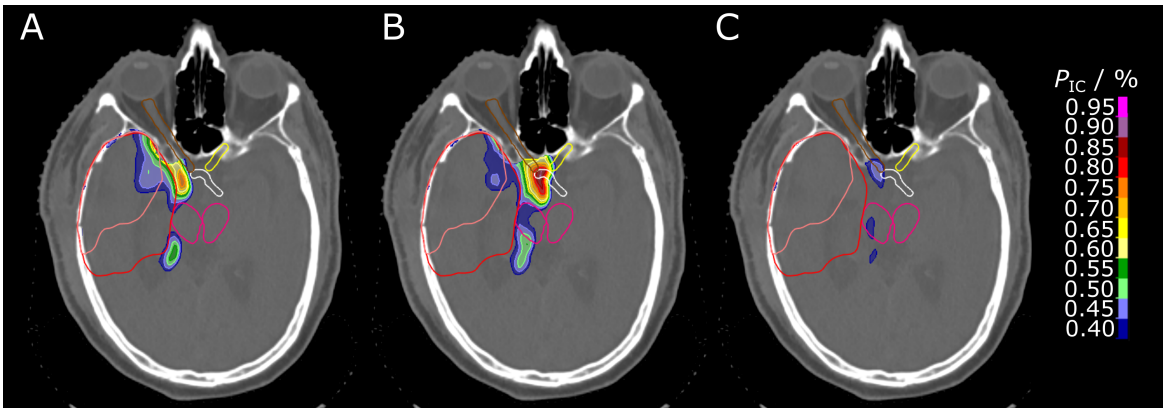

Figure 3.7: Probability for late radiation-induced magnetic resonance image changes (P_{IC}) calculated for the multi-field optimised treatment plan of brain case I for the range scenarios: **A** undershoot, **B** nominal and **C** overshoot. Clinical target volumes (CTV) for both dose levels (CTV_{low}: dark red, CTV_{high}: light red) and brainstem (magenta), chiasm (white), right and left optical nerves (brown, yellow) are displayed. Adapted from Hahn et al. (2020).

ent image modalities and time points. The investigation of radiation-induced toxicity can be divided into three steps: follow-up screening and contouring, image registration and treatment plan recalculation. The recalculation workflow will be presented for one exemplary patient who underwent PBS proton therapy at UPTD.

Patient characteristics and treatment plan information

The exemplary patient had a primary brain tumour and developed a signal abnormality after adjuvant proton therapy with SIB of 50 Gy(RBE) and 60 Gy(RBE) in 30 fractions to both CTVs, respectively. The contrast-enhancing lesion was found on MRI close to the CTV and in the periventricular region (PVR) 10 months after radiotherapy start (Figure 3.8). The contrast-enhancement was classified as radiation-induced brain injury (RIBI) by radiologists taking into account a methionine positron emission tomography. In the nominal dose distributions, prescription doses to the target were adequate with $D_{95\%}$ above 99 %. Tolerance doses with a constant RBE were met for all OARs (3.4) including the recently proposed $D_{1\%}$ below 54 Gy(RBE) to the CTV-free PVR (Eulitz, 2021). This triggered treatment plan recalculations for the selected patient case.

The treatment field parameters (spot positions, energies etc.) from the clinically delivered treatment plan were used to recalculate LET_d and included protons, deuterons and alphas. The voxelwise probability of image changes P_{IC} was derived with the logistic regression

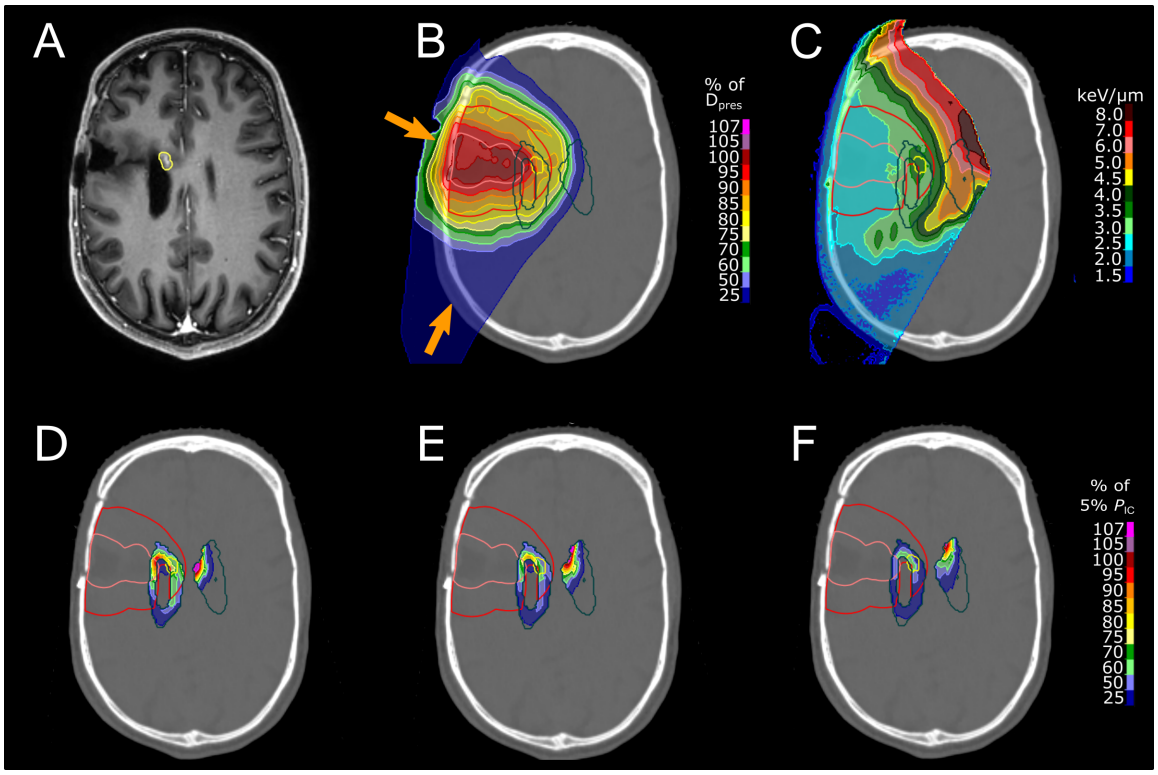

Figure 3.8: A Follow-up magnetic resonance image (MRI) 10 months after radiotherapy start shows radiation-induced image changes (yellow). **B** Nominal absorbed dose distribution together with the non-coplanar incident beam directions (arrows) covering the clinical target volumes (CTV_{low}: dark red, CTV_{high}: light red). The periventricular region is visualised as dark green contour. **C** The corresponding dose-averaged linear energy transfer (LET_d) distribution for absorbed doses larger than 1 Gy. The probability for image changes (P_{IC}) is shown for **D** the undershoot, **E** nominal, and **F** overshoot scenario, respectively. Adapted from Hahn et al. (2020).

model from Eulitz et al. (2019b), taking into account the potentially elevated radiosensitivity in the PVR by including an additional logistic regression coefficient (Bahn et al., 2020; Eulitz et al., 2019b). The PVR was defined as a 4 mm band around the segmented ventricles. The considered logistic regression coefficients were $\beta_0, \beta_1, \beta_2$ and β_3 of –8.2568, 0.0031 Gy^{-1}, 0.0293 µm Gy^{-1} keV^{-1} and 2.3458, respectively. All quantities were recalculated for the nominal as well as the under- and overshoot scenario by voxelwise scaling of the SPR maps.

3.3.1 Image registration and range prediction

The follow-up MRI was matched with the planning CT to overlap the toxicity area with the dose distribution and other information of the treatment fields. The image registration was

carried out with the framework developed by Eulitz (2021). First, the ventricular system, cerebro spinal fluid and white matter were segmented on the planning MRI using atlases. The planning MRI segments were subsequently co-registered to the planning CT and the corresponding deformation matrix for the cerebro spinal fluid was derived. First, contoured RIBI lesions from the follow-up MRI of first occurrence were co-registered with the planning MRI. Second, the cerebro spinal fluid deformation matrix from planning MRI to planning CT were used to non-linearly co-register RIBI lesions on the planning CT. An adapted and validated HLUT for UPTD from Peters (2021) was used to allow for treatment plan recalculations on the DECT-derived SPR maps with higher prediction accuracy in SPR and range than the conventional planning CT (Wohlfahrt et al., 2017).

3.3.2 Retrospective treatment plan assessment

Robustness evaluation with a range uncertainty of ±3.5 % revealed that range deviations induced systematic differences in mean and near-maximum constant RBE weighted doses of 2.1 Gy(RBE) and 1.9 Gy(RBE) within the RIBI lesion. However, this did not result in overdosages of the CTV-free PVR with a constant RBE. The RIBI also did not occur homogeneously in brain tissue receiving the same absorbed dose indicating that absorbed dose may not be the only predictor. Thus, it appeared unlikely that RIBI have been induced by range deviations and absorbed dose alone.

Instead, the location of RIBI was spatially correlated with the elevated LET_d, particularly in the PVR. Here, RIBI only occurred in areas where high absorbed dose of above 45 Gy coincided with elevated LET_d of above 3.1 keV µm^{-1}, i.e. in the distal dose gradient of the CTV boost volume where LET_d increased sharply and coincided with areas of still high absorbed dose (Figure 3.8). The predicted area of elevated risk for RIBI location based on absorbed dose, absorbed dose times LET_d and PVR matched the region of actual RIBI occurrence and may indicate the relevance of RBE-induced overdosages in toxicity-induction. The spatial correlation of predicted elevated P_{IC} and RIBI remained true also in the face of range deviations, but with slightly different absolute values in P_{IC} (Figure 3.8).

3.4 Benefit of an additional treatment field

Proton therapy centres are aware of the potentially elevated RBE at the end of proton range. However, it may be necessary in clinical practice to use treatment fields stopping in front of one or more OARs to avoid air cavities and steep density gradients in the beam path. This may be suboptimal in view of range and RBE uncertainties at the end of proton range. Increasing the number of treatment fields is considered to mitigate both range and RBE uncertainties. Using an additional treatment field allows to lower the field weight of the critical beam direction and thereby partially washing out high $\mathrm{LET_d}$ contributions through the lower $\mathrm{LET_d}$ contributions of the remaining fields (Bauer et al., 2021; Faught et al., 2022). However, whether a treatment plan with an additional treatment field is really superior may be patient-specific and requires the recalculation and assessment of both physical (range, setup) and biological (RBE) uncertainties and their complex interplay.

The following study assessed whether treatment plans with an additional third field reduce variable RBE-weighted dose (D_{RBE}) when compared to a two-field plan for the same patient. The results were produced as part of a master thesis (Sobolewski, 2021) and are summarised in this section to show the limitations of conventional treatment plan optimisation to counteract RBE variability.

3.4.1 Patient and treatment plan information

Nine brain tumour patients treated at WPE with prescription doses ($D_{50\%}$) of $36-54$ Gy(RBE) to one CTV were included. For each patient, two robust dose-optimised PBS treatment plans with two and three fields were analysed. Two of the incident beam directions were identical for both planning approaches, while one field was added for the three-field plan. The clinical plans applied robust objectives to the target volume with a range uncertainty of 3.5 % and a setup uncertainty of $3-4$ mm. The brainstem was the primary OAR. All treatment plans were clinically approved. Patient data usage was covered by an ethics approval for prospective registry trials (German Clinical Trial Register: DRKS00004384, DRKS00005363).

$D_{1\%}$ tolerance dose to the brainstem was 54 Gy(RBE). Variable RBE-weighted doses were recalculated with the RBE model from Wedenberg et al. (2013) and an α/β of 2 Gy for normal tissue and 10 Gy for the target volume. Additionally, the robustness evaluation

tool in RayStation version 9 for dose was extended via the scripting interface to allow for scoring LET and thus D_{RBE} on a set of setup and range uncertainty scenarios. Overall, 44 uncertainty scenarios were considered consisting of three range scenarios (no shift, $\pm 3.5\,\%$) and 14 translational setup errors ($3-4\,\mathrm{mm}$) along the axes and diagonals of a cube with side length twice the setup uncertainty.

3.4.2 Results of variable RBE recalculations

In the two field plans, the brainstem tolerance dose of 54 Gy(RBE) was exceeded in five cases when considering a variable RBE. In three of these cases, the three-field plans lowered the brainstem $D_{1\%}$ by more than 2.0 Gy(RBE) in the nominal scenario. These three-field plans were also superior in terms of robustness, since they lowered the brainstem $D_{1\%}$ in the worst-case uncertainty scenario of up to 5.5 Gy(RBE). However, the addition of a third treatment field was not beneficial for the other two patients at risk with $D_{1\%}$ differences in the nominal scenario below 0.1 Gy(RBE) and worsened robustness against setup and range uncertainty. Figure 3.9 illustrates two patient cases with prescription doses of 54 Gy(RBE) of whom one benefited of the third treatment field in terms of lower $D_{1\%}$ to the brainstem while the other did not. For the cohort, mean D_{RBE} to the healthy brain were slightly but systematically higher for three-field plans in six of the nine patients with average (range) differences of 0.2 Gy(RBE) (–0.9 – 1.1 Gy(RBE)). The maximum difference in $D_{50\%}$ to the CTV between the two planning strategies, also when accounting for range and setup uncertainties, remained below 0.9 Gy(RBE) with a variable RBE.

3.5 Discussion

The presented MC scoring extensions allowed to quantify and visualise LET and RBE distributions for proton treatment plans and were used to assess treatment plan safety in view of a variable RBE. LET distributions remained largely homogeneous in the target volume of multiple anatomical sites. This resulted in homogeneous RBE distributions, which however may be different from the clinically used value of 1.1, depending on the tumour-specific α/β. LET and variable RBE were particularly pronounced at the end of range and lateral treatment field edges, although IMPT offers the degrees of freedom to distribute the stopping protons and thus LET otherwise. This may be of concern for brain tumour patients where

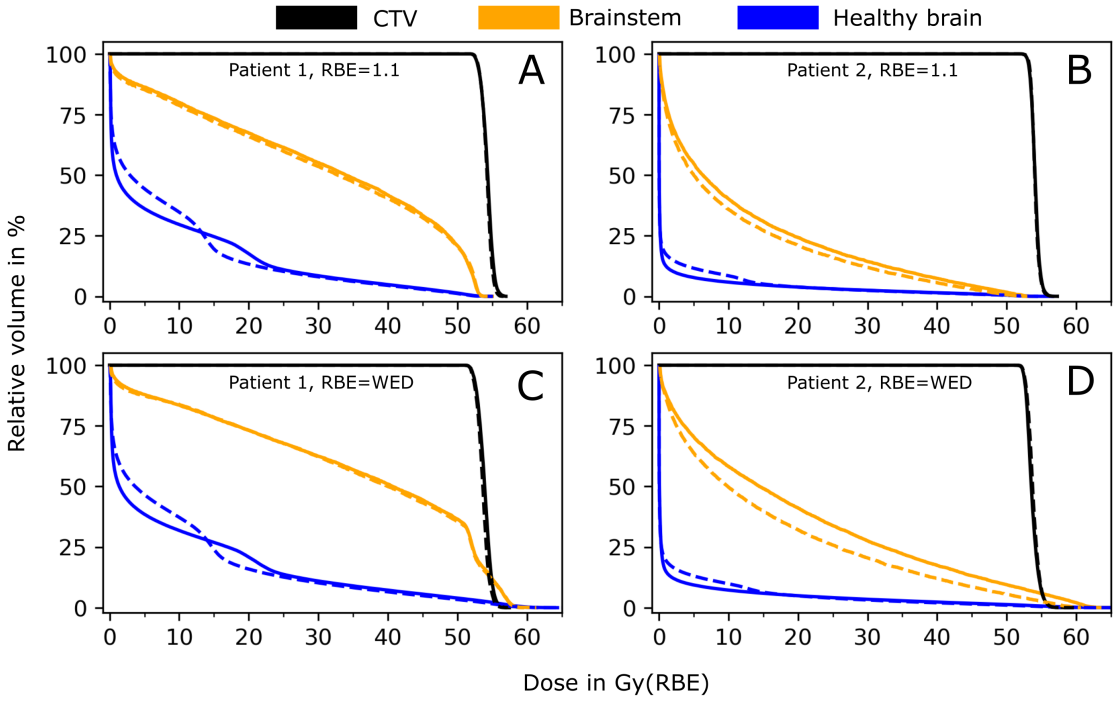

Figure 3.9: Dose-volume histograms (DVH) of treatment plans with two-fields (solid lines) and three fields (dashed lines) for two selected patient cases (left column, right column) from Sobolewski (2021). **A, B** show the DVH for absorbed dose weighted with a constant relative biological effectiveness (RBE). **C, D** DVH for a variable RBE-weighted dose (D_{RBE}, Wedenberg et al. (2013), WED) with α/β of 10 Gy for the clinical target volume (CTV) and 2 Gy otherwise. Patient 2 benefited from the third treatment field with lower maximum D_{RBE} in the brainstem.

high variable RBE values coincided with elevated absorbed dose leading to additional dose burden in serially structured OARs in vicinity to the target volume. Increasing the number of treatment fields and thereby reducing the relative weight of the critical beam direction was not feasible to systematically reduce RBE-induced extra dose burden in OARs.

The RayStation MC scoring extensions were integrated into a GUI (Sobolewski, 2021; Uber, 2018), which was implemented at UPTD and WPE. This overcomes the current lack of a ready-made solution for LET and RBE calculations in treatment plans and makes them easily accessible to clinicians and researchers. Recalculations for treatment plans ($2\times2\times2$ mm^3 grid) using clinical hardware (Intel Xeon E5-2680, 40×2.8 GHz, 128 GB RAM) typically took less than 20 minutes per treatment plan and can thus support clinical decision making in daily routine, for which a separate and simplified GUI was presented. The development of a semi-automated framework matches recently developed frameworks and efforts to recalculate LET and RBE in the inter-operating DICOM format (Aitkenhead et

al., 2020; Mein et al., 2022; Shin et al., 2020). The presented workflow was further simplified by the fact that RayStation was used as a clinical TPS enabling the use of the corresponding institution-specific clinical beam model and clinical HLUT in the research version. Otherwise, a thorough commissioning of the MC dose calculations against water phantom measurements would have been required (Eulitz et al., 2019a). Additionally, the LET_d calculations implemented in RayStation were recently validated against independent MC simulations with Open-MCsquare and microdosimetry measurements in a therapeutic proton beam of the IBA ProteusPlus (Wagenaar et al., 2020), which is also the proton therapy system used at UPTD and WPE. Still, when considering variable RBE as additional treatment plan information, it is of utmost importance to inform clinical personnel about the corresponding limitations. Variable RBE models and their biological input parameters underly substantial experimental uncertainties (Flint et al., 2022; McMahon, 2021), their translation to the clinical situation is debatable and they are not clinically validated yet (Paganetti, 2022; Paganetti et al., 2019).

Although the RBE driving LET_d is a free parameter in the inverse dose optimisation of IMPT, MFO did not present more pronounced LET_d hotspots in the target volume or OARs than SFO, in line with other studies (Faught et al., 2022). Placing the high-weighted spots at the distal and lateral edges of the treatment field appears to be the optimal solution in dose optimisation sparing dose to healthy normal tissue through steep dose gradients. Treatment field edges are placed in normal tissues due to mandatory range and setup margins (Tommasino & Durante, 2015). Consequently, for both optimisation strategies, LET_d distributions within the target volume were rather homogeneous and high LET values typically occurred in OARs close to the target volume.

LET and RBE distributions in clinical target volumes

LET_d distributions in the target volumes of all entities were rather homogeneous, comparable in LET_d magnitude, and essentially insensitive against range deviations. The nominal arithmetic mean of LET_d values in the target volumes ranged from approximately 2.3 keV µm^{-1} to 3.3 keV µm^{-1}, in agreement with other studies on proton therapy in brain, head and neck and prostate patients, respectively (Carabe et al., 2013; Fjæra et al., 2017; Frese et al., 2011; Ödén et al., 2017a, 2017b; Ödén et al., 2020; Resch et al., 2017; Traneus & Ödén, 2019; Wedenberg & Toma-Dasu, 2014). The slightly higher average LET_d values

in prostate CTVs result from their smaller field sizes in beam direction leading to less contribution from lower LET radiation in the target (Marteinsdottir et al., 2019; Paganetti, 2014). Within the range scenarios of each patient, lower beam ranges led to slightly but systematically increased LET_d in the CTV. This effect was biggest, though still small, in smaller sized targets, such as prostate, where a larger part of the target volume is located closer to the steep distal LET_d gradients. The observed LET_d homogeneity in all target volumes obtained here with robust optimisation is consistent with other studies (Fjæra et al., 2017; Ödén et al., 2017b; Ödén et al., 2020; Resch et al., 2017; Traneus & Ödén, 2019; Wedenberg & Toma-Dasu, 2014).

The use of a constant RBE in target volumes appears reasonable for the evaluated robust dose-optimised treatment plans. Robust dose optimisation was sufficient to generate homogeneous LET_d distributions in the CTVs that were robust against range deviations. Considering a homogeneous radiosensitivity throughout the tumour volume, these narrow and robust LET_d value ranges translated into an approximately constant RBE in the target volumes of all investigated entities, in accordance with other studies (Ödén et al., 2017a, 2017b; Resch et al., 2017; Wedenberg & Toma-Dasu, 2014). Until dedicated studies with large patient numbers determine tumour-specific RBE values, the use of a constant RBE in the target appears justified, in line with a recent review (Paganetti et al., 2019). Differences in tumour-specific radiosensitivity could thus still be taken into account by tumour-specific prescription doses. This may be accompanied with a robustness analysis of RBE that accounts for the relevant α/β uncertainty (Ödén et al., 2017b). Still, this neglects a potential heterogeneous radiosensitivity throughout the tumour volume, and even within a single voxel, due to the coexistence of hypoxic and well-oxygenated cell regions, which influences RBE estimations (Dahle et al., 2020).

LET and RBE distributions in organs at risk

LET_d distributions in OARs were more inhomogeneous and exhibited higher maximum LET_d values than those in the target volumes. Additionally, LET_d distributions in OARs were highly susceptible to range deviations. OARs placed laterally or distally to the target volumes received particularly high LET_d. Maximum LET_d values in the rectum and bladder ranged from approximately $4.0\,\mathrm{keV\,\mu m^{-1}}$ to $5.0\,\mathrm{keV\,\mu m^{-1}}$ and LET_d maxima of up to $6.0\,\mathrm{keV\,\mu m^{-1}}$ were found in the parotid glands. This was consistent with other studies on

prostate (Carabe et al., 2013; Ödén et al., 2017a; Resch et al., 2017) and head and neck cases (Traneus & Ödén, 2019) using similar treatment field arrangements. Since, in IMPT, the dose to these structures is typically far from tolerance dose and the LET_d is only a dose-enhancing factor, these elevated LET_d values in small volumes do not necessarily translate to unforeseen toxicity. An exception to this may be the occurrence of rectal bleeding which was recently reported to depend on the combination of local high dose and high LET_d in small volumes after IMPT (Yang et al., 2021).

Brain tumour patients featured LET_d maxima of up to 9.0 keV µm^{-1} in OARs, which was also observed in other planning studies (Carabe et al., 2013; Ödén et al., 2020; Traneus & Ödén, 2019). These high LET_d values were a result of less range straggling due to lower initial beam energies and fewer inhomogeneities in the beam path (Grün et al., 2013). This was further increased by the highly weighted beam spots placed at the end of range to achieve steep dose gradients to fulfil the clinical goals to adjacent OARs.

The estimated variable RBE above 1.1, caused by the high LET_d and low α/β, and the dose values close to OAR tolerance dose may render brain tumour patients particularly susceptible to unexpected toxicity after IMPT. In a recent review on clinical studies investigating variable proton RBE (Underwood et al., 2022), six out of 22 studies concluded that they had found clinical evidence for variable proton RBE. Five of these studies reported a clinically variable RBE after cranial proton therapy for radiation-induced image changes on MRI (Bahn et al., 2020; Eulitz et al., 2019b; Peeler et al., 2016; Roberts et al., 2019) or temporal lobe necrosis (Zhang et al., 2021) and one study reported on asymptomatic lung density changes after breast cancer proton therapy (Underwood et al., 2018). The overall statistical clinical evidence for RBE variability in proton therapy remains statistically weak at the moment (Underwood et al., 2022). A more conservative OAR tolerance dose could be considered for brain tissues with low α/β ($\approx$ 2 Gy). For instance, this could be applied in the brainstem and optical apparatus (Paganetti, 2022), receiving high LET_d ($\approx$ 5 keV µm^{-1}) to mimic a potentially elevated RBE, in line with recent propositions (Haas-Kogan et al., 2018; Paganetti et al., 2019). These results indicate that LET and RBE distributions should be considered in the evaluation of proton therapy treatment plans (Toma-Dasu et al., 2020).

Sources of uncertainties and their impact on LET and RBE

Systematic range deviations can be considered one of the main contributors to LET uncertainty. Systematic and random uncertainties may be present during treatment delivery and may thus alter dose, LET_d and RBE distributions delivered to the patient from that shown on the planning CT. Since systematic uncertainties are likely present throughout the entire fractionated treatment, they may have an actual impact on the treatment outcome. The relevance of systematic error components is also reflected in its higher weight in CTV margin calculations over the random components (Van Herk et al., 2000).

The impact of random uncertainties is, however, likely to be washed out over a fractionated treatment with daily random errors. State-of-the-art image guidance, robust patient immobilisation, and MC dose calculations limit the effect of patient setup, calculation accuracy and model parameters to approximately 2 mm (Lowe et al., 2016; Paganetti, 2012). In contrast, systematic range uncertainties are introduced at the initial stage of treatment planning by the imperfect conversion of HU to mass density or to SPR and in mean excitation energy (Lomax, 2008; Paganetti, 2012). The range error for a proton beam with energies of 100 – 227 MeV is in the order of 0.3 – 1.1 cm. The considered range shift can also include the influence of other uncertainties as long as the total effect does not exceed 3.5 %.

Range deviations caused maximum variations in the mean LET_d in the CTV of 0.5 $keV\,\mu m^{-1}$, in line with other studies investigating the impact of range uncertainties on LET_d distributions (Rana et al., 2022). Accordingly, range deviations showed a small impact on RBE estimation in the target volumes, particularly in those with high α/β. Their impact on RBE was lower than that from the uncertainty in α/β itself and comparable to the impact of the uncertainty in the fit parameter q of the Wedenberg RBE model (Resch et al., 2017). The observed LET_d increase and decrease to the CTV in the under- and overshoot scenarios, respectively, was consistent with other studies (Rana et al., 2022). This also remains true when adding systematic setup uncertainties, which increase the overall LET_d variation in the CTV by approximately 0.2 $keV\,\mu m^{-1}$ (Rana et al., 2022). These results suggest that the range uncertainties, as well as the combination of range and setup uncertainties, produced homogeneous LET_d and RBE distributions in the CTV.

Range deviations predominantly impacted LET_d distributions in OARs being close to the target volume and coinciding spatially with the location where each beam stopped. Accord-

ingly, OARs placed distally and laterally to the target volume were particularly susceptible to range deviations, as LET_d was already elevated and range deviations caused voxelwise changes of up to 3 keV µm^{-1}. This effect was particularly relevant in brain tumour patients where the high LET_d at the end of range coincided with high dose resulting in elevated P_{IC} in healthy brain tissue. Although range deviations caused changes in absolute estimations, the identified risk regions occurred at the target volume border and in healthy brain tissue, the optical apparatus and the brainstem.

Radiation-induced brain injury

The presented toxicity region in patient follow-up did not occur homogeneously in brain tissue suggesting that the constant RBE-weighted dose in a given normal tissue structure shown on the planning CT may not be the only predictor for radiation-induced toxicity in proton therapy. This observation is in line with other studies evaluating follow-up images after proton therapy (Bahn et al., 2020; Eulitz et al., 2019b; Peeler et al., 2016). The spatial location close to the CTV border and the time of occurrence of the RIBI at about 10 months after radiotherapy start were representative for a large patient cohort from the same institution with similar prescription doses but using double-scattering proton therapy (Eulitz et al., 2023). Although only presented for a single patient case, the analysis suggested that range deviations had a small impact on the dose received in the RIBI lesion close to the CTV, in accordance with other studies investigating the spatial correlation of LET_d and toxicity regions in view of physical and biological uncertainties (Ödén et al., 2020).

When considering a varying spatial radiosensitivity and the LET_d in addition to absorbed dose, the predicted elevated P_{IC} and the region of actual lesion occurrence coincided spatially. From a clinical point of view, however, the predicted absolute probabilities of less than 5 % may not appear relevant. This may be a result of neglecting inter-patient radiosensitivity in model building of the applied P_{IC} model from Eulitz et al. (2019b), which was observed to influence model building in other studies investigating brain injuries after proton therapy (Engeseth et al., 2021; Niemierko et al., 2021). The applied RIBI model may thus identify risk regions for RIBI occurrence, but not whether they occur (Eulitz et al., 2023). Similarly, absorbed dose alone may discriminate between regions of lower and higher risk but failed to identify a small region of increased risk as reflected in the best model performance when predicting P_{IC} based on absorbed dose, absorbed dose times LET_d and the periventricular

region (Eulitz et al., 2023). Still, the applied model from Eulitz et al. (2019b) was built for double scattering proton therapy and has not been validated for PBS yet, where clinical LET_d distributions may exhibit larger maximum values (Wilson et al., 2021).

Most of the current models to estimate voxel- and patient-wise side-effects are based on the dose on the nominal planning CT and do not consider the dose actually delivered to the patient, and thus the accuracy of these models is limited by the accuracy of dose reporting itself (Paganetti et al., 2021). The robustness of these voxelwise models could be tested in the future, when including range and setup uncertainties to more accurately reflect the dose delivered to the patient over the whole treatment course (Lowe et al., 2016).

Clinical mitigation strategies

The addition of a third treatment field was not effective in systematically reducing D_{RBE}, as it lowered $D_{1\%}$ in the brainstem for only three out of nine patient cases. The benefit of using a third field was found to be patient-specific, consistent with other studies (Faught et al., 2022). The patients who benefited from a third treatment field featured a small opening angle in their two-field plan and the third field was placed in opposition to one of the existing treatment fields. The patients who did not benefit from a third field presented an (approximately) opposing field arrangement already in the two-field plan. Accordingly, the opening angles between two incident beams in a multiple-field treatment plan should be maximised as much as possible, keeping in mind a potential increase of irradiated volume, or a lower weighted opposing treatment field should be added to lower the variable RBE-weighted dose to OARs. This rule of thumb considers that the high LET_d portions of one field are partially washed out by the lower LET_d contributions from the opposing field (Faught et al., 2022) and is already practiced at European proton therapy institutions (Heuchel et al., 2022; Sørensen et al., 2021; Toma-Dasu et al., 2020).

In line with the findings in this thesis, more fields and larger opening angles were postulated to mitigate the role of LET_d in radiation-induced brain toxicity (Bertolet et al., 2022). However, whether to use an additional treatment field or not should be considered for each patient individually and the decision should be complemented by balancing the potential reduction in variable RBE-weighted dose to selected OARs with the increased integral dose to the healthy brain and the increased treatment delivery time per fraction. Solely increasing the number of treatment fields may be insufficient to reduce the elevated RBE in the pres-

ence of varying tissue radiosensitivity (Bauer et al., 2021), as this variation is geometrically complex and not explicitly included in the treatment plan optimisation. The MC scoring extensions and the developed GUI are therefore still relevant and may help to scrutinise potential clinical RBE mitigation strategies and novel planning approaches.

3.6 Summary

LET and RBE distributions can be recalculated for clinical treatment plans by using the MC scoring extensions of RayStation and the presented GUI. When considering RBE variability, doses to the tumour volume remained homogeneous indicating that the use of a constant (entity-specific) RBE may be maintained. In contrast, higher LET_d and RBE values occured at the lateral and distal edges of the proton treatment fields. This RBE variability is of particular concern for brain tumour patients, where high LET_d values coincide with high doses causing extra dose burden to healthy tissue which may translate into unforeseen side-effects. Using three instead of two treatment fields to indirectly wash out high LET was effective only when placing the additional field opposed to one of the other two fields but must be balanced with the increased mean dose to the remaining brain in most patient cases. In brain cases, and especially when using small opening angles or treatment field terminating in front of an OAR near the target volume, recalculation of quantities other than absorbed dose can inform treatment planners and medical staff about the safety of the treatment plan in terms of a variable RBE. The consideration of RBE variability in patient treatment plans may help to better understand its clinical relevance and to better exploit the potential and safety of proton therapy.

4 Status of LET and RBE calculations in European proton therapy

The clinical use of a generic RBE of 1.1 in proton therapy allows for straightforward treatment plan comparisons and outcome reporting between individual therapy centres and between protons and photons. However, the inter-centre comparability might worsen when accounting for quantities other than absorbed dose, which are not standardised yet. In view of emerging evidence for the relevance of clinical proton RBE variability (Underwood et al., 2022), an increasing number of proton therapy centres uses LET and variable RBE recalculations to produce clinical data to better understand radiation response or to inform clinical staff on variable RBE retrospectively or even during treatment planning (Heuchel et al., 2022; Mein et al., 2022; Sørensen et al., 2021). However, LET and RBE recalculations are not available in clinical TPS (Wagenaar et al., 2020). Thus, each proton facility may have its own technical solution for obtaining patient-specific LET and RBE distributions and the corresponding research tools are under different stages of development in Europe (Toma-Dasu et al., 2020).

Centres are faced with a variety of possible LET and variable RBE definitions. The reported average LET per voxel depends on the weighting used in averaging, the secondary particles considered, the calculation method used and the physics model and parameters set in the specific research simulation environment, as shown in numerous monocentric studies (Cortés-Giraldo & Carabe, 2015; Granville & Sawakuchi, 2015; Grzanka et al., 2018; Guan et al., 2015; Koh et al., 2020; Mairani et al., 2017). Despite their evident impact on LET, so far, no standard has been established for calculating and reporting LET in experiments, in clinical practice or for evaluating patient follow-up data (Kalholm et al., 2021; Koh et al., 2020; Paganetti et al., 2019; Smith et al., 2021; Underwood et al., 2022). The voxelwise averaged LET can then be used as input for numerous *in-vitro* LET-driven phenomenological variable RBE models (Rørvik et al., 2018). Consequently, differences in RBE modeling resulting from differences in input parameters may complicate inter-centre

comparability. Therefore, it needs to be carefully considered and reported which quantities, definitions and algorithms to use (Hernandez et al., 2020). The same is true also for LET and variable RBE, i.e. to avoid bias and inconsistencies when collecting, reporting and exchanging data on treatment efficacy.

Thus, the proton therapy community recently urged for harmonising the reporting of LET and RBE-weighted dose calculations. This includes the choice of RBE model and physical and biological input parameters to maintain consistent clinical dose prescription and outcome reporting between centres (Heuchel et al., 2022; Underwood et al., 2022). This may increase size and homogeneity of patient outcome reports, which may improve clinical evidence on variable RBE effects in multi-centric studies (Sørensen et al., 2021).

In direct response, two multi-centric studies were initiated to assess and compare the status of calculating and reporting, first, LET and, second, variable RBE-weighted dose at proton therapy institutions in Europe. The primary goal of this multi-centric study was to assess the inter-centre variability for the same treatment planning situation. Parts of this chapter were presented at conferences (Hahn et al., 2021a; Hahn et al., 2022d; Hahn et al., 2021c) and published (Hahn et al., 2022c).

4.1 Study design

Eight proton therapy institutions active in work package 9 of the European project *Infrastructure in Proton International Research* (INSPIRE) and technically capable of performing LET and RBE recalculations of treatment plans participated in this multi-centric study (Table 4.1). An ethics approval was granted (EK601122019). CT datasets for a homogeneous water phantom and five anonymised patient cases were distributed to all participating institutions.

A coherent set of TPS-specific look-up tables was used to ensure a consistent HU to material assignment (based on mass density, material composition) and SPR prediction among the different TPS and simulation environments used (Table 4.1) (Permatasari et al., 2020; Wohlfahrt et al., 2020). This deliberately reduced the variability between centre-specific TPS and simulation environments originating solely from different HU to material and SPR conversions. The set of look-up tables consisted of a CT number to SPR conversion for Eclipse (Varian Medical Systems, Palo Alto, USA), an adapted CT number to mass

Table 4.1: Participating proton therapy institutions and their centre-specific hard- and software.

Institution	Nozzle design	Simulation environment	
		dose	LET
University Proton Therapy Dresden, Germany	IBA universal	RayStation v6	RayStation R6 [1,2]
The Skandion Clinics Uppsala, Sweden	IBA dedicated	RayStation v9	RayStation R6 [2,3]
Danish Center for Particle Therapy Aarhus, Denmark	Varian ProBeam	Eclipse 13.7	FRoG [4,5] TOPAS 3.5 [6,7,8]
Institut Curie Paris/Orsay, France	IBA universal	Eclipse 15.5	TOPAS 3.5 [6,7,8]
Proton Beam Therapy Centre Christie Manchester, United Kingdom	Varian ProBeam	Eclipse 15.6	GATE 8.1 [8,9,10,11]
Internet-Simulation Evaluation Envision Torino, Italy	PBS sample	PlanIt 3.0 4SeePlan R3	PlanIt 3.0 [12] 4SeePlan R3 [13]
GSI Helmholtz Centre for Heavy Ion Research, Darmstadt, Germany	GSI	TRiP98 1805a	TRiP98 1805a [14]
Institute of Nuclear Physics Krakow, Poland	IBA dedicated	TRiP98 1310	TRiP98 1310 [14]

Eclipse, Varian Medical Systems, Palo Alto, CA, USA. FRoG: Fast dose Recalculation on GPU (Graphics Processing Unit). GATE: GEANT4 Application for Emission Tomography. GEANT4: GEometry ANd Tracking. IBA: Ion Beam Applications SA, Louvaine-la-Neuve, Belgium. RayStation, RaySearch Laboratories AB, Stockholm, Sweden. TOPAS: TOol for PArticle Simulation. TRiP: TReatment plannIng for Particles.
References: [1] (Hahn et al., 2020), [2] (Wagenaar et al., 2020), [3] (Ödén et al., 2020), [4] (Mein et al., 2018), [5] (Choi et al., 2018), [6] (Perl et al., 2012), [7] (Faddegon et al., 2020), [8] (Allison et al., 2016), [9] (Sarrut et al., 2014), [10] (Grevillot et al., 2020), [11] (Aitkenhead et al., 2020), [12] (Russo et al., 2015), [13] (Bourhaleb et al., 2011), [14] (Krämer et al., 2000)

density for RayStation and a direct SPR to material conversion for Tool for Particle Simulation (TOPAS) and GEANT4 Application for Emission Tomography (GATE), respectively.

This chapter presents two multi-centric studies among different European proton beam facilities comparing, first, the calculated absorbed dose and LET spatial distributions and, second, the applied approaches to model RBE variability for a selected set of proton therapy patients. Each study was divided in two parts. In the first part, the local routine applied at each institution was reported and their comparability was assessed. In the second part, definitions and parameters to harmonise LET and RBE reporting are suggested based on the consensus of the participating institutions.

Table 4.2: Patient and treatment planning information to compare linear energy transfer (LET) and relative biological effectiveness (RBE) calculations at European proton therapy centres.

Case	Prescribed dose in Gy(RBE)		Fx	Treatment field angles (gantry, couch) in °			
	CTV_{high}	CTV_{low}		Field 1	Field 2	Field 3	Field 4
Waterphantom							
Single field SOBP	60.0	–	30	270, 0	–	–	–
Perpendicular fields	60.0	–	30	270, 0	180, 0	–	–
Opposing fields	60.0	–	30	270, 0	90, 0	–	–
Patients							
Brain	60.0	50.0	30	60, 270	170, 0	285,15	–
Base of skull	70.0	57.0	33	70,350	140, 0	210,0	300, 10
Head and neck	70.0	57.0	33	0, 0	40, 350	180, 0	320,10
Pancreas	55.8	50.4	31	160, 0	180, 0	225,0	–
Prostate	60.0	48.0	20	90, 0	270, 0	–	–

CTV: Clinical target volume. Fx: Number of fractions. SOBP: Spread-out Bragg peak.

4.1.1 Treatment planning information

PBS treatment plans were created by each institution using their site-specific, if available, clinical TPS and beam model for treatment plan dose optimisation and calculation. Centre-specific research simulation environments with their characteristic MC implementation parameters, if applicable, were used for LET and RBE recalculations (Table 4.1).

A set of patient-specific plan properties were commonly agreed on prior to treatment planning based on suggestions by a subgroup of treatment planners. All participating institutions used the same treatment field angles for treatment planning, prescription and fractionation for the water phantom and patient cases, respectively (Table 4.2). Centre-specific treatment plans were created by their individual treatment planner using centre-specific optimisation objectives and constraints to fulfil the commonly agreed on clinical goals including prioritisation (Table 4.3). Doses to OARs were kept as low as reasonably achievable and in line with the quantitative analyses of normal tissue effects in the clinic (QUANTEC) (Bentzen et al., 2010). Maximum doses were restricted to below 107 % of the prescription dose.

Water phantom cases

Every proton therapy institution generated three non-robust SFO treatment plans that homogeneously dose-cover a cubic target volume of $5 \times 5 \times 5\,\mathrm{cm}^3$ placed in different depths

Table 4.3: Clinical goals for dose-volume histogram (DVH) parameters used in the INSPIRE patient study. Priority 1: Must not be violated. Priority 2: May be exceeded to achieve target coverage. Priority 3: May be exceeded when contralateral side is spared. Priority 4: Should be aimed for. DVH parameters are given for normo-fractionation, except rectum and bladder with hypo-fractionation.

Organ at risk	Parameter	Clinical goal
Priority 1: Robust.		
Brainstem	$D_{1\%}$	54 Gy(RBE)
Optical apparatus	$D_{1\%}$	54 Gy(RBE)
Spinal cord	$D_{1\%}$	45 Gy(RBE)
Duodenum, Bowel	$D_{1\,\mathrm{cm}^3}$	52 Gy(RBE)
	$V_{45\,\mathrm{Gy(RBE)}}$	195 cm^3
	$V_{15\,\mathrm{Gy(RBE)}}$	120 cm^3
Stomach	$D_{1\,\mathrm{cm}^3}$	54 Gy(RBE)
	$V_{50\,\mathrm{Gy(RBE)}}$	2 %
	$V_{45\,\mathrm{Gy(RBE)}}$	25 %
Rectum	$V_{61\,\mathrm{Gy(RBE)}}$	3 %
(hypofractionated)	$V_{57\,\mathrm{Gy(RBE)}}$	15 %
	$V_{40.8\,\mathrm{Gy(RBE)}}$	60 %
Bladder	$V_{48.6\,\mathrm{Gy(RBE)}}$	25 %
(hypofractionated)	$V_{40.8\,\mathrm{Gy(RBE)}}$	50 %
Priority 2: Robust.		
CTV	D_{mean}	D_{pres}
	$D_{98\%}$	95 %
Priority 2: Non-robust.		
Healthy brain	$D_{1\%}$	60 Gy(RBE)
	D_{mean}	40 Gy(RBE)
Lacrimal glands	$D_{1\%}$	40 Gy(RBE)
	D_{mean}	35 Gy(RBE)
Parotids	D_{mean}	25 Gy(RBE)
Liver	$V_{30\%}$	30 Gy(RBE)
Priority 3: Non-robust.		
Kidneys	D_{mean}	15 Gy(RBE)
Cochlea	D_{mean}	45 Gy(RBE)
Priority 4: Non-robust.		
Lens	$D_{1\%}$	5 Gy(RBE)
Femoral heads	$V_{52\,\mathrm{Gy(RBE)}}$	5 %

CTV: Clinical target volume. D: Dose. D_{pres}: Prescribed dose. V: Volume.

of a homogeneous water phantom. The three different planning cases covered a single-field spread-out Bragg peak (SOBP), two perpendicular fields and two opposing fields, respectively (Table 4.2). The isocentre was at target volume centre in 12.5 cm depth for the single-field SOBP and both perpendicular fields and 20 cm for the opposing field setup, respectively. For plan evaluation, additional regions of interest were created in all CT slices

of the target volume in the proximal dose build-up and the distal dose-fall and measured 15 mm in beam direction. The study in the water phantom aimed to compare the underlying physics and simulation engines applied at different centres and to compare the calculation of averaged LET. Additionally, it aimed to initiate the data exchange with the unambiguous and interoperable DICOM format, as there is no DICOM object for LET and RBE yet, a basis for the comparison of simulations in patients.

LET calculations in the phantom were divided in two methodological parts. First, every centre independently employed the LET averaging approach and considered the secondary particles according to their local practice to assess the inter-centre variability in LET calculation. Second, it was jointly concluded to harmonise LET reporting among the institutions and the benefit of such a harmonised reporting was quantified.

Patient cases

Clinical contours were used for patient tumour volumes and OARs, respectively. The distributed patient cohort included five patients, each with a different primary tumour site and site-specific fractionation schedule: brain tumour, base of skull tumour, head and neck tumour, pancreas tumour and prostate tumour, respectively (Figure 4.1). MFO was used to plan the prescription doses with SIB to two CTVs of higher (CTV_{high}) and lower prescription dose (CTV_{low}), respectively. Centres used their TPS specific framework for robust plan optimisation (probabilistic or minimax) in the CTVs considering 3.5 % range and 3 mm setup uncertainty, except for the pancreas tumour patient with a setup uncertainty of 4 mm. Other uncertainties were accounted for in the internal CTVs (iCTV).

The patient study aimed to report and compare the status of centre-specific approaches to recalculate variable RBE-weighted dose in patients. Here, a harmonised LET definition as proposed in the water phantom study was considered as an input parameter by all centres for the centre-specific variable RBE model. Thereby, the comparison of harmonised LET calculations between different centres was extended to heterogeneous patient geometries with non-water and non-unit density conditions.

The RBE calculations of the patient study were divided in two methodological parts. Firstly, centres independently chose a variable RBE model and biological input parameters to report variable RBE-weighted doses for each patient in accordance to their local practice. Secondly, based on the centre-specific absorbed dose and LET distributions, the Weden-

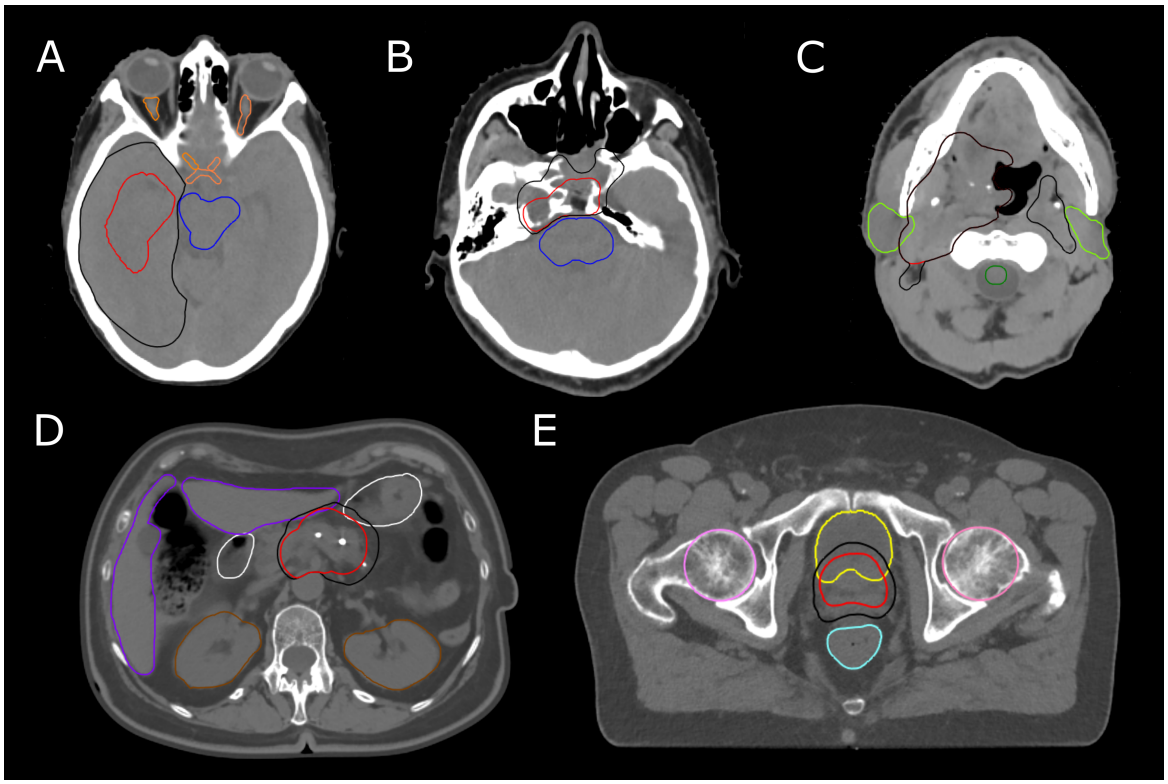

Figure 4.1: Exemplary axial computed tomography slice for each of the five patient cases distributed to all participating proton therapy institutions and used for treatment planning: the **A** brain, **B** base of skull, **C** head and neck, **D** pancreas and **E** prostate cases. Contours for higher-risk clinical target volume (CTV_{high}, red) and lower-risk CTV (CTV_{low}, black) are shown together with the organs at risk: brainstem (blue), optical apparatus (orange), parotid glands (green), colon (purple), stomach (white), kidneys (brown), bladder (yellow), rectum (cyan) and femoral heads (purple).

berg et al. (2013) RBE model was applied with α/β of 2 Gy in normal tissues and 10 Gy for all CTVs but prostate with 2 Gy.

4.1.2 Data processing and treatment plan evaluation

Resulting dose, LET, RBE and D_{RBE} distributions from all centres for the water phantom and patient study were collected and centrally stored. Institution-specific scoring grid sizes were $\leq 2 \times 2 \times 2\,mm^3$. For plan evaluation, all distributions were interpolated and evaluated on the respective CT grid size of the water phantom ($1 \times 1 \times 1\,mm^3$) and the patient cases ($0.9765625 \times 0.9765625 \times 2.0\,mm^3$), respectively, using self-written and benchmarked Python scripts (Python Software Foundation, version 3.6.10). This was done to circumvent differences in calculating DVH statistics between different TPS (Pepin et al., 2022),

which could bias the inter-centre comparison. Dose distributions were analysed without any rescaling. Only distributions in DICOM format were accepted in both the water phantom and the patient study. A consistent data format allowed for performing unambiguous data exchange between institutions that used different simulation environments, grid sizes, grid resolutions and, consequently, for correctly sampling the simulation on the CT grid.

HI and CI were used as additional measures for treatment plan acceptability and comparability. The dose distribution from the centre with the most homogeneous dose, i.e. HI closest to zero, was used as reference for three dimensional global gamma analyses (Wendling et al., 2007) considering voxels above 50 Gy(RBE) with dose and distance to agreement set to 3 % and 3 mm, respectively. Near-maximum, mean and near-minimum $\mathrm{LET_d}$ ($\mathrm{LETd_{1\%}}$, $\mathrm{LETd_{mean}}$, $\mathrm{LETd_{99\%}}$) were evaluated in voxels above 2 Gy. The model from Wedenberg et al. (2013) was applied for voxelwise variable RBE estimation with α/β of 2 Gy for the entire water phantom.

Treatment plans were deemed acceptable if they complied with OAR tolerance doses and showed adequate CTV coverage (Table 4.3). Near-maximum, mean and near-minimum $\mathrm{LET_d}$ ($\mathrm{LET_{d,2\%}}$, $\mathrm{LET_{d,mean}}$, $\mathrm{LET_{d,98\%}}$) were evaluated in voxels above 2 Gy. Absorbed dose, LET, variable RBE-weighted doses and their volume-histogram statistics were compared among the institutions for all clinically acceptable plans.

Variations in volume histogram parameters between institutions were quantitatively summarised by the relative standard deviation σ_n. It was defined as one standard deviation in the given LET or dose metric across all institutions divided by its arithmetic mean. Levene's test for equality of variances was applied to test whether a variable RBE would affect the inter-centre variances in LET- and dose-volume parameters. A level of 0.05 was considered statistically significant.

4.2 Treatment plan comparisons in the water phantom

Treatment planning results from six out of eight institutions were provided in DICOM format and used for further analyses. Results from the two institutions using TRiP were provided in the proprietary VOXELPLAN format. Since the VOXELPLAN format did not allow to unambiguously reconstruct the dose and LET distributions in the DICOM coordinate system, TRiP data was excluded from analyses in this multi-centre comparison, i.e. methods IX and

X were also excluded from LET analyses (Table 4.4).

4.2.1 Absorbed dose evaluation

Centre-specific absorbed dose weighted with RBE of 1.1 ($D_{1.1}$) distributions were comparable in the target volume (Figure 4.2). For all three treatment field arrangements, adequate target coverage was reached with $D_{95\%}$ above 95.1 % and $D_{99\%}$ above 92.0 %. Dose hotspots remained within tolerance with $D_{1\%}$ below 105.4 %.

Maximum relative inter-centre variations (σ_n) and absolute differences in near-minimum, mean and near-maximum $D_{1.1}$ were below 2.7 % and 3.6 Gy(RBE), respectively. Gamma pass rates (3 %, 3 mm) in the high dose region above 50 Gy(RBE) were above 91.8 %, except for one single field SOBP dose distribution with a pass rate of 81.9%. All $D_{1.1}$ distributions achieved adequate homogeneity (HI ≤ 0.13) and conformity to the CTVs with deviations from a CI of 1 below 0.16, except for two planning cases of one institution presenting maximum CI deviations of 0.22 and 0.32. In the proximal dose build-up and the steep distal dose fall-off regions, inter-institutional variations in DVH parameters were larger and up to 33.5 % and 18.8 %, respectively, as they were not explicitly included in plan optimisation (Figure 4.2).

4.2.2 Centre-specific LET calculations

For LET calculations, the participating institutions used different simulation environments, scoring techniques and considered different averaging methods and secondary particles (Table 4.4). At all institutions, analytical or MC-based solutions were available for LET calculations. Institutions either used research versions of clinically available TPS (RayStation, TRiP) or dedicated research simulation environments (FRoG, TOPAS, GATE, PlanIt, 4SeePlan) (Table 4.4). All institutions scored the unrestricted LET. Calculation methods I to VI were used for non-harmonised reporting. While one institution considered trackaveraging for LET, all others performed dose-averaging. Different secondary particle spectra were considered in LET scoring:

1. only primary protons,
2. all protons, i.e. primary and later proton generations,
3. all ions with atomic charge $Z = 1$, or
4. primary protons and all ions with atomic charge $Z \leq 2$.

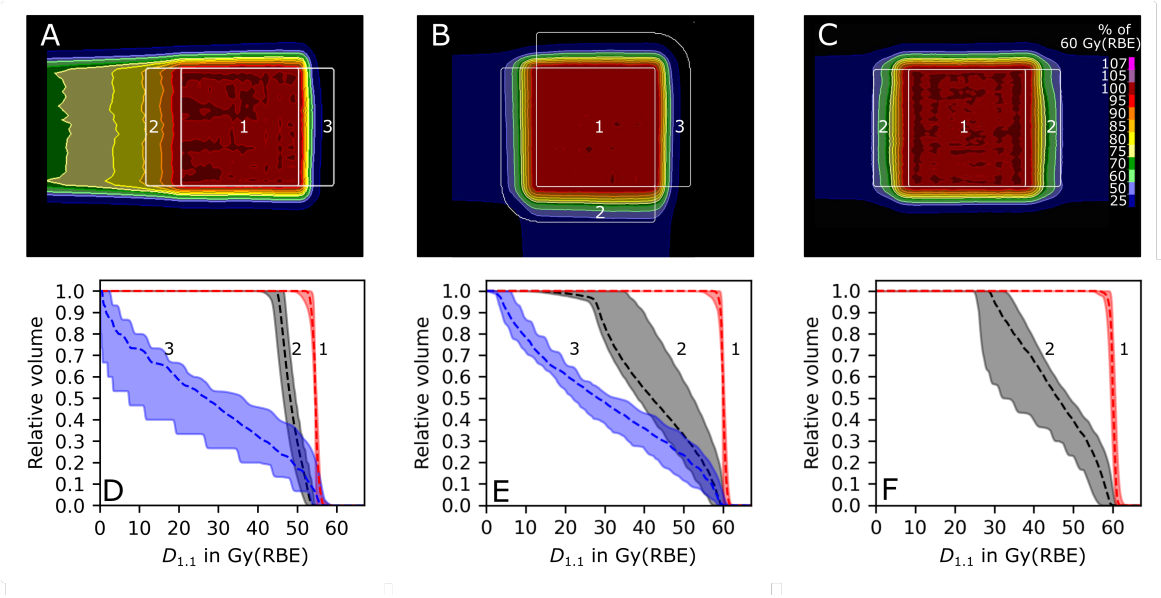

Figure 4.2: Exemplary dose distributions from one institution for a **A** single-field spread out Bragg-peak (SOBP), **B** perpendicular and **C** opposing field arrangement. Median (dashed) and range (shaded) dose-volume histograms (DVH) of the six institutions are shown for the **D** single field SOBP, **E** perpendicular fields and **F** opposing fields, respectively. $D_{1.1}$: absorbed dose weighted with a constant relative biological effectiveness. Regions of interest: (1) target volume, (2) proximal dose build-up region, (3) steep distal dose fall-off region. Adapted from (Hahn et al., 2022c), with permission from Taylor & Francis Group.

Differences in LET scoring technique, LET definitions and considered secondary particles resulted in inter-institutional variability (σ_n) in near-minimum, mean and near-maximum LET of 13.9 – 57.1 %. Absolute differences in mean LET increased from proximal dose-build up and target volume towards the distal fall-off region from 1.0 – 2.8 keV µm^{-1} and 1.5 – 4.2 keV µm^{-1} for the single-field SOBP and both perpendicular fields, respectively (Figure 4.3). Absolute mean differences in average LET for the opposing field setup were 1.8 keV µm^{-1} in the target volume and 4.8 keV µm^{-1} in the adjacent regions of interest, respectively.

Using centre-specific non-harmonised LET calculations (Table 4.4, methods I to VI) as input for the same variable RBE model considerably increased the inter-centre variability in reported dose values compared to consistently using a constant RBE. The inter-centre variation in mean dose to the target volume increased significantly for the perpendicular and opposing field setup ($p < 0.05$) and by 5.5 percentage points and 6.5 percentage points, respectively. Non-harmonised D_{RBE} calculations increased variations in reported dose values substantially for all but one evaluated DVH parameter and with up to 10.4 percentage points

Table 4.4: Specification of linear energy transfer (LET) calculations as implemented at the eight proton therapy institutions. Methods in bold were used for reporting the harmonised LET definition in the water phantom and used in the patient cases.

Method	**LET definition**		**Scoring parameters for unrestricted LET**		
	Averaging	Ions	Technique	Medium	Normalisation
I	dose	all protons	Ref.[1], Method 1	material	unit density tissue
II	dose	primary protons	Ref.[2]	material	unit density tissue
III	dose	$Z = 1$	Ref.[3]	water	none
IV	dose	$Z \leq 2$	Ref.[4], Method C	material	unit density tissue
V	dose	all protons	Ref.[4], Method C	water	none
VI	track	all protons	Ref.[4], Method C	material	unit density tissue
VII	dose	all protons	Refs.[5,6]	material	none
VIII	dose	all protons	Ref.[1], Method 1	water	none
IX	dose	all particles	Refs.[7,8]	water	unit density tissue
X	dose	all particles	Ref.[8]	material	none
harmonised	dose	all protons	centre-specific	water or material	unit density tissue

Z: atomic charge. References: [1] (Granville & Sawakuchi, 2015), [2] (Russo et al., 2015), [3] (Kopp et al., 2020), [4] (Cortés-Giraldo & Carabe, 2015), [5] (Guan et al., 2015), [6] (Romano et al., 2014), [7] (Heinrich et al., 1991), [8] (Krämer et al., 2000).

compared to an RBE of 1.1.

4.2.3 Harmonised LET calculations

As a result, it was jointly proposed to harmonise the scoring of LET by specifying which averaging technique and secondary particles to consider, thereby increasing the consistency in D_{RBE}. For this harmonisation, the unrestricted dose-averaged LET to water or unit density tissue was collectively agreed on, while continuing to use the centre-specific scoring technique. For resimulating the LET using harmonised settings, two centres changed their simulation environment (Table 4.4: from method II to VII and method III to VIII). Using the harmonised LET definition decreased the relative LET variability among the institutions (σ_n) in all evaluated regions by 9.0 – 52.8 percentage points and resulted in a remaining LET variability of generally below 10 % (Figure 4.4). As an exception to this, slightly higher variations remained for near-maximum $\mathrm{LET_d}$ in the target volume for all beam arrangements with a maximum difference of 14.0 % and near-minimum $\mathrm{LET_d}$ in the proximal regions for opposing fields with absolute differences of up to 1.6 keV µm^{-1}.

The proposed harmonisation of averaged LET calculations translated into substantially reduced D_{RBE} variations among the centres (Figure 4.4). Inter-centre D_{RBE} variations de-

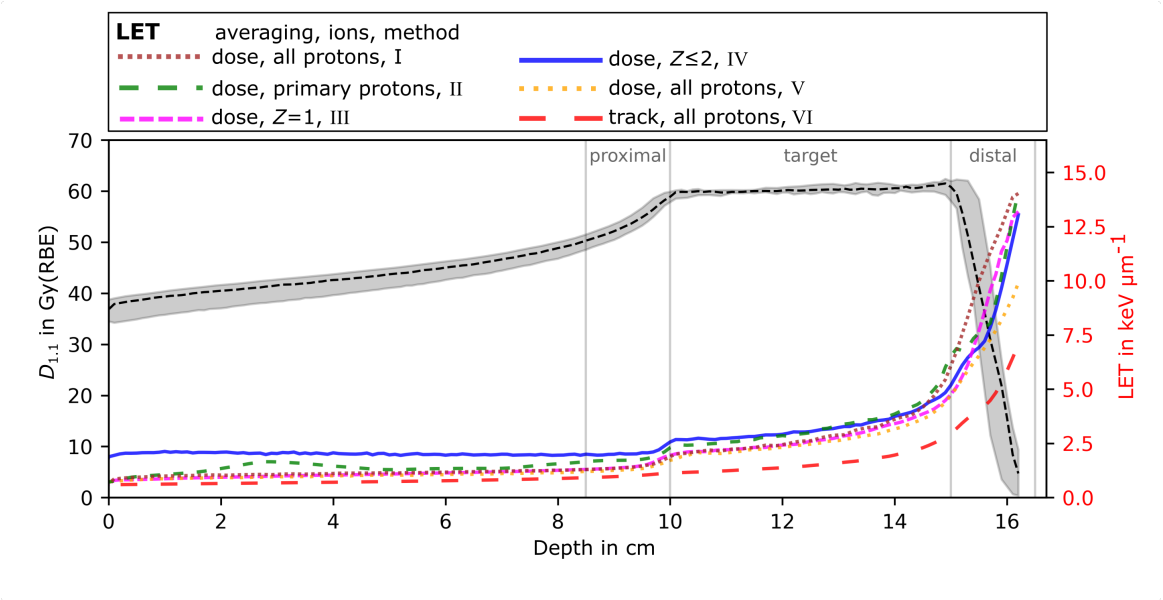

Figure 4.3: Line profiles of the six institutions along the beam central axis for an absorbed dose weighted with relative biological effectiveness of 1.1 ($D_{1.1}$, gray, upper) and centre specific averaged linear energy transfer (LET) profiles (color-coded, lower). Median $D_{1.1}$ (dashed, black) with minimum and maximum values (shaded area) and detailed depiction of LET line profiles for all six centre-specific LET calculations show inter-institutional variability. Roman numerals correspond to the characteristic implementation parameters for LET calculation according to Table 4.4. $\mathcal{Z}$: atomic charge. Adapted from (Hahn et al., 2022c), with permission from Taylor & Francis Group.

creased by 4.6 – 6.1 percentage points when reporting the proposed harmonised LET_d definition instead of the centre-specific definitions. Reported harmonised D_RBE distributions were no longer significantly different from the corresponding variation in $D_{1.1}$ for any of the investigated DVH-parameters, regions or field arrangements ($p > 0.136$). The remaining variability in D_RBE volume-histogram parameters was below 2.0 percentage points. Gamma pass rates (3 %, 3 mm) generally exceeded 90 % for regions receiving D_RBE above 50 Gy(RBE). Thus, the harmonisation of LET_d calculations reduced the inter-centre differences in D_RBE substantially and the remaining variability was driven by the variability in absorbed dose.

4.3 Treatment plan comparisons in patient cases

Five institutions generated clinically acceptable robust treatment plans for all patient cases. All five institutions scored the LET according to the harmonised definition and provided the data in DICOM format (Table 4.4: methods I, IV, V, VI, VIII). Thus, 25 dose and LET

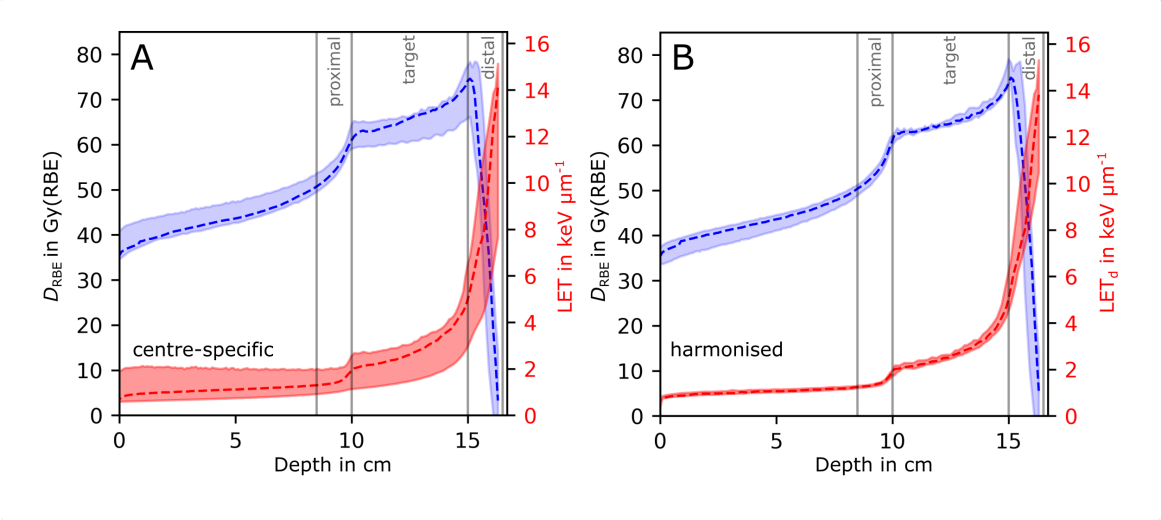

Figure 4.4: Line profiles from the six institutions along beam-central axis of the single-field spread-out Bragg peak for averaged linear energy transfer (LET, red, lower) and for variable relative biological effectiveness (RBE)-weighted dose (D_{RBE}, blue, upper) considering **A** centre-specific averaged LET and **B** harmonised dose-averaged LET_d. D_{RBE} was calculated with the RBE model from Wedenberg et al. (2013) with α/β of 2 Gy. Median (dashed) D_{RBE} and LET are shown together with their minimum and maximum values (shaded area) showing inter-institutional variability. Evaluation regions are indicated in grey. Adapted from (Hahn et al., 2022c), with permission from Taylor & Francis Group.

distributions were available for analyses.

$D_{98\%}$ above 95 % in the CTVs was met in the brain and prostate case, respectively (Figure 4.5). Target volume underdosages were tolerated in the base of skull, head and neck and pancreas patients to fulfil tolerance doses of adjacent OARs. Centre-wise dose- and volume-metrics did not exceed first priority OAR clinical goals by more than 0.6 Gy(RBE) and 0.4 percentage points, respectively.

4.3.1 Dose-averaged linear energy transfer for protons

LET_d distributions in the target volume were rather homogeneous and comparable between the centres (Figure 4.6). The median LET_d mean in the CTV_{low} from all centres over all plans was 2.5 keV µm^{-1} and ranged from 2.2 keV µm^{-1} to 3.1 keV µm^{-1}. Similar median values (2.4 keV µm^{-1}) and ranges (2.1 keV µm^{-1} to 3.3 keV µm^{-1}) were found in the CTV_{high}. Patient-wise inter-centre differences in the average LET_d in the target volumes were on median 0.2 keV µm^{-1} and ranged from 0.1 keV µm^{-1} to 0.7 keV µm^{-1}. Inter-centre variations, characterised by the normalised standard deviation (σ_n), in average LET_d of the target

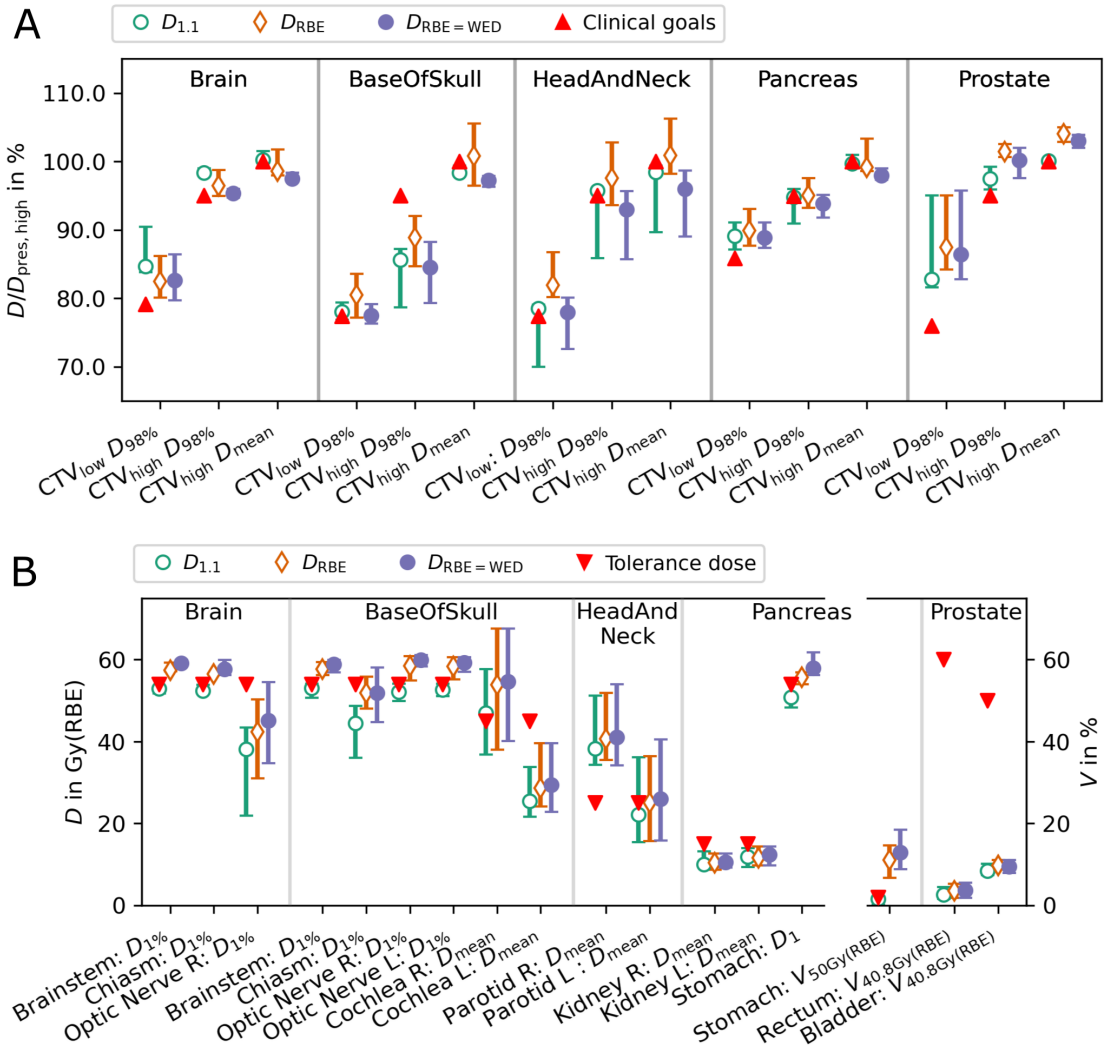

Figure 4.5: Dose-volume histogram values are shown for **A** clinical target volumes (CTV) of both prescription levels (CTV_{high}, CTV_{low}) relative to the prescribed high dose $D_{pres,high}$ and **B** for organs at risk in absolute dose. Each distribution contains the median (symbol) and range (whiskers) of all centre-wise dose-volume histogram statistics for all clinically acceptable treatment plans. For each structure, constant relative biological effectiveness (RBE) weighted dose ($D_{1.1}$, green), variable RBE-weighted dose using centre-specific models and tissue radiosensitivity (D_{RBE}, brown) and variable RBE-weighted dose using the Wedenberg RBE model with identical radiosensitivities at all centres ($D_{RBE=WED}$, blue) are shown. The red triangles indicate in subplot A the clinical goal for the target volume and in B the tolerance dose for each structure.

volumes were comparable for all patients and below 9.8 %.

LET_d was higher in OARs than in the target volumes (Figure 4.6). The largest near-maximum LET_d values occurred in patients with acute opening angles between incident

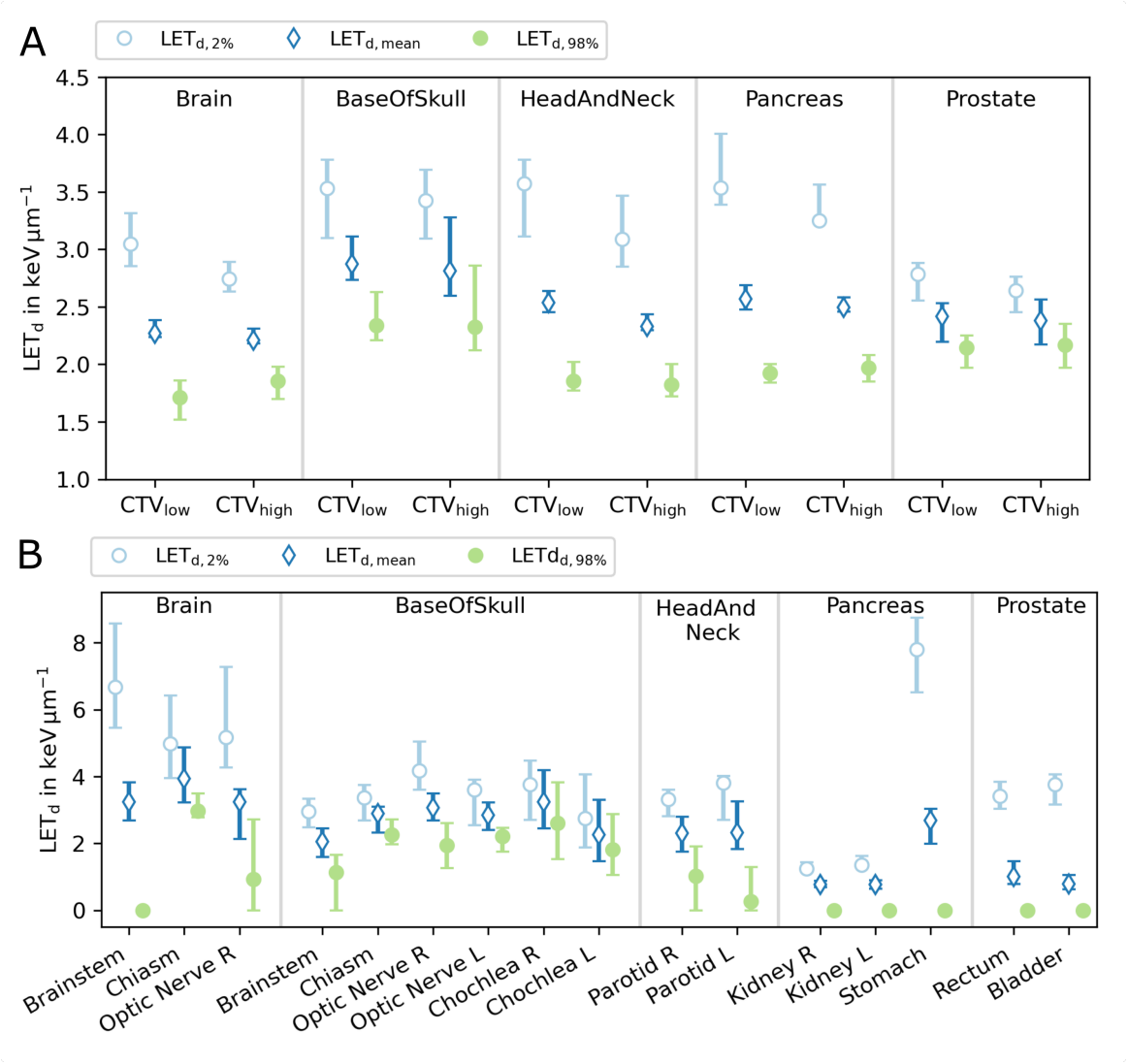

Figure 4.6: Dose-averaged linear energy transfer (LET$_d$) values are shown for **A** clinical target volumes of both prescription levels (CTV$_{high}$, CTV$_{low}$) and **B** organs at risk. Each distribution contains the median (symbol) and range (whiskers) of the centre-specific near-maximum, mean and near-minimum LET$_d$ (LETd$_{d,2\%}$, LET$_{d,mean}$, LET$_{d,98\%}$), respectively. Note the different scale of the y-axis in subplots A and B.

treatment fields and steep dose gradients (Table 4.2, Figure 4.6). Near-maximum LET$_d$ exceeded 8 keV µm^{-1} in the brain and pancreas case, while it remained below 5 keV µm^{-1} in the other entities. Centre-specific LET$_d$ volume histogram parameters in the OARs differed on median by 0.7 keV µm^{-1} and up to 3.1 keV µm^{-1}. Average LET$_d$ in OARs varied by 14.9 % (9.6 – 28.5 %). Similar inter-centre variations were observed for near-maximum LET$_d$ with inter-centre variations of 12.3 % (6.6 – 34.0 %).

Table 4.5: Centre-specific choices for variable relative biological effectiveness (RBE) models and tissue radiosensitivity α/β are shown for organs at risk (OAR) and the (internal) clinical target volumes (CTVs).

Site	RBE model	α/β in Gy					
		Brain CTVs	BoS CTVs	H & N CTVs	Panc. iCTVs	PCa iCTVs	OARs
Aarhus	McNamara et al. (2015)	10.0	3.5	3.5	10.0	2.5	3.0 2.0[§]
Dresden	Wedenberg et al. (2013)	10.0	10.0	10.0	10.0	2.0	2.0
Manchester	McMahon et al. (2018)	no α/β dependence					
Orsay	not provided	–					
Uppsala	Wedenberg et al. (2013)	10.0	10.0	10.0	10.0	1.5	3.0
harmonised	Wedenberg et al. (2013)	10.0	10.0	10.0	10.0	2.0	2.0

BoS: Base of skull. H & N: Head and neck. Panc: Pancreas. PCa: Prostate.
[§]: applied in the optic nerves, chiasm and spinal cord.

4.3.2 Centre-specific RBE models and parameters

D_{RBE} recalculations were reported by four of the five centres (Table 4.5). They all chose phenomenological *in-vitro* data based LET-driven RBE models with (3 centres) or without (1 centre) α/β dependency. The institutions considered generic α/β values for early (10 Gy) and late reacting tissue ($\approx$ 2 Gy), except for one centre, which chose more specific α/β values for the target volumes in the base of skull and head and neck case (Table 4.5).

Inter-centre variations in DVH parameters remained largely comparable when considering a variable RBE instead of a constant RBE. Exceptions to this were the $\mathrm{CTV}_{\mathrm{low}}$ $D_{98\%}$ of the base of skull case and $\mathrm{CTV}_{\mathrm{high}}$ mean dose of the base of skull case and prostate case, respectively ($p < 0.04$), where substantially different α/β values were considered (Table 4.5). Variations were in general small and increased significantly only for stomach $V_{50\,\mathrm{Gy(RBE)}}$ of the pancreas case ($p < 0.01$).

The use of the same RBE model and α/β at each centre reduced inter-centre variability in most cases and significantly for the mean dose to $\mathrm{CTV}_{\mathrm{high}}$ and $D_{98\%}$ to the $\mathrm{CTV}_{\mathrm{low}}$ in the base of skull as well as the stomach $V_{50\,\mathrm{Gy(RBE)}}$ of the pancreas case. Compared to variations in $D_{1.1}$, the remaining inter-centre variations were not significantly different in any OARs and only in mean dose in $\mathrm{CTV}_{\mathrm{high}}$ of the prostate case ($p < 0.02$) where an α/β of 2 Gy was considered.

4.4 Discussion

The current status of LET calculations and RBE modelling at European proton therapy institutions was assessed and their differences were quantified. The impact of centre-specific treatment planners, beam models, TPS and recalculation frameworks on LET recalculation was found to be low. Instead, differences in averaging technique and considered secondary particles in LET scoring were found to be the main contributors to inter-centre differences in LET calculations. To overcome the lack of a standard, it was commonly agreed to report the unrestricted dose-averaged LET to water or unit density tissue to mitigate the observed inconsistencies and harmonise the calculations and reporting. The observed inter-centre variability in D_{RBE} using the same LET definition was comparable to and mostly determined by that of the underlying absorbed dose. In other words, it is possible to obtain D_{RBE} and $D_{1.1}$ with equivalent precision, which enables consistent analysis and reporting of tumour control and side effects in view of a variable biological effect among proton therapy centres in upcoming studies.

In the first part of the water phantom study, proton therapy centres independently carried out LET calculations using individual LET definitions. In line with these findings, monocentric studies showing a spatial correlation of radiation-induced injury with elevated LET in brain tumour, breast tumour and chest-wall patients after proton therapy reported inconsistently on LET (Bahn et al., 2020; Eulitz et al., 2019b; Ödén et al., 2020; Peeler et al., 2016; Underwood et al., 2018; Wang et al., 2020). LET definitions differed particularly in reported averaging methods and secondary particle spectra. Additionally, a recent review observed highly inconsistent LET reporting in 354 studies quantifying RBE in *in-vitro* studies (Kalholm et al., 2021). However, the current RBE data basis is insufficient to identify the *correct* LET definition for proton therapy (Kalholm et al., 2021). Still, tools to visualise LET distributions in clinical practice are sought after (Heuchel et al., 2022) and are likely to be used before knowing which LET definition might be best suited (Wagenaar, 2022). Therefore, this multi-centric study aimed to suggest a harmonised LET calculation and reporting, that

1. is in line with current dose reporting,
2. is a meaningful input for LET-driven variable RBE models, and
3. can be calculated consistently among proton therapy centres.

This study found that the observed influence of institution-specific simulation software,

simulation settings, and beam model on LET variability was relatively small if the same treatment planning situation was planned by multiple proton therapy institutions and the same (harmonised) LET definition was considered.

Rationale for the proposed harmonised LET definition

In this multi-centric study, it was jointly proposed to report the unrestricted dose-averaged LET for all protons to water or to unit density tissue, which will be discussed in the following.

When calculating the averaged LET in a voxel, the kinetic energy of delta rays must be considered. The unrestricted LET includes the contribution of all secondary electrons in the energy lost. However, not all electrons produced might be absorbed locally, as their kinetic energy is large enough to leave the voxel, and thus might not contribute to the local RBE. This is considered in the restricted LET, where secondary delta-rays above a specified threshold kinetic energy are disregarded in local LET scoring (Seltzer et al., 2011), rendering the restricted LET sensitive to the cut-off energy selected (Deng et al., 2021). However, there is no evidence that restricted LET better correlates with RBE than unrestricted LET (Deng et al., 2021). At the end of range, the difference between unrestricted and restricted diminishes due to the short range of secondary electrons around the proton track (Bertolet et al., 2020). Furthermore, delta electron production is also often neglected in dose calculation, since the electron range remains below typically used voxelsizes of 2 mm for most of the treatment field. The unrestricted LET considered by all participating institutions thus appears as a reasonable and stable consideration.

Voxelwise averaging of the LET spectra is typically done by either dose- or track-averaging (Kalholm et al., 2021). Although no rigorous comparison exists between these two methods, LET_d is thought to better correlate with RBE than track-averaged linear energy transfer (LET_t) (Granville & Sawakuchi, 2015; Resch et al., 2020). LET_t may underestimate the biological effect (Deng et al., 2021), potentially due to the fact that a high-LET particle deposits more dose locally than a low-LET particle thus contributing more to the biological effect (McMahon et al., 2018). Most centres in this study chose dose- over track-averaging, which is in line with proton therapy institutions reporting mainly dose-averaged LET for in-vitro experiments (Kalholm et al., 2021) and clinical data (Underwood et al., 2022).

There is an active debate on which secondary particles to include in LET scoring in

proton therapy (Mairani et al., 2017). For conventional treatment planning in proton therapy, secondary protons originating from non-elastic nuclear interactions are the secondary particles that contribute most to the dose deposition (Paganetti, 2002). Accordingly, proton TPS typically include dose contributions from primary protons and later generations to avoid dose underestimation (Farr et al., 2021). For fragments heavier than protons, helium nuclei are the main contributors to biological effect (Paganetti, 2002). Due to their short range, the detection and measurement of these low energetic fragments is challenging and their biological relevance needs to be quantified more accurately (Bellinzona et al., 2021; Kalholm et al., 2021). Still, over 90 % of helium nuclei produced by a 160 MeV proton beam have ranges large enough to cross and inactivate cells and may thus contribute to the biological effect (Grassberger & Paganetti, 2011). However, these short ranged helium nuclei are mainly produced and absorbed in the entrance region of the beam into the body (Ödén, 2019), which is in line with the simulation data presenting the largest $\mathrm{LET_d}$ differences between all protons and $Z \leq 2$ for small penetration depth and low doses (Figure 4.3). Thus, neglecting the relatively small contribution of heavier particles to biological effect in proton therapy appears reasonable. Moreover, it is favourable to avoid mixing ion-types in RBE calculations since RBE as a function of LET depends on the ion-type, more specifically Z (Tian et al., 2022).

Reporting LET to water or to unit density tissue is consistent with reporting dose to water, as currently done in radiotherapy (Paganetti, 2009). This material independence takes into account that the main biological target in radiotherapy is the cell nucleus, which mainly consists of water, independent of the medium of the voxel (Grassberger & Paganetti, 2011). LET to unit density tissue minimises local material dependence by multiplying the LET to material with the density of water and dividing it by the local density, in accordance with the report of the American Association of Physicists in Medicine on proton RBE and other studies (Giantsoudi et al., 2013; Grassberger & Paganetti, 2011; Paganetti, 2014; Paganetti et al., 2019). In inhomogeneous patient geometries, the material independence smooths out LET spikes at boundaries between low- and high-density tissues (Grassberger & Paganetti, 2011) or when a more coarse dose grid overlaps with multiple CT voxels of different densities (Smith et al., 2021). Still, LET to material in unit density tissue is not exactly the same as LET to water. We found differences between the two definitions in air (and bone) in the order of 1.5 % or 0.01 $\mathrm{keV\,\mu m^{-1}}$ (and 5 % or 0.3 $\mathrm{keV\,\mu m^{-1}}$) for a monoenergetic proton beam of 100 MeV and 10 MeV, respectively.

LET_d values are influenced by the scoring technique used in the specific simulation (Granville & Sawakuchi, 2015). For the harmonised LET_d calculations in our study using the centre-specific simulation environments, LET was derived either by scoring the ratio of energy deposited along the simulation step and particle step length for each simulation step or by using the pre-step proton kinetic energy to derive the mean energy loss per unit path length in the material. Harmonisation of simulation protocols for LET_d by further specifying the scoring parameters, as recently suggested (Koh et al., 2020), may further standardise LET calculations across institutions. On the other hand, consistent reporting of LET by specifying averaging technique and secondary particle spectrum – both are typically easily available in LET simulations – resulted already in substantially increased inter-centre LET comparability. Therefore, an adaptation of the suggested harmonised LET_d calculations and reporting by other institutions appears feasible and could be the starting point for designing quality control that will be needed for clinical LET calculations and reporting in proton therapy.

LET benchmarking and input for variable RBE models

MC engines from RayStation and GEANT4 (as implemented in TOPAS and GATE) were previously benchmarked against independent MC simulations of LET_d as well as measurements of their microdosimetrical equivalent mean lineal energy (Tran et al., 2017; Wagenaar et al., 2020). Here, RayStation- and GEANT4-based simulations provided consistent results with one another and other simulation environments in terms of harmonised LET_d. However, the present inter-centre LET comparison does not replace the validation of a site-specific implementation of LET_d calculations (Granville & Sawakuchi, 2015; Wagenaar et al., 2020).

The LET definition used as input parameter when applying an LET-driven RBE model should coincide with the definition considered in model construction (Grzanka et al., 2018). However, model parameters for several phenomenological RBE models were fitted to *in-vitro* data from multiple experimental publications with various inconsistent LET definitions (Kalholm et al., 2021). Therefore, there typically exists no 'correct' LET to be used for these RBE models. An exception to the mixed reporting of underlying LET data is the model from McNamara et al. (2015), which is solely based on retrospectively simulated dose-averaged LET using the reported proton range and modulation width for all experiments (Paganetti,

2014). As range and modulation cannot be used to fully characterise the treatment field and all simulations were based on the beam model from the Massachusetts General Hospital, the McNamara model also underlies uncertainties. The inconsistent LET data used in *in-vitro* RBE models further underline the need for harmonised LET reporting. To overcome this limitation and to allow for an application in patient treatment, it is recommended to update the current parameters of empirical models based on a consistent analysis of patient instead of pre-clinical response data – as recently requested by the European Particle Therapy Network (Sørensen et al., 2021).

Inter-centre comparability and data storage

When using the same variable RBE model, LET_d definition and α/β, inter-institutional variability in reported DVH parameters remained comparable to that with a constant RBE. A variable RBE increased inter-centre variability by only about 1 percent point in patient target volumes. Similarly, an increase below 1.5 percent points was observed in all but two reported OAR DVH parameters, i.e. stomach $V_{50\,\text{Gy(RBE)}}$ for the pancreas case and $D_{1\%}$ in the right optic nerve of the brain case. These findings are compatible with the recently postulated requirement prior to using LET_d for RBE-weighted dose calculations (Wagenaar et al., 2020), suggesting that LET_d inaccuracy should impact the average D_RBE in the target volume by less than 1 %. The remaining increase in inter-centre variability from using a constant RBE of 1.1 to harmonised D_RBE calculations, appears remarkably low, given that different beam models, robust optimisation algorithms, planning systems, LET simulation environments, scoring techniques and individually optimised treatment plans were used among the institutions. Thus, the remaining inter-centre D_RBE variability was driven by the variability in absorbed dose. The observed high inter-institutional agreement in harmonised D_RBE suggests the conceptual feasibility of multi-centric studies to derive clinical tumour RBE data and NTCP models with increased total patient numbers.

Six out of eight centres were able to convert their LET and D_RBE simulation data to DICOM format for both non-TPS MC engines and non-clinical research versions of commercially available TPS. Firstly, this enables consistent archiving of both dose and LET_d data for upcoming patient outcome analysis on clinical RBE (Sørensen et al., 2021; Toma-Dasu et al., 2020). Secondly, making LET distributions accessible in a clinical setting further informs clinicians on treatment plan safety in view of a variable RBE (Paganetti et al., 2019).

Thirdly, sharing LET and D_{RBE} in a consistent data format (i.e., DICOM) allows for inter-centre comparisons and finding a consensus on what may be regarded as safe in clinical treatment planning. In this regard, it is of utmost importance to report the RBE model and input parameters considered as well as an unambiguous description of the LET definition, i.e. including information on the averaging, included particles, medium and density normalisation (Kalholm et al., 2021). Still, it remains a critical task to collectively agree on how to utilise variable RBE models in clinical practise to ensure future comparability of results between proton therapy centres and to realise the full potential of proton radiotherapy.

4.5 Summary

A harmonisation of LET reporting was jointly proposed among eight European proton therapy institutions to overcome the existing inter-centre differences in reporting LET with respect to averaging methods and secondary particle spectra. Scoring the unrestricted dose-averaged LET for all protons to water or to unit density tissue is in line with current absorbed dose reporting, a meaningful input for variable RBE models and could be calculated consistently among proton therapy centres. Other centre-specific factors such as beam characteristics and calculation settings had a minor impact. Thereby, harmonised LET reporting reduced inter-centre variability in LET and RBE reporting to a clinically acceptable level and can be easily adapted by other proton therapy centres. This allows for consistent analysis and reporting of tumour control and side effects after proton therapy in view of a variable biological effect. The harmonisation of LET reporting may help to compare and combine outcome data from different proton therapy institutions thereby complementing the currently scarce and inconsistently reported outcome data. In this way, harmonising LET reporting contributes to a more rapid and reliable implementation of variable RBE in proton therapy and may help to exploit the full potential of proton beam therapy. This may become even more important when including LET in treatment plan optimisation.

5 Biological treatment plan optimisation

Proton therapy centres consider RBE variability mainly in OARs and not in the tumour volume. For most tumours and for normalfractionated treatments, a constant RBE of 1.1 is chosen conservatively to avoid tumour underdosage, although caution is warranted for tumours with low α/β and small modulation widths (Paganetti et al., 2019). For OARs, proton therapy centres strive to mitigate variable RBE-induced dose burden therein mainly by special beam angle considerations (Heuchel et al., 2022). However, this and other clinically available forward-based planning strategies such as spot-location restrictions, increasing the number of treatment fields, range shifter usage for larger spot sizes or decreasing the degree of intensity-modulation do not represent effective planning strategies to counteract RBE-induced overdosages (Faught et al., 2022), since the LET and RBE are not included in the plan optimisation process. Additionally, current clinical treatment planning strategies do not provide the means to actively account for LET_d or different tissue-specific radiosensitivities, let alone their complex interplay (Bauer et al., 2021). For an effective risk reduction in view of a variable RBE, this urges the exploration of novel plan optimisation approaches beyond the clinically used absorbed dose and the assumption of a constant RBE.

In IMPT, the host of (pristine) Bragg peaks placed in the patient by each treatment field allows to produce multiple dosimetrically equivalent solutions to a patient-specific optimisation problem (Lomax, 1999). This plan degeneracy can be used to actively influence the LET_d distribution, and thus RBE, without significantly altering the absorbed dose in the same anatomical region (Grassberger et al., 2011). Proton treatment plan optimisation approaches beyond absorbed dose were studied by multiple groups and include the optimisation of LET_d (An et al., 2017; Cao et al., 2017; Giantsoudi et al., 2013; Liu et al., 2020; Unkelbach et al., 2016), variable RBE with different *in-vitro* data based models (Henjum et al., 2021; Sánchez-Parcerisa et al., 2019) or proton track-end fractions (Traneus & Ödén, 2019). However, it is unclear which of the presented novel optimisation approaches performs best under clinically relevant conditions. Additionally, it requires optimisation approaches in line with current clinical practice to allow for translating these approaches into

clinical studies.

In this chapter, four optimisation strategies beyond absorbed dose are introduced and compared among each other and with the conventional absorbed dose-based optimisation. Treatment plans are designed in line with current clinical practice and aim to reduce D_{RBE} in OAR, while maintaining clinical plan quality with a constant RBE. This study aims towards safely translating optimisation with variable RBE into clinical practice. Large parts of the work presented in this chapter were presented at a conference (Hahn et al., 2022b) and have been published (Hahn et al., 2022a).

5.1 Treatment plan design

This study included ten patients with primary cranial tumour with at least one serial OAR adjacent to the CTV (Table 5.1), who previously underwent IMPT at WPE. Patient data usage was covered by an ethics approval of prospective clinical trials (German Clinical Trial Register: DRKS00004384, DRKS00005363). Prescribed median doses to the CTVs were 54 Gy(RBE) or higher, using a constant RBE of 1.1 (Table 5.1).

PBS treatment plan optimisation was based on the clinical beam model, machine parameters and commissioned beam line objects for the IBA Proteus Plus (IBA PT, Louvain-la-Neuve, Belgium) installed at WPE. PBS treatment plans were created with MFO and the clinically used three treatment fields and angles for each patient. The PTV, defined as 5 mm isotropic expansion of the CTV, was used in treatment planning to account for range and setup uncertainties of 3.5 % and 2 mm, respectively. SIB concept was used for patients with two dose levels to a higher ($\mathrm{CTV_{high}}$) and lower ($\mathrm{CTV_{low}}$) dose target volume, respectively (Table 5.1). The treatment field configurations used clinically for that patient were considered for both the constant RBE-weighted dose optimisation (DOSEopt) reference treatment plans and the plans using biological effectiveness guided optimisation (BGopt), respectively (Table 5.1). Robust optimisation was not available for BGopt at the time of this study. Therefore, the DOSEopt reference treatment plans were created using the objectives from the clinically delivered and robust dose optimised treatment plan as starting point in optimisation to allow for a fair comparison with non-robust BGopt treatment plans. Treatment plan optimisation was done with the research version of RayStation (v8.99.30).

Five treatment plans were created per patient. The DOSEopt plan aimed to achieve the

Table 5.1: Patient and treatment planning characteristics for plan optimisation beyond dose.

Case	Diagnosis	Prescribed median dose in Gy(RBE)		Fx	Critical OAR	Field angles in °	
		CTV_{high}	CTV_{low}			Gantry	Couch
1	Meningioma	54.00	–	30	Brainstem	90 120 70	310 0 0
2	Glioneuronal tumour (relapse)	54.00	–	30	Opticus R+L Chiasm Brainstem	90 120 70	350 320 180
3	Meningioma	54.00	–	30	Opticus R+L Chiasm Brainstem	90 90 90	350 320 180
4	Meningioma	54.00	–	30	Opticus L Chiasm Brainstem	90 90 90	0 320 270
5	Meningioma	54.00	–	30	Opticus R+L Chiasm Brainstem	290 240 90	0 0 0
6	Chondrosarcoma	69.30	54.45	33	Opticus R+L Chiasm Brainstem	90 90 90	190 350 250
7	Adeonoidcystic carcinoma	70.00	63.00	35	Opticus L Chiasm Brainstem	240 25 105	10 0 0
8	Clivus Chordoma	73.50	56.00	35	Opticus R+L Chiasm Brainstem	60 120 270	0 0 0
9	Chordoma	73.50	56.00	35	Opticus R+L Chiasm Brainstem	100 55 240	355 290 0
10	Clivus Chordoma	73.50	56.00	35	Opticus R+L Chiasm Brainstem	100 250 60	0 5 0

CTV: Clinical target volume. Fx: Number of fractions. L: Left. OAR: Organ at risk. R: Right.

optimal absorbed dose distribution for each patient and did not consider any variable RBE-related objectives in plan optimisation. The four BGopt treatment plans were designed to satisfy two criteria. Firstly, the absorbed dose distribution of BGopt plans should be similar to that in DOSEopt, since the latter encompasses the optimal absorbed dose distribution for that patient. Secondly, the BGopt aimed to reduce D_{RBE} to selected OARs.

Therefore, the BGopt treatment plans were created to reduce D_{RBE} in dose-limiting serial OARs (Table 5.1), while keeping $D_{1.1}$ to the CTVs comparable to the corresponding DOSEopt reference plan. First, reference treatment plans were created with DOSEopt using solely DVH based objectives for absorbed dose times a constant RBE of 1.1 that fulfil the clinical dose volume goals. Second, the weights and levels of the $D_{1.1}$-based objectives found with DOSEopt were transferred without modification to the optimisation of the BGopt treatment plans. Third, for each plan using BGopt, specific objective functions beyond $D_{1.1}$ were added to reduce D_{RBE} to dose-limiting serial OARs close to the target volume, hereafter termed critical OARs (Table 5.1). To allow for a D_{RBE} reduction through a redistribution of stopping protons, a small increase in mean $D_{1.1}$ to healthy brain tissue is expected in BGopt compared to DOSEopt. This increase was kept below 3 %, in accordance with similar previous studies (Traneus & Ödén, 2019; Unkelbach et al., 2016). A statistical MC uncertainty of 0.5 % was used for the final dose calculation in all treatment plans.

5.1.1 Clinical goals

Treatment plans were deemed clinically acceptable when their $D_{1.1}$ distribution complied with the following dose-volume goals. CTV coverage was defined relative to their prescription dose with $D_{50\%}$ of 100 % and $D_{95\%}$ above 95 %. Near-maximum and near-minimum doses were defined as the dose to 1 % and 99 % of the volume of interest, respectively. For patients with prescribed dose of 54 Gy(RBE) to the primary CTV ($\mathrm{CTV_{high}}$, Table 1), $D_{1\%}$ tolerance doses to the brainstem and optical apparatus were 54 Gy(RBE). For patients with higher prescription doses to the $\mathrm{CTV_{high}}$, doses up to 60 Gy(RBE) were tolerated in the optical structures (Mayo et al., 2010a). Similarly for these patients, higher brainstem doses were tolerated if the dose to the brainstem core, defined as a 4 mm circular ROI in the geometric centre of the brainstem, did not exceed 54 Gy(RBE) (Lambrecht et al., 2018). Doses to other healthy tissue were kept as low as reasonably achievable (Bentzen et al., 2010).

Treatment plan quality was defined by dose coverage ($D_{95\%} > 95\,\%$) and robustness in the CTV, dose conformity and dose homogeneity in the PTV as well as adherence to OAR tolerance dose. It was assessed for all DOSEopt and BGopt plans based on their respective $D_{1.1}$ distribution. Dose conformity index and dose homogeneity index for $D_{1.1}$ were quantified with:

$$\mathrm{CI} = \frac{V_{\mathrm{PTV}}(\text{covered by } 95\,\%\text{ isodose})}{V_{95\,\%\text{isodose}}} \tag{5.1}$$

and

$$\mathrm{HI} = \left(\frac{D_{2\,\%}}{D_{98\,\%}}\right)_{\mathrm{PTV}} \quad , \tag{5.2}$$

with V being the volume of interest. Robustness analysis based on $D_{1.1}$ distributions was performed for all DOSEopt and BGopt plans with twelve scenarios for each treatment plan considering $\pm 3.5\,\%$ density uncertainty and an isotropic setup uncertainty of $\pm 2\,\mathrm{mm}$ along the cardinal directions in the patient coordinate system, for which the percentage of scenarios passing $D_{95\%}$ above 95 % in the CTV was assessed.

5.1.2 Novel treatment plan optimisation approaches

Four different BGopt treatment plans were created for each patient using physical to biological optimisation approaches of variable RBE-driving factors and covered the optimisation of one of the following quantities:

- proton track-end distributions (TEopt),
- proton dose-averaged LET in voxels above a dose threshold (LETopt),
- dose contributed by high-LET protons, i.e. dirty dose (DDopt), or
- variable RBE-weighted dose (DRBEopt).

Proton track-ends were defined as the location where protons stop, i.e. the voxel where the proton transport was terminated. Track-end optimisation (TEopt) exploits that the maximum of the proton track-end depth distribution spatially correlates with the absorbed dose maximum and elevated $\mathrm{LET_d}$ area (Figure 5.1). Thereby, it intrinsically focusses on areas with elevated D_{RBE} and thus elevated biological effect. In TEopt, the track-end fraction, defined as the number of track-ends in the ROI divided by the total number of track-ends in the patient, was minimised within the ROI. TEopt objectives acted on primary protons and aimed to reduce the track-end fraction in the critical OARs. Here, a reduction of track-end fractions in critical OARs by 50% relative to those in the corresponding DOSEopt plan was applied to all patients.

$\mathrm{LET_d}$ optimisation (LETopt) minimises the $\mathrm{LET_d}$, which is a dose-weighted mean value of the LET-spectrum within a voxel. LETopt requires a sensible weighting with local absorbed dose to effectively reduce D_{RBE}, since the highest $\mathrm{LET_d}$ values usually occur in volumes

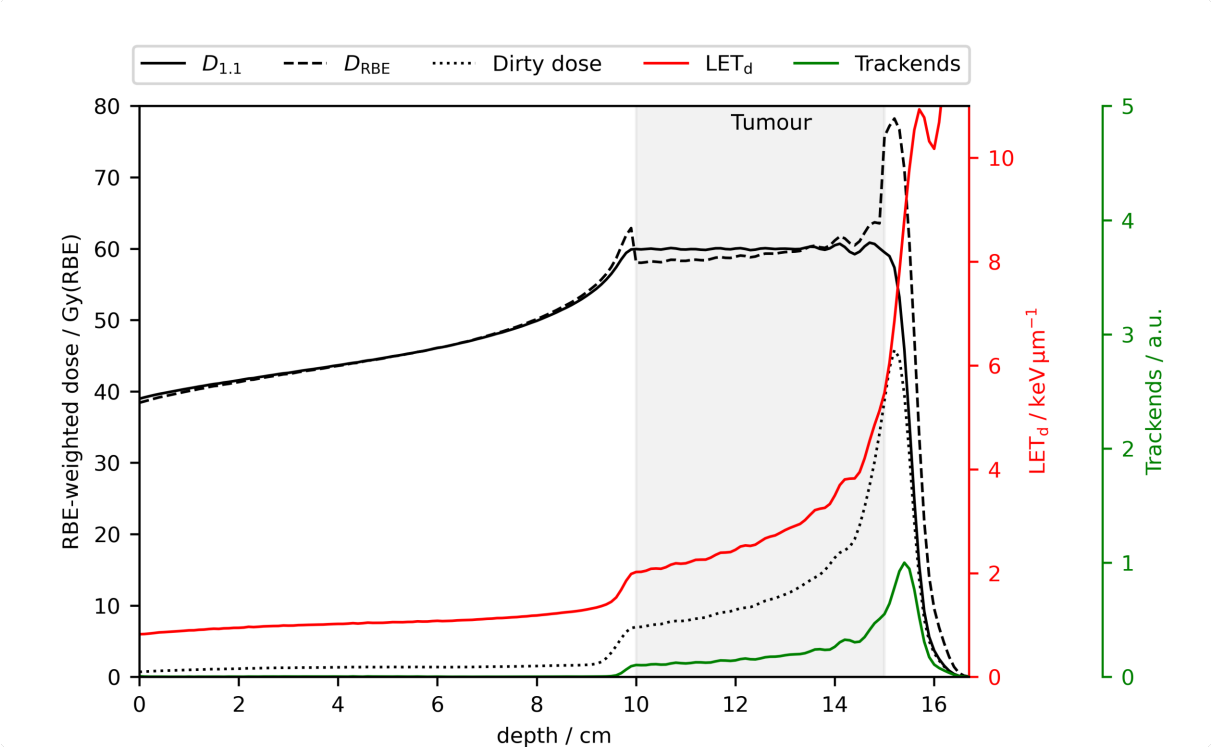

Figure 5.1: Lineprofiles for a spread-out Bragg peak that homogeneously covers the tumour volume with a constant relative biological effectiveness (RBE) weighted dose ($D_{1.1}$). Variable RBE-weighted dose (D_{RBE}) was recalculated with the RBE model from Wedenberg et al. (2013) and an α/β of 10 Gy in the tumour and 2 Gy otherwise. Additionally, the proton dose-averaged linear energy transfer (LET_d), the trackends of primary protons and the dose contributed by high LET protons ($>$2.5 keV µm^{-1}, dirty dose) were scored. All these quantities are eligible to reduce D_{RBE} at the end of proton range when included in treatment plan optimisation.

of negligible dose and are biologically irrelevant (Figure 5.1). Therefore in LETopt, LET_d values above a set LET_d level were only penalised in voxels with a dose above a user-specified threshold. Here, LET_d values above 2.5 keV µm^{-1} were penalised in critical OARs but only in voxels with $D_{1.1}$ above 40 Gy(RBE). These levels were derived from reported mean $D_{1.1}$ and mean LET_d levels observed in toxicity volumes on MRI after cranial proton therapy (Bahn et al., 2020; Bertolet et al., 2022; Garbacz et al., 2021; Giantsoudi et al., 2016; Niemierko et al., 2021; Ödén et al., 2020). Additionally, 90 % of voxels developing RIBI showed doses of more than 40 Gy(RBE) in the region of signal abnormalities (Eulitz, 2021).

The dirty dose optimisation (DDopt) objective is designed to penalise dose depositions from individual protons with an LET above a set LET threshold. The total absorbed dose in each voxel was separated in two categories: the absorbed dose deposited by individual

protons with LET above the LET threshold (dirty dose) and that below the LET threshold (clean dose). Typically, the dirty dose portions of each treatment field are located at the distal field edge (Figure 5.1). DDopt is a dose-optimisation approach where only the dirty dose portion, contributed by high LET protons, is minimised. In this thesis, the absorbed dose contributed by protons with an LET above 2.5 keV µm^{-1} in critical OAR was considered as dirty dose and reduced in critical OARs. A reduction of near-maximum dirty dose ($D_{1\%}$) in critical OARs by 50% relative to those in the corresponding DOSEopt plan was applied. This study was the first to report on the application of dirty dose optimisation in a larger patient cohort.

Variable RBE-weighted dose optimisation (DRBEopt) minimises the product of total absorbed dose and variable RBE in OARs (Figure 5.1). Thus, absorbed dose or variable RBE or both can be optimised in order to lower the D_{RBE} in the OARs. DRBEopt used the variable RBE model from Wedenberg et al. (2013) with an α/β of 2 Gy in the critical OARs and the proton dose and $\mathrm{LET_d}$ as input parameters. Objective levels for RBE-weighted dose applied in DRBEopt with a variable RBE were identical to the $D_{1.1}$ levels applied in the corresponding DOSEopt plan.

During BGopt, track-end fractions, $\mathrm{LET_d}$, dirty dose or D_{RBE} were scored voxelwise and were consequently minimised within all critical OARs of the patient. Each of the BG objectives was added as quadratic penalty function to the standard composite objective function in the research TPS for critical OARs. All BGopt objectives were implemented as maximum objectives meaning that a penalty is applied when a certain quantity is above a user-specified threshold value.

All treatment plans were recalculated with the RBE model from Wedenberg et al. (2013) to quantify their potential of reducing D_{RBE} to critical OAR. Model input parameters were α/β of 10 Gy in the CTVs, 2 Gy otherwise (Lambrecht et al., 2018) and proton $\mathrm{LET_d}$. All OARs were assumed free of tumour cells. The relative seriality model (Källman et al., 1992) was used to estimate NTCP for D_{RBE} distributions with equivalent doses delivered in 2 Gy fractions using an α/β of 2 Gy. NTCP values were determined for brainstem necrosis and blindness in the optical structures using variable RBE-weighted doses and model parameters of relative seriality $s = 1$, $\gamma = 2.4$, $TD_{50} = 65.1$ Gy(RBE) and $s = 1$, $\gamma = 2.5$, $TD_{50} = 65.0$ Gy(RBE), respectively (Ågren Cronqvist, 1995), and denoted as NTCP(D_{RBE}). Intra-patient differences in $D_{1.1}$, $\mathrm{LET_d}$, D_{RBE} and NTCP(D_{RBE}) between the one DOSEopt and the four BGopt plans were derived and statistically tested with a Wilcoxon signed-rank

test on a significance level of 0.05.

5.2 Treatment plan quality assessment with a constant RBE

All 50 patient treatment plans featured clinically acceptable and deliverable $D_{1.1}$ distributions (Figure 5.2). $D_{1.1}$ distributions were conformal to and homogeneous in the PTV, with average (range) HI of 0.87 (0.73 – 0.95) and CI of 0.91 (0.78 – 1.00), respectively. All treatment plans adhered to the respective CTV prescription doses (Figure 5.3) with average (range) $D_{50\%}$ to the CTV_{high} of 99.8 % (99.1 – 100.1 %) and $D_{95\%}$ to the CTV_{high} and CTV_{low} of 96.4 % (84.9 – 99.0 %) and 99.6 % (99.4 – 102.8 %), respectively (Figure 5.3). Minor intra-patient differences between DOSEopt and BGopt plans were found in CTV coverage [$\Delta D_{50\%} < 0.1$ Gy(RBE), $\Delta D_{95\%} < 1.4$ Gy(RBE)] as well as PTV homogeneity (ΔHI < 0.04) and conformity (ΔCI < 0.07). For patients 8 and 10, CTV coverage and PTV homogeneity were compromised in all plans to fulfill tolerance doses of overlapping critical OARs (Figures 5.2, 5.3). Increases in mean $D_{1.1}$ to the healthy brain tissue by BGopt were below 3.0 %. For all treatment plans and patients, near-maximum $D_{1.1}$ values in the brainstem, brainstem core and optical apparatus complied with the clinical goals.

Robust CTV coverage was achieved with DOSEopt and BGopt. Overall, $D_{95\%}$ above 95 % in the CTV was fulfilled by on average (range) 96 % (67 – 100 %) and 94 % (75 – 100 %) uncertainty scenarios in the DOSEopt and BGopt treatment plans, respectively. In patients with prescription doses above 54 Gy(RBE), slightly but systematically worse robustness was found for DRBEopt (average: 92 %) than the other BGopt strategies (average: >97 %).

5.3 Assessment of NTCP reductions with a variable RBE

BGopt systematically reduced D_{RBE} and corresponding NTCP to OARs compared to DOSEopt treatment plans (Table 5.2). Using a variable RBE for dose evaluation in the DOSEopt plans, OAR tolerance doses were exceeded in more than 86 % of the cases. Additionally, NTCP(D_{RBE}) for brainstem necrosis and blindness increased in the optical apparatus to on average above 6.6 % and 9.7 %, respectively (Table 5.2). BGopt reduced near-maximum D_{RBE} by up to 8.3 Gy(RBE). The observed D_{RBE} reductions in critical OARs with BGopt translated into significant average (range) NTCP(D_{RBE}) reductions in brainstem

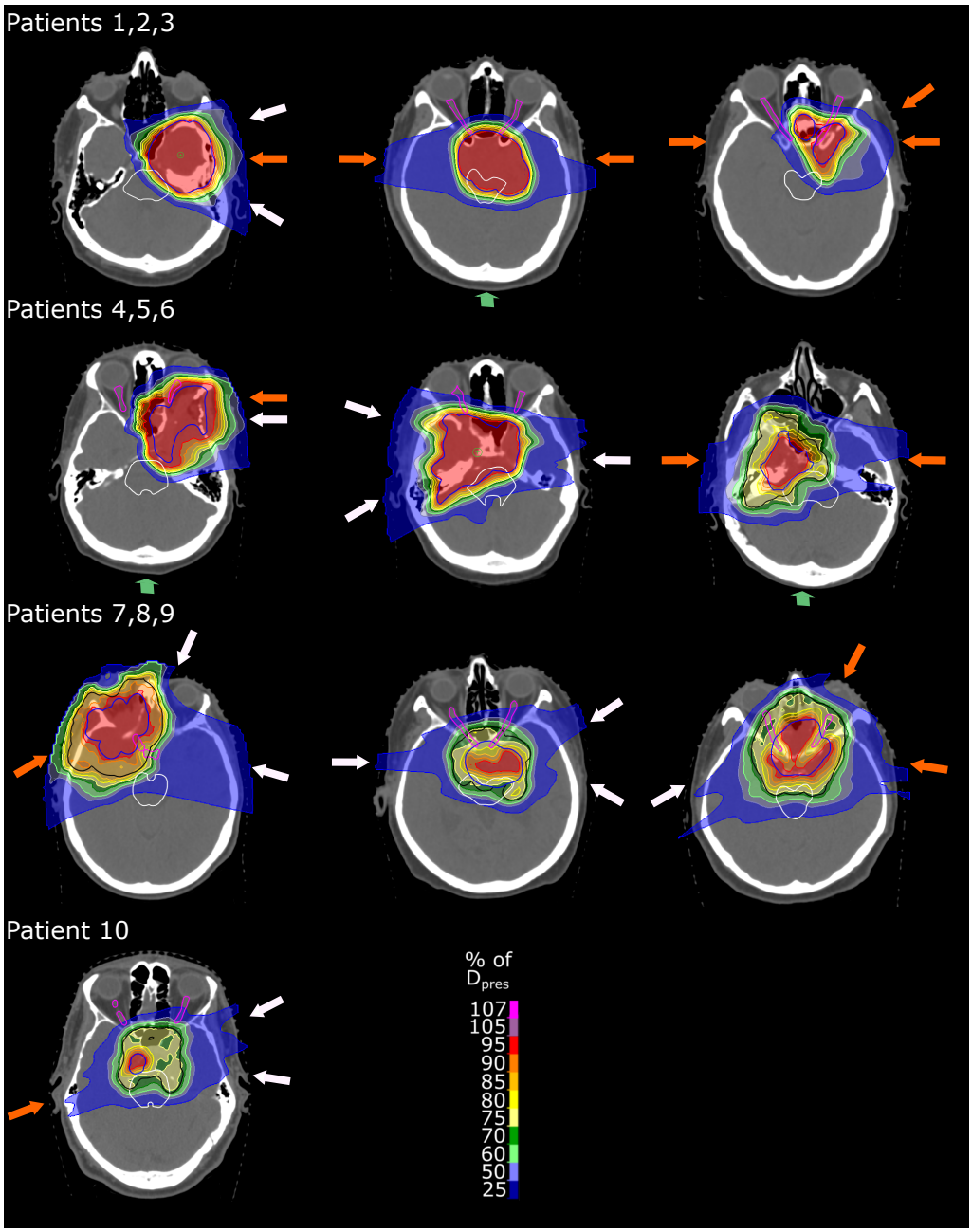

Figure 5.2: Constant relative biological effectiveness weighted dose distributions of the dose-only optimised reference plans in representative computed tomography slices for patients one to ten. Isodoses are displayed relative to the prescription dose to the primary (high-dose) clinical target volume. Arrows depict coplanar (white) and non-coplanar beams (orange) as well as beams passing through the skullcap (green), respectively. Contours show the primary (high-dose) planning target volume (PTV, blue), secondary (low-dose) PTV (black), brainstem (white) and both optic nerves and chiasm (all magenta). Reproduced from (Hahn et al., 2022a), with permission from Springer Nature.

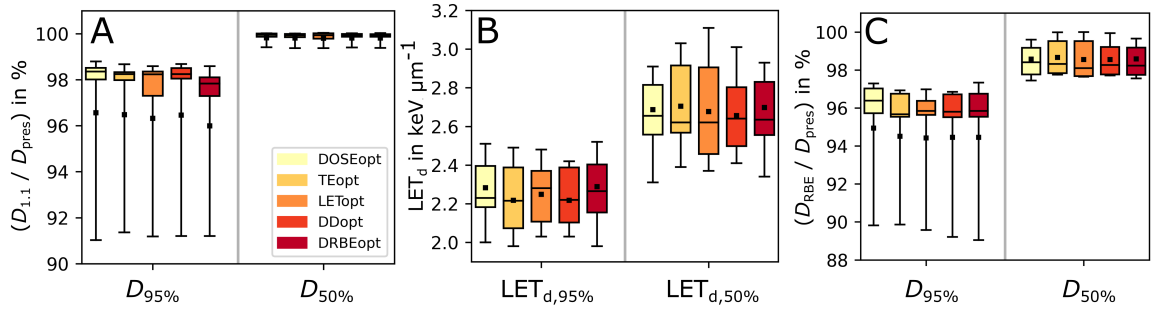

Figure 5.3: Each boxplot contains near-minimum (95 %) or median (50 %) values of all patients in the primary clinical target volume (CTV_{high}). Volume histogram parameters for **A** absorbed dose-weighted with a constant relative biological effectiveness of 1.1 ($D_{1.1}$) **B** dose-averaged linear energy transfer (LET_d) and **C** variable RBE-weighted dose (D_{RBE}). Doses were normalised to their prescription dose (D_{pres}). Abbreviations: optimisation with dose only (DOSEopt), trackends (TEopt), LET_d with dose threshold (LETopt), dirty dose (DDopt) and D_{RBE} (DRBEopt) are shown. Adapted from (Hahn et al., 2022a), with permission from Springer Nature.

necrosis and blindness of 47.4 % (33.3 – 63.9 %) and ranged from 2.2 to 10.7 percentage points (Table 5.2). The highest NTCP(D_{RBE}) reductions were achieved in patients with high initial NTCP(D_{RBE}) in the DOSEopt plans and none of the BGopt strategies was systematically superior. In the CTV, DOSEopt and BGopt treatment plans showed similar absorbed dose and LET_d distributions and D_{RBE} differed by less than 0.3 Gy(RBE) in $D_{95\%}$ and $D_{50\%}$, respectively (Figure 5.3).

BGopt achieved D_{RBE} reductions in critical OARs by altering the absorbed dose, LET_d or both therein (Figure 5.4). TEopt, LETopt and DDopt treatment plans did not significantly alter the mean absorbed dose in any critical OAR compared to DOSEopt treatment plans ($p > 0.05$). These three physical strategies reduced mean and near-maximum LET_d on average by 0.5 keV µm^{-1} and 0.8 keV µm^{-1} in OARs, respectively, which in both LET_d parameters was significantly lower than DOSEopt for three of four critical OARs. In contrast, the DRBEopt approach primarily reduced the mean and near-maximum absorbed dose to critical OARs by on average 2.0 Gy and 2.2 Gy, respectively ($p < 0.05$, Figure 5.4). Accordingly, these absorbed dose values were significantly lower in DRBEopt than for DOSEopt for all but one comparison. No significant LET_d reduction was observed for DRBEopt where minor changes in mean and near-maximum LET_d and average differences remained below 0.1 keV µm^{-1}.

Figure 5.5 illustrates the effect of BGopt for one exemplary patient case. D_{RBE} reduc-

Table 5.2: Normal tissue complication probabilities (NTCPs) for necrosis and blindness in the dose-only optimised (DOSEopt) treatment plans and the NTCP reductions achieved by optimisation strategies beyond dose. Group 1 includes patients with prescription doses of 54 Gy(RBE) and group 2 with higher prescription doses, respectively.

OAR Endpoint	**Group**	**Mean (range) NTCP** NTCP(D_{RBE}) / %	**Mean (range) NTCP reduction** $\triangle$NTCP(D_{RBE}) to DOSEopt / percentage points			
		DOSEopt	TEopt	LETopt	DDopt	DRBEopt
Brainstem Necrosis	All	6.6 (0.7–18.0)	3.0 * (0.5–8.6)	2.6 * (0.4–8.0)	2.5 * (0.6–6.0)	2.2 * (0.2–7.0)
	Group 1	2.6 (0.7–4.8)	1.5 (0.5–2.3)	1.4 (0.5–2.3)	1.4 (0.6–2.1)	1.0 (0.2–2.2)
	Group 2	10.6 (1.0–18.0)	4.5 (0.5–8.6)	3.8 (0.4–8.0)	3.6 (0.7–6.0)	3.5 (0.5–7.0)
Chiasm Blindness	All	16.8 (11.0–22.0)	8.8 * (4.5–16.9)	7.7 * (2.0–16.8)	9.5 * (4.5–16.2)	10.7 * (1.0–18.4)
	Group 1	16.3 (11.0–21.0)	6.1 (4.6–16.9)	6.1 (2.0–16.8)	5.7 (4.5–16.2)	7.1 (2.0–16.2)
	Group 2	17.2 (12.0–22.0)	7.8 (4.5–10.7)	5.7 (2.3–8.0)	8.6 (4.9–10.9)	11.9 (1.0–18.4)
Opticus R Blindness	All	9.7 (0.2–20.0)	5.3 * (0.2–9.0)	5.3 * (0.2–10.4)	4.9 * (0.2–10.0)	3.7 * (0.1–16.5)
	Group 1	5.4 (0.2–9.3)	2.0 (0.2–3.0)	2.8 (0.2–6.1)	2.8 (0.2–5.4)	1.7 (0.1–3.0)
	Group 2	13.0 (5.4–20.0)	6.2 (3.0–9.0)	5.6 (2.9–10.4)	6.4 (3.6–10.0)	9.2 (2.8–16.5)
Opticus L Blindness	All	11.2 (1.0–30.0)	5.2 * (0.5–15.0)	4.8 * (0.5–15.0)	4.9 * (0.6–13.0)	6.0 * (1.0–17.3)
	Group 1	13.5 (6.2–30.0)	6.5 (2.8–15.0)	6.6 (3.6–15.0)	6.4 (2.8–13.0)	5.7 (2.8–13.0)
	Group 2	9.3 (1.0–27.0)	4.2 (0.5–12.0)	3.3 (0.5–8.0)	3.8 (0.6–9.0)	6.2 (1.0–17.3)

*$p < 0.05$ tested with Wilcoxon signed-rank test for group 'all patients'. OAR: organ at risk. D_{RBE}: absorbed dose weighted with a variable RBE. TEopt: track-end optimisation. DDopt: dirty dose optimisation. LETopt: $\mathrm{LET_d}$ optimisation. DRBEopt: variable RBE-weighted dose optimisation. R: right. L: left.

tions in critical OARs were realised by a redistribution of stopping protons, thus proton track-ends, to areas that were not included in BGopt (Figure 5.5). Initially with DOSEopt, proton track-ends were placed at the PTV border to produce steep absorbed dose gradients to fulfill the tolerance dose of adjacent OARs. This causes areas with $\mathrm{LET_d}$ above 2.5 keV µm^{-1} in and around the critical OARs. TEopt, LETopt and DDopt redistributed track-ends from the critical OARs to the PTV and healthy brain tissue, which were not subject to BGopt objectives, and thereby largely reduced $\mathrm{LET_d}$ in all critical OARs. TEopt strictly

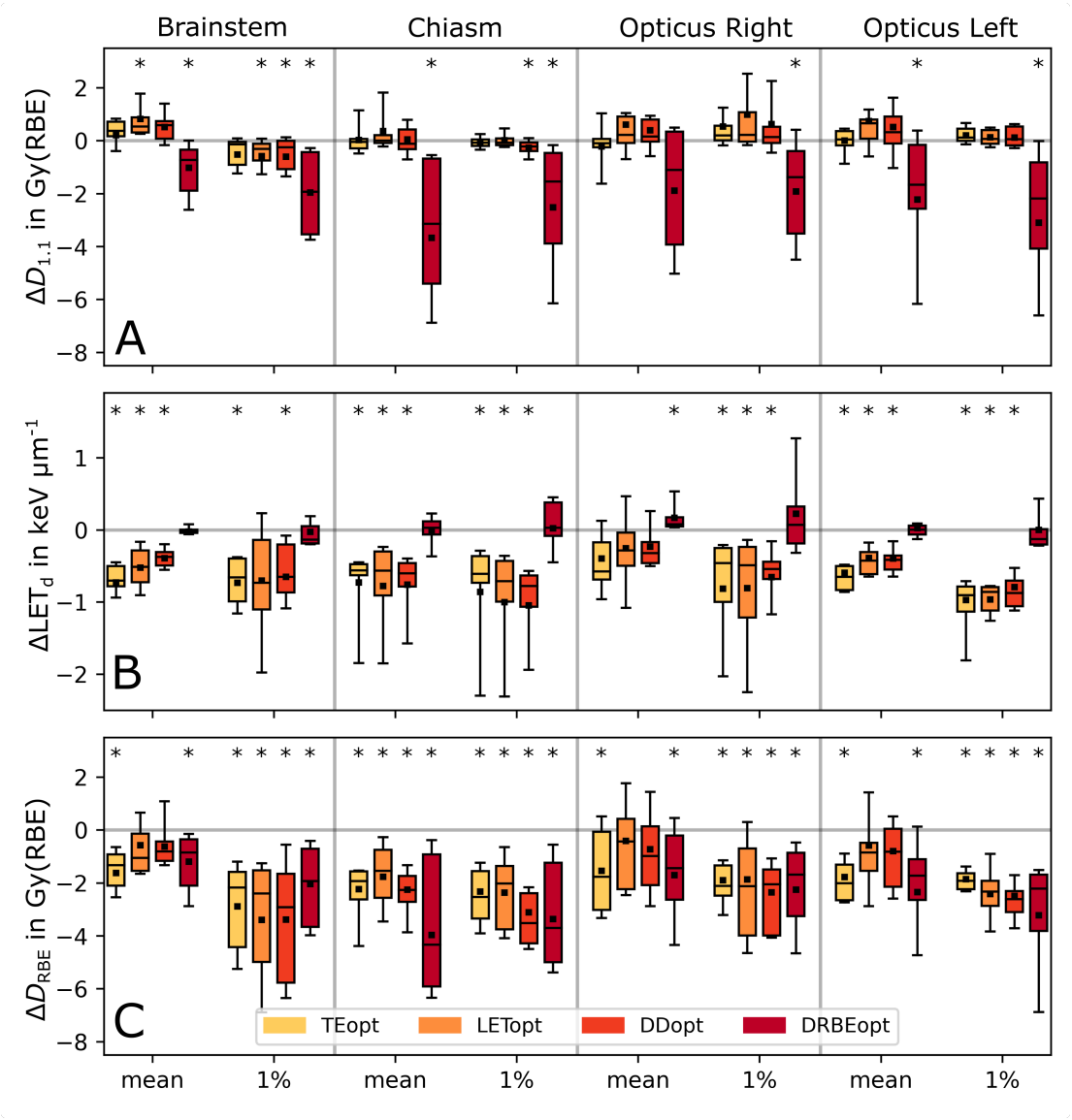

Figure 5.4: Each boxplot contains differences (Δ) in mean or near-maximum (1 %) values between biological effectiveness guided plans and dose-only optimised plans in critical organs at risk for all patients. Absolute differences in **A** constant relative biological effectiveness weighted dose ($D_{1.1}$), **B** dose-averaged linear enery transfer (LET_d) and **C** variable RBE-weighted dose (D_RBE) are shown. Statistically significant differences ($p < 0.05$) are marked with an arterisk. Abbreviations: optimisation with dose only (DOSEopt), trackends (TEopt), LET_d with dose threshold (LETopt), dirty dose (DDopt) and D_RBE (DRBEopt) are shown. Adapted from (Hahn et al., 2022a), with permission from Springer Nature.

penalised track-ends and, thus, avoided elevated LET_d to large volumes of the OARs, while LETopt and DDopt focussed on reducing hotspots of track-ends and LET_d. DRBEopt did not change the track-end distribution within the critical OARs substantially. Instead, it pro-

duced a track-end hotspot at the border between CTV and OAR to obtain an even steeper absorbed dose fall-off. Accordingly, LET_d values in the brainstem and optical apparatus with DRBEopt remained comparable to those in DOSEopt (Figure 5.4, Figure 5.5).

5.4 Discussion

The majority of toxicity reports after proton therapy originate from cranial irradiations (Underwood et al., 2022), so that patients undergoing cranial proton therapy may benefit particularly from BGopt. Short beam ranges, low range straggling, sharp distal dose gradients and high patient positioning reproducibility contribute to D_{RBE} uncertainties and hotspots in normal tissue of cranial irradiations that are not washed out over the course of the fractionated treatment (Grün et al., 2013; Hahn et al., 2020). There, the highly radiosensitive brainstem and optical apparatus in close vicinity to the CTV may be particularly prone to variable RBE induced toxicity urging the development of treatment plan optimisation beyond dose (Deng et al., 2021). In contrast, entities with parallel structured OARs, such as liver or lungs, are rarely at a high initial risk of the spatially limited RBE-induced overdosages, which may limit the extend of RBE induced toxicities and the measurable benefit of BGopt.

Optimisation beyond dose may deteriorate plan quality, i.e. in terms of target volume coverage (Sørensen et al., 2021), compared to the clinical treatment plans currently planned and delivered. In this thesis, the changes to the original reference DOSEopt plan were kept as low as possible by using the clinically used beam angles, beam line objects and machine parameters to generate clinically deliverable treatment plans without sacrificing plan quality with a constant RBE. In principle, BGopt can be applied for either the target volume or OARs or both and may optimise absorbed dose and dose-enhancing factors simultaneously or sequentially (Deng et al., 2021). Here, a sequential optimisation approach was considered and applied to OARs only. This strategy is in line with recent recommendations suggesting variable RBE-based optimisation objectives should primarily be applied at highly radiosensitive critical structures at the end of range, while maintaining a constant RBE for dose prescription to the tumour to avoid CTV underdosage with D_{RBE} due to low radiosensitivity and moderately high LET_d values in the CTV (Paganetti et al., 2019). This optimisation approach allows for consistent dose reporting while acquiring more clinical data on RBE variability and is in line with other research works on novel optimisation

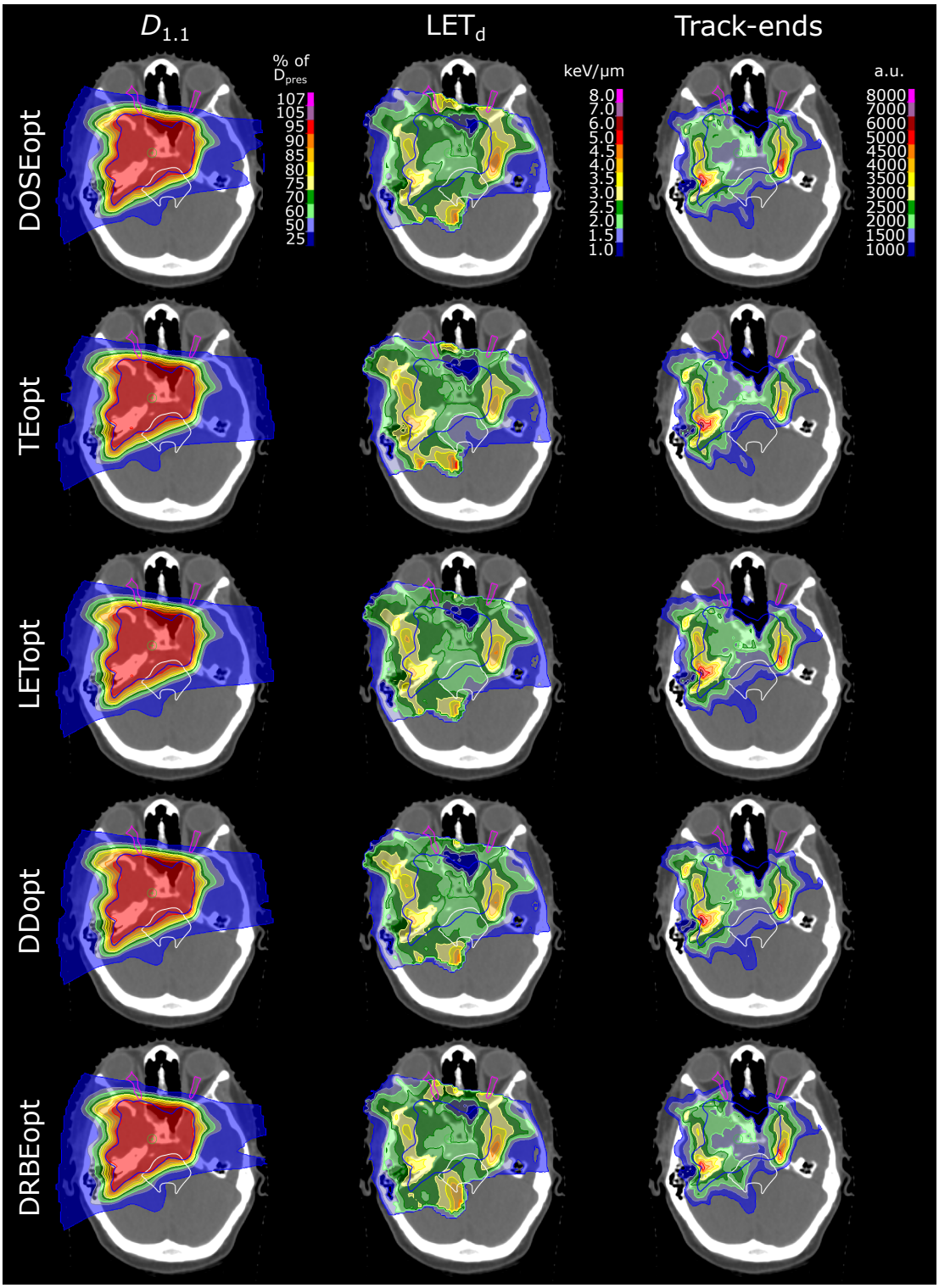

Figure 5.5: Patient 5: Columns display distributions of absorbed dose weighted with RBE of 1.1 ($D_{1.1}$), dose-averaged linear energy transfer (LET_d) in voxels above 10 Gy and proton track-ends. Each row shows $D_{1.1}$, LET_d and track-end distributions for one optimisation strategy. The planning target volume (blue) is shown together with the brainstem (white) and both optic nerves (magenta). DOSEopt: dose-only optimisation, TEopt: track-end optimisation, LETopt: LET_d optimisation with dose threshold, DDopt: Dirty dose optimisation, DRBEopt: variable RBE-weighted dose optimisation. Reproduced with permission from Springer Nature (Hahn et al., 2022a).

strategies (An et al., 2017; Ödén et al., 2020; Sánchez-Parcerisa et al., 2019; Unkelbach et al., 2016). Although simultaneous absorbed dose and LET_d optimisation offer additional degrees of freedom and may reduce D_{RBE} and NTCP even further (Deng et al., 2021), two-step optimisation as applied in our study was considered closer to current clinical practice. Therefore, sequentially reducing D_{RBE} to OARs while maintaining current dose constraints to the target volume and OARs may be regarded as a first and safe step towards translating optimisation with variable RBE into clinical practice.

BGopt strategies as implemented in this thesis could be categorised in primarily LET_d optimising and primarily absorbed dose-optimising strategies (Figure 5.4). TEopt, LETopt and DDopt are classified primarily LET_d optimising as they decreased the near-maximum LET_d in critical OARs by on average 19.0 %, 19.0 % and 18.9 %, respectively. This is comparable to earlier studies optimising track-ends or LET_d with reductions of 25.7 % (Traneus & Ödén, 2019) and 23.7 % (Cao et al., 2017), respectively. In contrast, LET_d distributions remained virtually unchanged in DRBEopt, which can thus be considered a primarily absorbed dose optimising stratey. For DRBEopt, the benefit of reducing LET_d may be mitigated by entering the variable RBE formula in the square root favouring the optimisation of absorbed dose instead to reduce D_{RBE}.

Altering LET_d instead of absorbed dose to reduce D_{RBE} was found to be more robust against range uncertainties. Although the static cloud assumption does not necessarily hold for proton therapy, the applied CTV to PTV achieved $D_{95\%}$ above 95 % in the CTV in more than 90 % of all BGopt treatment plans, in line with clinical requirements on plan robustness (Korevaar et al., 2019). Plan robustness was lower for patients where the CTV overlapped with critical OARs, as target coverage in the entire volume could also not be ensured in the nominal scenario, but BGopt and DOSEopt showed similar robustness for these cases. An exception to this was DRBEopt in our current implementation, which generated steep absorbed dose gradients to reduce D_{RBE} and thereby slightly but systematically decreased robustness in the primary CTV when prescription doses exceeded 54 Gy(RBE). In contrast, optimising LET_d did not decrease robustness in CTV coverage. Thus, BGopt treatment plans should be complemented by robustness evaluation when used clinically. Combining BGopt with a robust optimisation framework in the future would allow to directly balance D_{RBE} sparing in OARs with robustness in the optimisation process. In this regard, robust optimisation may alter the absorbed dose and LET_d distributions at the end of range (Paganetti & Giantsoudi, 2018) compared to the PTV-based DOSEopt reference

plans used in this thesis. In its current implementation, the absorbed-dose optimising DRBEopt may contradict the goal of robust optimisation aiming for smoother dose gradients at the end of range. Similarly, the smoother dose gradients produced by robust dose optimisation may smoothen the LET_d gradients at the end of range, which may impact the potential of primarily LET_d-optimising approaches. Yet, it was shown that the robust dose optimisation frameworks can be extended to include LET_d (Liu et al., 2020) or biological effect, approximated by the product of absorbed dose and LET_d (Bai et al., 2019), to consider robustness in biologically optimised treatment plans while lowering D_{RBE} in OARs.

Clinically relevant threshold values are required for BGopt to optimally balance D_{RBE} reductions with maintaining plan quality and to systematically apply BGopt in a larger patient cohort prior to clinical translation, e.g. in prospective studies. Using tolerance doses formulated for a constant RBE of 1.1 as dose objectives for critical OARs in DRBEopt appears safe since variable RBE typically exceeds 1.1 in critical OARs with high radiosensitivity and elevated LET_d. Consequently, the absorbed dose in these OARs decreases as was also observed in this thesis.

Clinically relevant LET_d and dose levels are available and emerging for LETopt. Since many proton therapy centres are equipped to provide LET information for treatment plans in an unambiguous clinically data format (Hahn et al., 2021a), this will likely augment the database for clinically relevant LET levels from retrospective clinical toxicity reports in the near future. In this regard, a more harmonised reporting of voxelwise averaged LET in terms of averaging technique and secondary particle spectra would ensure a consistent reporting of the not yet standardised voxelwise averaged LET calculations (Kalholm et al., 2021; Koh et al., 2020), e.g. reporting the recently proposed unrestricted LET_d of protons to water or unit density tissue (Hahn et al., 2022c).

Since voxelwise particle-energy spectra were not reported in radiation-induced brain injuries or similar side-effects, a generic LET level of $2.5\,\mathrm{keV\,\mu m^{-1}}$ was applied as LET threshold in DDopt to separate dirty dose from clean dose. Similarly, track-end levels to be penalised were found in trial-and-error iterations, as they are not yet reported in patient follow-up and may also depend on the incident field directions and the volumes of the CTVs and OARs (Traneus & Ödén, 2019). Although a generic 50 % reduction in track-ends and near-maximum dirty dose kept plan quality and translated in NTCP(D_{RBE}) reductions comparable to those in LETopt and DRBEopt, these objective levels may still not be optimal. Clearly, more studies reporting volume histogram parameters or voxelwise information for

absorbed dose, LET_d and dirty dose or track-ends in toxicity volumes are needed to better define the objectives to be used in biology-guided plan optimisation.

For plan optimisation with BGopt, user-defined threshold values and objective weights are required. However, the user-defined threshold values and weights to create a clinically acceptable treatment plan are correlated. For an exploratory study of the correlated threshold-values and objectives, their uncertainties and their quantitative impact on the resulting treatment plan, multi-criteria optimisation (MCO) including BGopt strategies is required and may be part of future studies, given the technical availability of an MCO implementation for BGopt strategies. Instead, in the optimisation process to create the final plans presented in this thesis, the BGopt objective weights were increased incrementally, while keeping the threshold values fixed, until the resulting CTV coverage started to decrease. Finally, the plans with the highest BGopt objective weight were selected that maintained acceptable CTV coverage.

In this thesis, BGopt systematically reduced NTCP(D_{RBE}). Compared to DOSEopt, BGopt reduced the probability for brainstem necrosis and blindness in the optical apparatus, using the Wedenberg et al. (2013) RBE model, by about 50 % with average (maximum) reductions of 5.4 (18.4) percentage points, respectively. BGopt was particularly beneficial in patients with elevated initial NTCP for necrosis and blindness in the DOSEopt plans. There, at dose values close to the OAR tolerance doses, changes in D_{RBE} translate directly into substantial reductions in the sigmoid-shaped NTCP function. The observed NTCP reductions in our study seem to reach a relevant level, as similar NTCP differences are used for patient selection to proton therapy by the model based approach (Langendijk et al., 2013), as adopted in the Netherlands and Denmark. Still, the presented absolute values for D_{RBE} and NTCP(D_{RBE}) reductions must be considered with caution (Paganetti, 2022), since the transferability of *in-vitro* data based RBE models to the clinical situation is limited, the applied NTCP models are based on photon data, and the presented NTCP values for DOSEopt treatment plans do not correlate with clinical findings at WPE.

Clinical treatment planning strategies beyond absorbed dose are not yet considered clinically for several reasons. First, it remains debatable which of the multitude of available *in-vitro* data based RBE models, as summarised elsewhere (Rørvik et al., 2018), best describes how clinical RBE varies as a function of LET_d. Second, the uncertainty in *in-vitro* and *in-vivo* experiments assessing the biological response after proton irradiation underly substantial uncertainties (Paganetti et al., 2019), which may obscure other functional RBE

dependencies and complicates accuracy assessment of individual RBE models (Flint et al., 2022). Third, proton therapy centres demand for more clinical data on RBE variability before changing RBE-related clinical guidelines on dose prescription and treatment field selection (Heuchel et al., 2022). Fourth, it remains unclear which of the physical or biological RBE driving factors should be considered in novel treatment planning strategies, as explored in this thesis. Despite these uncertainties, proton therapy centres showed interest in the development of LET_d and RBE optimisation tools but changes to current treatment plan quality should be kept as low as reasonably achievable (Heuchel et al., 2022). In this thesis, the presented novel optimisation approaches beyond absorbed dose optimisation showed that D_{RBE} to OARs can be reduced substantially while maintaining plan quality with a constant RBE of 1.1. The absorbed dose distributions of BGopt strategies, that primarily altered the LET_d distributions, remained comparable to the optimal solution found with DOSEopt. Clinical translation of the presented BGopt strategies thus appears feasible in principal but should be considered with caution and done in line with current clinical practice, since it is unlikely that a validated clinical (site-specific) RBE model will become available in the near future (Deng et al., 2021).

5.5 Conclusion

Clinical data on the relevance of RBE variability in patients undergoing cranial proton therapy is emerging. While proton therapy centres aim to mitigate RBE uncertainties through clinically available strategies such as changing orientation and number treatment fields, safe and effective plan optimisation strategies beyond absorbed are not yet available. In this chapter, multiple variable RBE guided optimisation strategies were introduced and compared. It was shown that the selective optimisation of track-end fractions, LET_d, dirty dose and D_{RBE} in serially structured OARs allows to reduce expected NTCP therein considerably. At the same time, all novel optimisation strategies provided adequate target volume coverage and sufficient robustness with a constant RBE. Primarily LET-optimising strategies featured absorbed dose distributions similar to the optimal solution found with DOSEopt. This allows to reduce the RBE hotspots in relevant OARs effectively, without changing current clinical practice. Currently, only LETopt can be based on clinically meaningful, though still scarce, LET_d volume histogram parameters from toxicity reports. Paired with its robust-

ness against range and setup uncertainties as well as the current awareness of proton therapy centres to report LET_d for toxicity observations, makes LETopt a good candidate to be explored in the clinics, while collecting more clinical data on RBE variability. In line with the findings in this thesis, but not based on them, a phase I pilot trial on LET optimised IMPT for pediatric patients with ependymoma was recently initiated in the USA and its safety will be evaluated as primary endpoint (NCT03750513).

6 Summary

Background

Proton therapy better conforms the dose distribution to the tumour volume and is biologically more effective than photon therapy. However, the uncertainty in relative biological effectiveness (RBE) limits the exploitation of the full potential of proton therapy. The current clinical practice of using a generic RBE of 1.1 neglects a multitude of preclinical and emerging clinical evidence for a variable proton RBE. It was shown that radiation-induced side effects are not caused by absorbed dose alone but depend on the linear energy transfer (LET) which varies throughout the treatment field. This urges proton therapy centres to account for RBE variability in treatment planning. However, LET and variable RBE calculations are neither implemented in clinical treatment planning systems (TPSs) nor standardised. This hampers a rapid clinical implementation and consistent reporting of RBE variability in proton therapy.

Purpose and hypotheses

This thesis considers RBE variability in clinical pencil beam scanning (PBS) proton treatment planning to further enhance patient safety. This includes both the retrospective treatment plan assessment as well as the optimisation with a variable RBE. It is assumed that solutions to obtain patient-specific LET and RBE distributions differ between proton therapy centres due to the current lack of a standard. Furthermore, it is hypothesised that PBS treatment plan optimisation can be extended to actively counteract RBE variability by including RBE driving factors in the process.

Material and methods

A framework to recalculate LET and variable RBE for PBS treatment plans was established in the research version of the clinical TPS RayStation and implemented at two German

proton therapy centres. First, this framework was applied in mono-centric studies to assess the RBE variability and the benefit of clinical dose-based mitigation strategies in treatment plans of patients with brain, head and neck and prostate tumour. Second, a European multi-centric treatment planning study was conducted to assess the status and comparability of centre-specific approaches to recalculate LET and RBE variability in specific water phantom and patient cases. Finally, the existing dose-based treatment plan optimisation was extended. Four physical to biological strategies to actively reduce variable RBE in organs at risk (OARs) were implemented and compared for cranial proton therapy.

Results

LET and variable RBE values were particularly elevated at the treatment field edges in all investigated patients. Accordingly, RBE variability affected OARs more than the clinical target volumes (CTVs). Brain tumour patients were found at elevated risk for side effects, since the regions of high LET spatially coincided with high absorbed dose. This was confirmed for one brain tumour patient showing radiation induced toxicity in areas of combined high dose and LET. Adding an opposing field may help to reduce RBE hotspots in healthy tissue at the cost of higher low-dose exposure of brain tissue.

European proton therapy centres used different research frameworks to recalculate LET. The initial differences in LET averaging technique and considered secondary particles were overcome by proposing a harmonised LET definition. This resulted in comparable patient dose distributions among the centres even when recalculating variable RBE weighted doses. Other centre-specific parameters had a minor impact on the reported dose values.

All novel optimisation strategies reduced the estimated normal tissue complication probability for brainstem necrosis and blindness in the optical apparatus substantially. Similarly, they kept plan robustness and the absorbed dose distribution in line with current clinical practice when using a constant RBE. The optimisation of LET in high dose areas may be favourable since tolerance values are already available from patient follow-up.

Conclusions

Patient-specific LET and variable RBE recalculations were enabled and are recommended when using small opening angles or treatment fields stopping in front of an OAR near the target volume. This may inform treatment planners and clinical staff on treatment plan safety

in view of a variable RBE. The proposed harmonised LET definition allows for consistent analysis and reporting of tumour control and side effects in view of a variable biological effect of protons in upcoming multi-centric studies. Meanwhile, the presented optimisation strategies allow to actively mitigate RBE variability in OARs, despite the limited proton-specific outcome data to date. In this way, this thesis contributes to a more rapid and reliable implementation of variable RBE to further enhance safety and efficacy of proton therapy.

7 Zusammenfassung

Hintergrund

Die Protonentherapie passt die Dosisverteilung besser an das Tumorvolumen an und ist biologisch wirksamer als die Photonentherapie. Die Unsicherheit in ihrer relativen biologischen Wirksamkeit (RBW) schränkt jedoch die Ausschöpfung des vollen Potenzials der Protonentherapie ein. Derzeit wird klinisch eine konstante RBW von 1.1 verwendet, was jedoch sowohl präklinische als auch erste klinische Studienergebnisse einer variablen RBW vernachlässigt. Es wurde gezeigt, dass strahleninduzierte Nebenwirkungen nicht allein von der absorbierten Dosis, sondern auch vom linearen Energietransfer (LET) bestimmt werden, welcher im Bestrahlungsfeld variiert. Daher sollten Protonentherapiezentren die RBW-Variabilität bei der Bestrahlungsplanung berücksichtigen. Allerdings sind die Berechnungen weder im klinischen Planungssystem implementiert, noch sind sie standardisiert. Dies erschwert die zeitnahe klinische Berücksichtigung einer variablen RBW sowie eine einheitliche Dokumentation des Therapieergebnisses in der Protonentherapie.

Fragestellung und Hypothesen

Diese Arbeit berücksichtigt die RBW-Variabilität in der klinischen Pencil Beam Scanning (PBS) Protonentherapie. Dies umfasst sowohl die retrospektive Auswertung von Bestrahlungsplänen als auch die Optimierung mit einer variablen RBW. Es wird davon ausgegangen, dass sich die Ansätze zur Berechnung patientenspezifischer LET- und RBW-Verteilungen zwischen einzelnen Protonentherapiezentren unterscheiden, da es derzeit keinen Standard gibt. Ferner wird postuliert, dass die Optimierung von PBS-Bestrahlungsplänen erweitert werden kann, um der RBW-Variabilität aktiv entgegenzuwirken, indem Einflussfaktoren einer variablen RBW in den Prozess implementiert werden.

Material und Methoden

Eine Methode zur Nachberechnung von LET und variabler RBW für PBS Bestrahlungspläne wurde für die Forschungsversion des klinischen Planungssystems RayStation an zwei deutschen Protonentherapiezentren implementiert. Die RBW-Variabilität und der Nutzen klinischer dosisbasierter Strategien zur RBW-Reduktion wurde in Bestrahlungsplänen für Patienten mit Hirn-, Kopf-Hals- und Prostatatumoren in monozentrischen Studien untersucht. Die Vergleichbarkeit zentrumsspezifischer Ansätze zur Berechnung von LET und RBW wurde in einer multi-zentrischen europäischen Studie für ausgewählte Phantom- und Patientenfälle quantifiziert. Abschließend wurde die konventionelle dosisbasierte Optimierung von Bestrahlungsplänen erweitert. Vier physikalische bis biologische Strategien zur aktiven Reduzierung variabler RBW in Risikoorganen wurden für die kraniale Protonentherapie integriert und verglichen.

Ergebnisse

LET- und variable RBW-Werte waren bei allen untersuchten Patienten besonders am Rand der Bestrahlungsfelder erhöht. Dementsprechend wirkte sich die RBW-Variabilität stärker auf die Risikoorgane als auf das klinische Zielvolumen aus. Bei Hirntumorpatienten wurde ein erhöhtes Nebenwirkungs-Risiko festgestellt, da Regionen mit hohem LET räumlich mit Bereichen hoher absorbierter Dosis zusammenfielen. Dies wurde bei einem Hirntumorpatienten bestätigt, der in Bereichen mit hoher Dosis und hohem LET eine strahleninduzierte Toxizität aufwies. Das Hinzufügen eines gegenüberliegenden Bestrahlungsfeldes kann dazu beitragen, Bereiche hoher RBW in gesundem Gewebe zu reduzieren, allerdings auf Kosten einer höheren Niedrigdosis-Exposition des Hirngewebes.

Die europäischen Protonentherapiezentren verwendeten unterschiedliche Methoden zur LET-Berechnung. Die anfänglichen Unterschiede in der LET-Mittelungstechnik und in den berücksichtigten Sekundärteilchen wurden durch den Vorschlag einer harmonisierten LET-Definition überwunden. Dies führte zu vergleichbaren Patientendosisverteilungen zwischen den Zentren, selbst unter Berücksichtigung einer variablen RBW. Andere zentrumsspezifische Parameter hatten einen geringen Einfluss auf die berichteten Dosiswerte.

Die Optimierungsstrategien zur Reduktion einer variablen RBW verringerten die berechnete Wahrscheinlichkeit für Nekrose im Hirnstamm und Erblindung im optischen Apparat erheblich. Ebenso blieben die Robustheit und die Verteilung der absorbierten Dosis in den

neuartigen Bestrahlungsplänen vergleichbar mit denen bei der Verwendung einer konstanten RBW in der Planoptimierung. Die Optimierung von LET in Hochdosis-Bereichen könnte besonders geeignet sein, weil Grenzwerte dafür aus der Patientennachsorge bereits verfügbar sind.

Schlussfolgerungen

Patientenspezifische LET- und variable RBW-Berechnungen sind implementiert worden. Ihre Anwendung wird für Patienten empfohlen, deren Bestrahlungsfelder kleine Öffnungswinkel haben oder vor einem Risikoorgan nahe des Zielvolumens stoppen. Damit kann das klinische Personal über die Sicherheit eines Bestrahlungsplans vor dem Hintergrund einer variablen RBW informiert werden. Die vorgeschlagene harmonisierte LET-Definition ermöglicht eine konsistente Analyse und Dokumentation über die Tumorkontrolle und Nebenwirkungen nach Protonentherapie, auch unter Berücksichtigung einer variablen RBW, in kommenden multizentrischen Studien. Gleichzeitig erlauben die vorgestellten Optimierungsstrategien, die RBW-Variabilität in den Risikoorganen aktiv abzuschwächen, auch wenn protonen-spezifische Behandlungsergebnisse zu einer variablen RBW bisher kaum verfügbar sind. Auf diese Weise trägt diese Arbeit zu einer schnelleren und zuverlässigeren Implementierung von variabler RBW bei, um die Sicherheit und Wirksamkeit der Protonentherapie weiter zu verbessern.

Bibliography

Ågren Cronqvist, A.-K. (1995). *Quantification of the response of heterogeneous tumours and organized normal tissues to fractionated radiotherapy* (Dissertation). Stockholm University.

Aitkenhead, A. H., Sitch, P., Richardson, J. C., Winterhalter, C., Patel, I., & Mackay, R. I. (2020). Automated Monte-Carlo re-calculation of proton therapy plans using Geant4/ Gate: implementation and comparison to plan-specific quality assurance measurements. *The British Journal of Radiology*, *93*(1114), 20200228. https://doi.org/10.1259/bjr.20200228

Allison, J., Amako, K., Apostolakis, J., Arce, P., Asai, M., Aso, T., Bagli, E., Bagulya, A., Banerjee, S., Barrand, G., Beck, B., Bogdanov, A., Brandt, D., Brown, J., Burkhardt, H., Canal, P., Cano-Ott, D., Chauvie, S., Cho, K., ... Yoshida, H. (2016). Recent developments in Geant4. *Nuclear Instruments and Methods in Physics Research Section A: Accelerators, Spectrometers, Detectors and Associated Equipment*, *835*, 186–225. https://doi.org/10.1016/j.nima.2016.06.125

An, Y., Shan, J., Patel, S. H., Wong, W., Schild, S. E., Ding, X., & Liu, W. (2017). Robust intensity-modulated proton therapy to reduce high linear energy transfer in organs at risk. *Medical Physics*, *44*(12), 6138–6147. https://doi.org/10.1002/mp.12610

Anand, A., & Bues, M. (2022). Treatment planning for scanning beam proton therapy. In T. Malouff & D. Tifiletti (Eds.), *Principles and practice of particle therapy* (pp. 55–79). Wiley. https://doi.org/10.1002/9781119707530.ch5

Ares, C., Hug, E. B., Lomax, A. J., Bolsi, A., Timmermann, B., Rutz, H. P., Schuller, J. C., Pedroni, E., & Goitein, G. (2009). Effectiveness and safety of spot scanning proton radiation therapy for chordomas and chondrosarcomas of the skull base: First long-term report. *International Journal of Radiation Oncology*Biology*Physics*, *75*(4), 1111–1118. https://doi.org/10.1016/j.ijrobp.2008.12.055

Bahn, E., Bauer, J., Harrabi, S., Herfarth, K., Debus, J., & Alber, M. (2020). Late contrast enhancing brain lesions in proton-treated patients with low-grade glioma: clinical

evidence for increased periventricular sensitivity and variable RBE. *International Journal of Radiation Oncology Biology Physics*, *107*(3), 571–578. https://doi.org/10.1016/j.ijrobp.2020.03.013

Bai, X., Lim, G., Wieser, H.-P., Bangert, M., Grosshans, D., Mohan, R., & Cao, W. (2019). Robust optimization to reduce the impact of biological effect variation from physical uncertainties in intensity-modulated proton therapy. *Physics in Medicine & Biology*, *64*(2), 025004. https://doi.org/10.1088/1361-6560/aaf5e9

Baskar, R., Lee, K. A., Yeo, R., & Yeoh, K. W. (2012). Cancer and radiation therapy: Current advances and future directions. *International Journal of Medical Sciences*, *9*(3), 193–199. https://doi.org/10.7150/ijms.3635

Bauer, J., Bahn, E., Harrabi, S., Herfarth, K., Debus, J., & Alber, M. (2021). How can scanned proton beam treatment planning for low-grade glioma cope with increased distal RBE and locally increased radiosensitivity for late MR-detected brain lesions? *Medical Physics*, *48*(4), 1497–1507. https://doi.org/10.1002/mp.14739

Baumann, M., & Gregoire, V. (2009). Modified fractionation. In M. Joiner & A. van der Kogel (Eds.), *Basic clinical radiobiology* (4th ed., pp. 135–148). Hodder Arnold. https://doi.org/10.1201/b15450

Baumann, M., Krause, M., Overgaard, J., Debus, J., Bentzen, S. M., Daartz, J., Richter, C., Zips, D., & Bortfeld, T. (2016). Radiation oncology in the era of precision medicine. *Nature Reviews Cancer*, *16*(4), 234–249. https://doi.org/10.1038/nrc.2016.18

Bäumer, C., Ackermann, B., Hillbrand, M., Kaiser, F. J., Koska, B., Latzel, H., Lühr, A., Menkel, S., & Timmermann, B. (2017). Dosimetry intercomparison of four proton therapy institutions in Germany employing spot scanning. *Zeitschrift fur Medizinische Physik*, *27*(2), 80–85. https://doi.org/10.1016/j.zemedi.2016.06.007

Bäumer, C., Plaude, S., Khalil, D. A., Geismar, D., Kramer, P. H., Kröninger, K., Nitsch, C., Wulff, J., & Timmermann, B. (2021). Clinical implementation of proton therapy using pencil-beam scanning delivery combined with static apertures. *Frontiers in Oncology*, *11*(May), 1–11. https://doi.org/10.3389/fonc.2021.599018

Bellinzona, E. V., Grzanka, L., Attili, A., Tommasino, F., Friedrich, T., Krämer, M., Scholz, M., Battistoni, G., Embriaco, A., Chiappara, D., Cirrone, G. A. P., Petringa, G., Durante, M., & Scifoni, E. (2021). Biological impact of target fragments on proton treatment plans: An analysis based on the current cross-section data and a full mixed field approach. *Cancers*, *13*(19), 4768. https://doi.org/10.3390/cancers13194768

Bentzen, S. M., Constine, L. S., Deasy, J. O., Eisbruch, A., Jackson, A., Marks, L. B., Ten Haken, R. K., & Yorke, E. D. (2010). Quantitative Analyses of Normal Tissue Effects in the Clinic (QUANTEC): An introduction to the scientific issues. *International Journal of Radiation Oncology Biology Physics*, *76*(3 SUPPL.), 3–9. https://doi.org/10.1016/j.ijrobp.2009.09.040

Berger, M. J., Coursey, J., Zucker, M., & Chang, J. (2017). PSTAR stopping power and range tables for protons. Retrieved November 30, 2022, from https://physics.nist.gov/PhysRefData/Star/Text/PSTAR.html

Berger, M. J., Inokuti, M., Andersen, H. H., Bichsel, H., Powers, D., Seltzer, S. . M., Thwaites, D. ., & Watt, D. E. (1993). ICRU report 49: Stopping powers and ranges for protons and alpha particles. *Journal of the ICRU*, *os25*(2). https://doi.org/10.1093/jicru/os25.2.Report49

Bertolet, A., Abolfath, R., Carlson, D. J., Lustig, R. A., Hill-Kayser, C., Alonso-Basanta, M., & Carabe, A. (2022). Correlation of LET with MRI changes in brain and potential implications for normal tissue complication probability for patients with meningioma treated with pencil beam scanning proton therapy. *International Journal of Radiation Oncology Biology Physics*, *112*(1), 237–246. https://doi.org/10.1016/j.ijrobp.2021.08.027

Bertolet, A., Cortés-Giraldo, M. A., & Carabe-Fernandez, A. (2020). On the concepts of dose-mean lineal energy, unrestricted and restricted dose-averaged LET in proton therapy. *Physics in Medicine and Biology*, *65*(7), 075011. https://doi.org/10.1088/1361-6560/ab730a

Bethe, H. (1930). Zur Theorie des Durchgangs schneller Korpuskularstrahlen durch Materie. *Annalen der Physik*, *397*(3), 325–400. https://doi.org/10.1002/andp.19303970303

Bourhaleb, F., Attili, A., & Russo, G. (2011). Monte Carlo simulations for beam delivery line design in radiation therapy with heavy ion beams. In *Applications of monte carlo methods in biology, medicine and other fields of science* (pp. 115–131). InTech. https://doi.org/10.5772/15883

Cao, W., Khabazian, A., Yepes, P. P., Lim, G., Poenisch, F., Grosshans, D. R., & Mohan, R. (2017). Linear energy transfer incorporated intensity modulated proton therapy optimization. *Physics in Medicine and Biology*, *63*(1), 015013. https://doi.org/10.1088/1361-6560/aa9a2e

Carabe, A., España, S., Grassberger, C., & Paganetti, H. (2013). Clinical consequences of relative biological effectiveness variations in proton radiotherapy of the prostate, brain and liver. *Physics in Medicine and Biology*, *58*(7), 2103–2117. https://doi.org/10.1088/0031-9155/58/7/2103

Carabe, A., Moteabbed, M., Depauw, N., Schuemann, J., & Paganetti, H. (2012). Range uncertainty in proton therapy due to variable biological effectiveness. *Physics in Medicine and Biology*, *57*(5), 1159–1172. https://doi.org/10.1088/0031-9155/57/5/1159

Carlson, D. J., Stewart, R. D., Semenenko, V. A., & Sandison, G. A. (2008). Combined use of Monte Carlo DNA damage simulations and deterministic repair models to examine putative mechanisms of cell killing. *Radiation Research*, *169*(4), 447–459. https://doi.org/10.1667/RR1046.1

Chen, W., Unkelbach, J., Trofimov, A., Madden, T., Kooy, H., Bortfeld, T., & Craft, D. (2012). Including robustness in multi-criteria optimization for intensity-modulated proton therapy. *Physics in Medicine and Biology*, *57*(3), 591–608. https://doi.org/10.1088/0031-9155/57/3/591

Chen, Y., & Ahmad, S. (2012). Empirical model estimation of relative biological effectiveness for proton beam therapy. *Radiation Protection Dosimetry*, *149*(2), 116–123. https://doi.org/10.1093/rpd/ncr218

Choi, K., Mein, S. B., Kopp, B., Magro, G., Molinelli, S., Ciocca, M., & Mairani, A. (2018). FRoG—A new calculation engine for clinical investigations with proton and carbon ion beams at CNAO. *Cancers*, *10*(11), 1–14. https://doi.org/10.3390/cancers10110395

Cortés-Giraldo, M. A., & Carabe, A. (2015). A critical study of different Monte Carlo scoring methods of dose average linear-energy-transfer maps calculated in voxelized geometries irradiated with clinical proton beams. *Physics in Medicine and Biology*, *60*(7), 2645–2669. https://doi.org/10.1088/0031-9155/60/7/2645

Dahle, T. J., Rusten, E., Stokkevåg, C. H., Silvoniemi, A., Mairani, A., Fjæra, L. F., Rørvik, E., Henjum, H., Wright, P., Boer, C. G., Forsback, S., Minn, H., Malinen, E., & Ytre-Hauge, K. S. (2020). The FLUKA Monte Carlo code coupled with an OER model for biologically weighted dose calculations in proton therapy of hypoxic tumors. *Physica Medica*, *76*(November 2019), 166–172. https://doi.org/10.1016/j.ejmp.2020.07.003

Dasu, A., & Toma-Dasu, I. (2012). Prostate alpha/beta revisited an analysis of clinical results from 14 168 patients. *Acta Oncologica*, *51*(8), 963–974. https://doi.org/10.3109/0284186X.2012.719635

De Luca, P. (2007). ICRU report 78: Prescribing, recording and reporting proton beam therapy. *Journal of the ICRU*, *7*(2). https://doi.org/https://doi.org/10.1093/jicru/ndn001

De Luca, P., Jones, D., Gahbauer, R., Whitmore, G., & Wambersie, A. (2010). ICRU report 83: Prescribing, recording, and reporting photon-beam intensity-modulated radiation therapy (IMRT). *Journal of the ICRU*, *10*(1), 1–92. https://doi.org/10.1093/jicru/ndq001

Dearnaley, D., Syndikus, I., Mossop, H., Khoo, V., Birtle, A., Bloomfield, D., Graham, J., Kirkbride, P., Logue, J., Malik, Z., Money-Kyrle, J., O'Sullivan, J. M., Panades, M., Parker, C., Patterson, H., Scrase, C., Staffurth, J., Stockdale, A., Tremlett, J., ... Hall, E. (2016). Conventional versus hypofractionated high-dose intensity-modulated radiotherapy for prostate cancer: 5-year outcomes of the randomised, non-inferiority, phase 3 CHHiP trial. *The Lancet Oncology*, *17*(8), 1047–1060. https://doi.org/10.1016/S1470-2045(16)30102-4

Defraene, G., Van Den Bergh, L., Al-Mamgani, A., Haustermans, K., Heemsbergen, W., Van Den Heuvel, F., & Lebesque, J. V. (2012). The benefits of including clinical factors in rectal normal tissue complication probability modeling after radiotherapy for prostate cancer. *International Journal of Radiation Oncology Biology Physics*, *82*(3), 1233–1242. https://doi.org/10.1016/j.ijrobp.2011.03.056

Deng, W., Yang, Y., Liu, C., Bues, M., Mohan, R., Wong, W. W., Foote, R. H., Patel, S. H., & Liu, W. (2021). A critical review of LET-based intensity-modulated proton therapy plan evaluation and optimization for head and neck cancer management. *International Journal of Particle Therapy*, *8*(1), 36–49. https://doi.org/10.14338/ijpt-20-00049.1

Durante, M., Orecchia, R., & Loeffler, J. S. (2017). Charged-particle therapy in cancer: Clinical uses and future perspectives. *Nature Reviews Clinical Oncology*, *14*(8), 483–495. https://doi.org/10.1038/nrclinonc.2017.30

Dutz, A. (2020). *Towards patient selection for cranial proton beam therapy – Assessment of current patient-individual treatment decision strategies* (Dissertation). Technische Universität Dresden.

Ebert, M. A., Gulliford, S., Acosta, O., De Crevoisier, R., McNutt, T., Heemsbergen, W. D., Witte, M., Palma, G., Rancati, T., & Fiorino, C. (2021). Spatial descriptions of radiotherapy dose: Normal tissue complication models and statistical associations. *Physics in Medicine and Biology*, *66*(12). https://doi.org/10.1088/1361-6560/ac0681

Emami, B., Lyman, J., Brown, A., Coia, L., Goitein, M., Munzenrider, J., Shank, B., Solin, L., & Wesson, M. (1991). Tolerance of normal tissue to irradiation. *International Journal of Radiation Oncology Biology Physics*, *21*(1), 109–122.

Engelsman, M. (2011). Physics of treatment planning for single-field uniform dose. In H. Paganetti (Ed.), *Proton therapy physics* (pp. 305–334). CRC Press. https://ebookcentral.proquest.com/lib/dortmundtech/reader.action?docID=827022%7B%5C&%7Dppg=327

Engeseth, G. M., He, R., Mirkovic, D., Yepes, P., Mohamed, A. S. R., Stieb, S., Fuller, C. D., Wu, R., Zhang, X., Hysing, L. B., Pettersen, H. E. S., Stokkevåg, C. H., Mohan, R., Frank, S. J., & Gunn, G. B. (2021). Mixed effect modeling of dose and linear energy transfer correlations with brain image changes after intensity modulated proton therapy for skull base head and neck cancer. *International Journal of Radiation Oncology Biology Physics*, *111*(3), 684–692. https://doi.org/10.1016/j.ijrobp.2021.06.016

Eulitz, J. (2021). *Variable relative biological effectiveness (RBE) in proton therapy of gliomas* (Dissertation). Technische Universität Dresden.

Eulitz, J., Lutz, B., Wohlfahrt, P., Dutz, A., Enghardt, W., Karpowitz, C., Krause, M., Troost, E. G., & Lühr, A. (2019a). A Monte Carlo based radiation response modelling framework to assess variability of clinical RBE in proton therapy. *Physics in Medicine and Biology*, *64*(22). https://doi.org/10.1088/1361-6560/ab3841

Eulitz, J., Troost, E. G. C., Klünder, L., Raschke, F., Hahn, C., Schulz, E., Seidlitz, A., Thiem, J., Karpowitz, C., Hahlbohm, P., Grey, A., Engellandt, K., Löck, S., Krause, M., & Lühr, A. (2023). Increased relative biological effectiveness and periventricular radiosensitivity in proton therapy of glioma patients. *Radiotherapy and Oncology*, *178*, 109422. https://doi.org/10.1016/j.radonc.2022.11.011

Eulitz, J., Troost, E. G. C., Raschke, F., Schulz, E., Lutz, B., Dutz, A., Löck, S., Wohlfahrt, P., Enghardt, W., Karpowitz, C., Krause, M., & Lühr, A. (2019b). Predicting late magnetic resonance image changes in glioma patients after proton therapy. *Acta Oncologica*, *58*(10), 1536–1539. https://doi.org/10.1080/0284186X.2019.1631477

Faddegon, B., Ramos-Méndez, J., Schuemann, J., McNamara, A., Shin, J., Perl, J., & Paganetti, H. (2020). The TOPAS tool for particle simulation, a Monte Carlo simulation tool for physics, biology and clinical research. *Physica Medica*, *72*, 114–121. https://doi.org/10.1016/j.ejmp.2020.03.019

Farr, J. B., Moyers, M. F., Allgower, C. E., Bues, M., Hsi, W. C., Jin, H., Mihailidis, D. N., Lu, H. M., Newhauser, W. D., Sahoo, N., Slopsema, R., Yeung, D., & Zhu, X. R. (2021). Clinical commissioning of intensity-modulated proton therapy systems: Report of AAPM Task Group 185. *Medical Physics*, *48*(1), e1–e30. https://doi.org/10.1002/mp.14546

Faught, A. M., Wilson, L. J., Gargone, M., Pirlepesov, F., Moskvin, V. P., & Hua, C.-H. (2022). Treatment-planning approaches to intensity modulated proton therapy and the impact on dose-weighted linear energy transfer. *Journal of Applied Clinical Medical Physics*, *e13782*. https://doi.org/10.1002/acm2.13782

Ferlay, J., Colombet, M., Soerjomataram, I., Parkin, D. M., Piñeros, M., Znaor, A., & Bray, F. (2021). Cancer statistics for the year 2020: An overview. *International Journal of Cancer*, *149*(4), 778–789. https://doi.org/10.1002/ijc.33588

Fernández-Varea, J., Mayol, R., Baró, J., & Salvat, F. (1993). On the theory and simulation of multiple elastic scattering of electrons. *Nuclear Instruments and Methods in Physics Research Section B: Beam Interactions with Materials and Atoms*, *73*(4), 447–473. https://doi.org/10.1016/0168-583X(93)95827-R

Feuvret, L., Noël, G., Mazeron, J. J., & Bey, P. (2006). Conformity index: A review. *International Journal of Radiation Oncology Biology Physics*, *64*(2), 333–342. https://doi.org/10.1016/j.ijrobp.2005.09.028

Fjæra, L. F., Li, Z., Ytre-Hauge, K. S., Muren, L. P., Indelicato, D. J., Lassen-Ramshad, Y., Engeseth, G. M., Brydøy, M., Mairani, A., Flampouri, S., Dahl, O., & Stokkevåg, C. H. (2017). Linear energy transfer distributions in the brainstem depending on tumour location in intensity-modulated proton therapy of paediatric cancer. *Acta Oncologica*, *56*(6), 763–768. https://doi.org/10.1080/0284186X.2017.1314007

Flanz, J. (2011). Particle beam scanning. In H. Paganetti (Ed.), *Proton therapy physics* (pp. 157–190). CRC Press.

Flint, D. B., Ruff, C. E., Bright, S. J., Yepes, P., Wang, Q., Manandhar, M., Kacem, M. B., Turner, B. X., Martinus, D. K. J., Shaitelman, S. F., & Sawakuchi, G. O. (2022). An empirical model of proton RBE based on the linear correlation between x-ray and

proton radiosensitivity. *Medical Physics*, *49*(9), 6221–6236. https://doi.org/10.1002/mp.15850

Fossati, P., Vavassori, A., Deantonio, L., Ferrara, E., Krengli, M., & Orecchia, R. (2016). Review of photon and proton radiotherapy for skull base tumours. *Reports of Practical Oncology and Radiotherapy*, *21*(4), 336–355. https://doi.org/10.1016/j.rpor.2016.03.007

Fredriksson, A., & Bokrantz, R. (2014). A critical evaluation of worst case optimization methods for robust intensity-modulated proton therapy planning. *Medical Physics*, *41*(8). https://doi.org/10.1118/1.4883837

Fredriksson, A., Forsgren, A., & Hårdemark, B. (2011). Minimax optimization for handling range and setup uncertainties in proton therapy. *Medical Physics*, *38*(3), 1672–1684. https://doi.org/10.1118/1.3556559

Frese, M. C., Wilkens, J. J., Huber, P. E., Jensen, A. D., Oelfke, U., & Taheri-Kadkhoda, Z. (2011). Application of constant vs. variable relative biological effectiveness in treatment planning of intensity-modulated proton therapy. *International Journal of Radiation Oncology Biology Physics*, *79*(1), 80–88. https://doi.org/10.1016/j.ijrobp.2009.10.022

Garbacz, M., Cordoni, F. G., Durante, M., Gajewski, J., Kisielewicz, K., Krah, N., Kopeć, R., Olko, P., Patera, V., Rinaldi, I., Rydygier, M., Schiavi, A., Scifoni, E., Skóra, T., Tommasino, F., & Rucinski, A. (2021). Study of relationship between dose, LET and the risk of brain necrosis after proton therapy for skull base tumors. *Radiotherapy and Oncology*, *163*, 143–149. https://doi.org/10.1016/j.radonc.2021.08.015

Giantsoudi, D., Grassberger, C., Craft, D., Niemierko, A., Trofimov, A., & Paganetti, H. (2013). Linear energy transfer-guided optimization in intensity modulated proton therapy: Feasibility study and clinical potential. *International Journal of Radiation Oncology Biology Physics*, *87*(1), 216–222. https://doi.org/10.1016/j.ijrobp.2013.05.013

Giantsoudi, D., Sethi, R. V., Yeap, B. Y., Eaton, B. R., Ebb, D. H., Caruso, P. A., Rapalino, O., Chen, Y. L. E., Adams, J. A., Yock, T. I., Tarbell, N. J., Paganetti, H., & MacDonald, S. M. (2016). Incidence of CNS injury for a cohort of 111 patients treated with proton therapy for medulloblastoma: LET and RBE associations for areas of injury. *International Journal of Radiation Oncology Biology Physics*, *95*(1), 287–296. https://doi.org/10.1016/j.ijrobp.2015.09.015

Giovannini, G., Böhlen, T., Cabal, G., Bauer, J., Tessonnier, T., Frey, K., Debus, J., Mairani, A., & Parodi, K. (2016). Variable RBE in proton therapy: Comparison of different model predictions and their influence on clinical-like scenarios. *Radiation Oncology*, *11*(1), 1–16. https://doi.org/10.1186/s13014-016-0642-6

Goitein, M. (1985). Calculation of the uncertainty in the dose delivered during radiation therapy. *Medical Physics*, *12*(5), 608–612. https://doi.org/10.1118/1.595762

Gordon, K. B., Char, D. H., & Sagerman, R. H. (1995). Late effects of radiation on the eye and ocular adnexa. *International Journal of Radiation Oncology, Biology, Physics*, *31*(5), 1123–1139. https://doi.org/10.1016/0360-3016(95)00062-4

Gottschalk, B. (2011). Physics of proton interactions in matter. In H. Paganetti (Ed.), *Proton therapy physics* (pp. 27–66). CRC Press. https://www.taylorfrancis.com/books/9781351855754/chapters/10.1201/b22053-3

Goudsmit, S., & Saunderson, J. L. (1940a). Multiple scattering of electrons. *Physical Review*, *57*(1), 24–29. https://doi.org/10.1103/PhysRev.57.24

Goudsmit, S., & Saunderson, J. L. (1940b). Multiple scattering of electrons. II. *Physical Review*, *58*(1), 36–42. https://doi.org/10.1103/PhysRev.58.36

Granville, D. A., & Sawakuchi, G. O. (2015). Comparison of linear energy transfer scoring techniques in Monte Carlo simulations of proton beams. *Physics in Medicine and Biology*, *60*(14), N283–N291. https://doi.org/10.1088/0031-9155/60/14/N283

Grassberger, C., & Paganetti, H. (2011). Elevated LET components in clinical proton beams. *Physics in Medicine and Biology*, *56*(20), 6677–6691. https://doi.org/10.1088/0031-9155/56/20/011

Grassberger, C., Trofimov, A., Lomax, A., & Paganetti, H. (2011). Variations in linear energy transfer within clinical proton therapy fields and the potential for biological treatment planning. *International Journal of Radiation Oncology Biology Physics*, *80*(5), 1559–1566. https://doi.org/10.1016/j.ijrobp.2010.10.027

Grevillot, L., Boersma, D. J., Fuchs, H., Aitkenhead, A., Elia, A., Bolsa, M., Winterhalter, C., Vidal, M., Jan, S., Pietrzyk, U., Maigne, L., & Sarrut, D. (2020). Technical Note: GATE-RTion: a GATE/Geant4 release for clinical applications in scanned ion beam therapy. *Medical Physics*, *47*(8), 3675–3681. https://doi.org/10.1002/mp.14242

Grün, R., Friedrich, T., Krämer, M., Zink, K., Durante, M., & Engenhart-Cabillic, R. (2013). Physical and biological factors determining the effective proton range. *Medical Physics*, *40*(November), 1–10. https://doi.org/10.1118/1.4824321

Grzanka, L., Ardenfors, O., & Bassler, N. (2018). Monte carlo simulations of spatial LET distributions in clinical proton beams. *Radiation Protection Dosimetry*, *180*(1-4), 296–299. https://doi.org/10.1093/rpd/ncx272

Guan, F., Peeler, C., Bronk, L., Geng, C., Taleei, R., Randeniya, S., Ge, S., Mirkovic, D., Grosshans, D., Mohan, R., & Titt, U. (2015). Analysis of the track- and dose-averaged LET and LET spectra in proton therapy using the geant4 Monte Carlo code. *Medical Physics*, *42*(11), 6234–6247. https://doi.org/10.1118/1.4932217

Haas-Kogan, D., Indelicato, D., Paganetti, H., Esiashvili, N., Mahajan, A., Yock, T., Flampouri, S., MacDonald, S., Fouladi, M., Stephen, K., Kalapurakal, J., Terezakis, S., Kooy, H., Grosshans, D., Makrigiorgos, M., Mishra, K., Poussaint, T. Y., Cohen, K., Fitzgerald, T., ... Kun, L. (2018). National Cancer Institute workshop on proton therapy for children: Considerations regarding brainstem injury. *International Journal of Radiation Oncology Biology Physics*, *101*(1), 152–168. https://doi.org/10.1016/j.ijrobp.2018.01.013

Hahn, C., Eulitz, J., Peters, N., Wohlfahrt, P., Enghardt, W., Richter, C., & Lühr, A. (2020). Impact of range uncertainty on clinical distributions of linear energy transfer and biological effectiveness in proton therapy. *Medical Physics*, *47*(12), 6151–6162. https://doi.org/10.1002/mp.14560

Hahn, C., Heuchel, L., Ödén, J., Traneus, E., Wulff, J., Plaude, S., Timmermann, B., Bäumer, C., & Lühr, A. (2022a). Comparing biological effectiveness guided plan optimization strategies for cranial proton therapy: potential and challenges. *Radiation Oncology*, *17*(1), 169. https://doi.org/10.1186/s13014-022-02143-x

Hahn, C., Heuchel, L., Ödén, J., Wulff, J., Plaude, S., Timmermann, B., Bäumer, C., Traneus, E., & Lühr, A. (2022b). PO-1729 Novel optimization strategies to account for RBE variability in proton therapy. *Radiotherapy and Oncology*, *170*(Supplement 1), S1531–S1532. https://doi.org/10.1016/S0167-8140(22)03693-3

Hahn, C., Ödén, J., Dasu, A., Vestergaard, A., Fuglsang Jensen, M., Sokol, O., Pardi, C., Bourhaleb, F., Leite, A., de Marzi, L., Smith, E., Aitkenhead, A., Rose, C., Merchant, M., Kirkby, K., Grzanka, L., Pawelke, J., & Lühr, A. (2022c). Towards harmonizing clinical linear energy transfer (LET) reporting in proton radiotherapy: a European multi-centric study. *Acta Oncologica*, *61*(2), 206–214. https://doi.org/10.1080/0284186X.2021.1992007

Hahn, C., Ödén, J., Dasu, A., Vestergaard, A., Kallehauge, J. F., Pardi, C., Bourhaleb, F., Leite, A., Marzi, L. D., Smith, E., Aitkenhead, A., Merchant, M., Kirkby, K., Troost, E. G. C., & Lühr, A. (2021a). OC-0418 European multi-centric study on variable proton RBE dose calculations for multiple anatomical sites. *Radiotherapy and Oncology*, *161*, S314–S315. https://doi.org/10.1016/S0167-8140(21)06905-X

Hahn, C., Ödén, J., Dasu, A., Vestergaard, A., Kallehauge, J. F., Pardi, C., Bourhaleb, F., Leite, A., de Marzi, L., Smith, E., Aitkenhead, A., Merchant, M., Kirkby, K., Troost, E. G. C., & Lühr, A. (2022d). Multi-centric study on variable RBE dose calculations in European proton therapy institutions. *International Journal of Particle Therapy*, 124. https://doi.org/10.14338/IJPT-22-PTCOG59-9.3

Hahn, C., Peters, N., Wohlfahrt, P., Eulitz, J., Enghardt, W., Richter, C., & Lühr, A. (2019). Einfluss von Protonen-Reichweiteunsicherheiten auf LET-Verteilungen am Beispiel von Hirntumor-Patienten. In C. Gromoll & N. Wegner (Eds.), *Abstractband jahrestagung deutsche gesellschaft für medizinische physik* (pp. 77–78).

Hahn, C., Sobolewski, J., Uber, S., Wulff, J., Bäumer, C., Timmermann, B., & Lühr, A. (2021b). Introducing a semi-automated framework for variable relative biological effectiveness (RBE) recalculations of clinical proton treatment plans. In D. Georg & W. Birkfellner (Eds.), *Dreiländertagung der medizinischen physik* (pp. 72–73).

Hahn, C., Vestergaard, A., Sokol, O., Pardi, C., Leite, A., Rose, C., Ödén, J., Grzanka, L., & Lühr, A. (2021c). Multi-centric study to harmonize LET-calculations in proton therapy. *International Journal of Particle Therapy*, *7*(4), 78. https://doi.org/10.14338/IJPT.20-PTCOG-7.4

Hawkins, R. B. (1996). A microdosimetric-kinetic model of cell death from exposure to ionizing radiation of any LET, with experimental and clinical applications. *International Journal of Radiation Biology*, *69*(6), 739–755. https://doi.org/10.1080/095530096145481

Heinrich, W., Wiegel, B., & Kraft, G. (1991). β, zeff, dEdx, range and restricted energy loss of heavy ions in the region between 1 and 1000 MeV per nucleon. *GSI Preprint*, *30*, 1–24. https://cds.cern.ch/record/222110

Henjum, H., Dahle, T. J., Fjæra, L. F., Rørvik, E., Pilskog, S., Stokkevåg, C. H., Mairani, A., & Ytre-Hauge, K. S. (2021). The organ sparing potential of different biological optimization strategies in proton therapy. *Advances in Radiation Oncology*, *6*(6), 100776. https://doi.org/10.1016/j.adro.2021.100776

Hernandez, V., Hansen, C. R., Widesott, L., Bäck, A., Canters, R., Fusella, M., Götstedt, J., Jurado-Bruggeman, D., Mukumoto, N., Kaplan, L. P., Koniarová, I., Piotrowski, T., Placidi, L., Vaniqui, A., & Jornet, N. (2020). What is plan quality in radiotherapy? The importance of evaluating dose metrics, complexity, and robustness of treatment plans. *Radiotherapy and Oncology*, *153*, 26–33. https://doi.org/10.1016/j.radonc.2020.09.038

Heuchel, L., Hahn, C., Pawelke, J., Sørensen, B. S., Dosanjh, M., & Lühr, A. (2022). Clinical use and future requirements of relative biological effectiveness: Survey among all European proton therapy centres. *Radiotherapy and Oncology*, *172*, 134–139. https://doi.org/10.1016/j.radonc.2022.05.015

Holthusen, H. (1936). Erfahrungen über die Verträglichkeitsgrenze für Röntgenstrahlen und deren Nutzanwendung zur Verhütung von Schäden. *Strahlentherapie*, *57*, 254–269.

Hyer, D. E., Hill, P. M., Wang, D., Smith, B. R., & Flynn, R. T. (2014a). A dynamic collimation system for penumbra reduction in spot-scanning proton therapy: Proof of concept. *Medical Physics*, *41*(9). https://doi.org/10.1118/1.4837155

Hyer, D. E., Hill, P. M., Wang, D., Smith, B. R., & Flynn, R. T. (2014b). Effects of spot size and spot spacing on lateral penumbra reduction when using a dynamic collimation system for spot scanning proton therapy. *Physics in Medicine and Biology*, *59*(22), N187–N196. https://doi.org/10.1088/0031-9155/59/22/N187

Jereczek-Fossa, B. A., Marsiglia, H. R., & Orecchia, R. (2002). Radiotherapy-related fatigue. *Critical Reviews in Oncology/Hematology*, *41*(3), 317–325. https://doi.org/10.1016/S1040-8428(01)00143-3

Jones, B. (2015). A simpler energy transfer efficiency model to predict relative biological effect for protons and heavier ions. *Frontiers in Oncology*, *5*(Aug), 1–9. https://doi.org/10.3389/fonc.2015.00184

Kalholm, F., Grzanka, L., Traneus, E., & Bassler, N. (2021). A systematic review on the usage of averaged LET in radiation biology for particle therapy. *Radiotherapy and Oncology*, *161*, 211–221. https://doi.org/10.1016/j.radonc.2021.04.007

Källman, P., Ågren, A., & Brahme, A. (1992). Tumour and normal tissue responses to fractionated non-uniform dose delivery. *International Journal of Radiation Biology*, *62*(2), 249–262. https://doi.org/10.1080/09553009214552071

Karger, C. P., Glowa, C., Peschke, P., & Kraft-Weyrather, W. (2021). The RBE in ion beam radiotherapy: In vivo studies and clinical application. *Zeitschrift fur Medizinische Physik*, *31*(2), 105–121. https://doi.org/10.1016/j.zemedi.2020.12.001

Kellerer, A. M., & Rossi, H. D. (1972). Theory of dual radiation action. *Current Topics in Radiation Research Quarterly*, *8*(2), 85–158. https://www.osti.gov/biblio/4611340

Koh, W. Y. C., Tan, H. Q., Ang, K. W., Park, S. Y., Lew, W. S., & Lee, J. C. L. (2020). Standardizing Monte Carlo simulation parameters for a reproducible dose-averaged linear energy transfer. *The British journal of Radiology*, *93*(1112), 20200122. https://doi.org/10.1259/bjr.20200122

Kopp, B., Fuglsang Jensen, M., Mein, S., Hoffmann, L., Nyström, H., Falk, M., Haberer, T., Abdollahi, A., Debus, J., & Mairani, A. (2020). FRoG: An independent dose and LETd prediction tool for proton therapy at ProBeam® facilities. *Medical Physics*, *47*(10), 5274–5286. https://doi.org/10.1002/mp.14417

Korevaar, E. W., Habraken, S. J., Scandurra, D., Kierkels, R. G., Unipan, M., Eenink, M. G., Steenbakkers, R. J., Peeters, S. G., Zindler, J. D., Hoogeman, M., & Langendijk, J. A. (2019). Practical robustness evaluation in radiotherapy – A photon and proton-proof alternative to PTV-based plan evaluation. *Radiotherapy and Oncology*, *141*, 267–274. https://doi.org/10.1016/j.radonc.2019.08.005

Krämer, M., Jäkel, O., Haberer, T., Kraft, G., Schardt, D., & Weber, U. (2000). Treatment planning for heavy-ion radiotherapy: physical beam model and dose optimization. *Physics in Medicine and Biology*, *45*(11), 3299–3317. https://doi.org/10.1088/0031-9155/45/11/313

Kutcher, G. J., & Burman, C. (1989). Calculation of complication probability factors for non-uniform normal tissue irradiation: The effective volume method. *International Journal of Radiation Oncology Biology Physics*, *16*(6), 1623–1630. https://doi.org/10.1016/0360-3016(89)90972-3

Lambrecht, M., Eekers, D. B., Alapetite, C., Burnet, N. G., Calugaru, V., Coremans, I. E., Fossati, P., Høyer, M., Langendijk, J. A., Méndez Romero, A., Paulsen, F., Perpar, A., Renard, L., de Ruysscher, D., Timmermann, B., Vitek, P., Weber, D. C., van der Weide, H. L., Whitfield, G. A., … Troost, E. G. (2018). Radiation dose constraints for organs at risk in neuro-oncology; the European Particle Therapy Network consensus. *Radiotherapy and Oncology*, *128*(1), 26–36. https://doi.org/10.1016/j.radonc.2018.05.001

Langendijk, J. A., Lambin, P., De Ruysscher, D., Widder, J., Bos, M., & Verheij, M. (2013). Selection of patients for radiotherapy with protons aiming at reduction of side effects: The model-based approach. *Radiotherapy and Oncology*, *107*(3), 267–273. https://doi.org/10.1016/j.radonc.2013.05.007

Lawrence, J. H. (1957). Proton irradiation of the pituitary. *Cancer*, *10*(4), 795–798. https://doi.org/10.1002/1097-0142(195707/08)10:4<795::AID-CNCR2820100426>3.0.CO;2-B

Lawrence, Y. R., Li, X. A., el Naqa, I., Hahn, C. A., Marks, L. B., Merchant, T. E., & Dicker, A. P. (2010). Radiation dose-volume effects in the brain. *International Journal of Radiation Oncology Biology Physics*, *76*(3 SUPPL.), 20–27. https://doi.org/10.1016/j.ijrobp.2009.02.091

Liu, C., Patel, S. H., Shan, J., Schild, S. E., Vargas, C. E., Wong, W. W., Ding, X., Bues, M., & Liu, W. (2020). Robust optimization for intensity modulated proton therapy to redistribute high linear energy transfer from nearby critical organs to tumors in head and neck cancer. *International Journal of Radiation Oncology Biology Physics*, *107*(1), 181–193. https://doi.org/10.1016/j.ijrobp.2020.01.013

Lomax, A. (1999). Intensity modulation methods for proton radiotherapy. *Physics in Medicine and Biology*, *44*(1), 185–205. https://doi.org/10.1088/0031-9155/44/1/014

Lomax, A. (2008). Intensity modulated proton therapy and its sensitivity to treatment uncertainties 1: The potential effects of calculational uncertainties. *Physics in Medicine and Biology*, *53*(4), 1027–1042. https://doi.org/10.1088/0031-9155/53/4/014

Lomax, A., Boehringer, T., Coray, A., Egger, E., Goitein, G., Grossmann, M., Juelke, P., Lin, S., Pedroni, E., Rohrer, B., Roser, W., Rossi, B., Siegenthaler, B., Stadelmann, O., Stauble, H., Vetter, C., & Wisser, L. (2001). Intensity modulated proton therapy: A clinical example. *Medical Physics*, *28*(3), 317–324. https://doi.org/10.1118/1.1350587

Lomax, A., Pedroni, E., Rutz, H., & Goitein, G. (2004). The clinical potential of intensity modulated proton therapy. *Zeitschrift fur Medizinische Physik*, *14*(3), 147–152. https://doi.org/10.1078/0939-3889-00217

Lowe, M., Albertini, F., Aitkenhead, A., Lomax, A. J., & MacKay, R. I. (2016). Incorporating the effect of fractionation in the evaluation of proton plan robustness to setup errors. *Physics in Medicine and Biology*, *61*(1), 413–429. https://doi.org/10.1088/0031-9155/61/1/413

Lühr, A., von Neubeck, C., Krause, M., & Troost, E. G. (2018). Relative biological effectiveness in proton beam therapy – Current knowledge and future challenges. *Clinical and Translational Radiation Oncology*, *9*, 35–41. https://doi.org/10.1016/j.ctro.2018.01.006

Mairani, A., Dokic, I., Magro, G., Tessonnier, T., Bauer, J., Böhlen, T. T., Ciocca, M., Ferrari, A., Sala, P. R., Jäkel, O., Debus, J., Haberer, T., Abdollahi, A., & Parodi, K. (2017). A phenomenological relative biological effectiveness approach for proton therapy based on an improved description of the mixed radiation field. *Physics in Medicine and Biology*, *62*(4), 1378–1395. https://doi.org/10.1088/1361-6560/aa51f7

Marks, L. B., Yorke, E. D., Jackson, A., Ten Haken, R. K., Constine, L. S., Eisbruch, A., Bentzen, S. M., Nam, J., & Deasy, J. O. (2010). Use of normal tissue complication probability models in the clinic. *International Journal of Radiation Oncology Biology Physics*, *76*(3), S10–S19. https://doi.org/10.1016/j.ijrobp.2009.07.1754

Marteinsdottir, M., Schuemann, J., & Paganetti, H. (2019). Impact of uncertainties in range and RBE on small field proton therapy. *Physics in Medicine and Biology*, *64*(20). https://doi.org/10.1088/1361-6560/ab448f

Mayo, C., Martel, M. K., Marks, L. B., Flickinger, J., Nam, J., & Kirkpatrick, J. (2010a). Radiation dose–volume effects of optic nerves and chiasm. *International Journal of Radiation Oncology Biology Physics*, *76*(3), S28–S35. https://doi.org/10.1016/j.ijrobp.2009.07.1753

Mayo, C., Yorke, E., & Merchant, T. E. (2010b). Radiation associated brainstem injury. *International Journal of Radiation Oncology Biology Physics*, *76*(3), S36–S41. https://doi.org/10.1016/j.ijrobp.2009.08.078

McMahon, S. J. (2021). Proton RBE models: commonalities and differences. *Physics in Medicine and Biology*, *66*(4), 04NT02. https://doi.org/10.1088/1361-6560/abda98

McMahon, S. J., Paganetti, H., & Prise, K. M. (2018). LET-weighted doses effectively reduce biological variability in proton radiotherapy planning. *Physics in Medicine and Biology*, *63*(22). https://doi.org/10.1088/1361-6560/aae8a5

McNamara, A. L., Schuemann, J., & Paganetti, H. (2015). A phenomenological relative biological effectiveness (RBE) model for proton therapy based on all published in vitro cell survival data. *Physics in Medicine and Biology*, *60*(21), 8399–8416. https://doi.org/10.1088/0031-9155/60/21/8399

Mein, S., Choi, K., Kopp, B., Tessonnier, T., Bauer, J., Ferrari, A., Haberer, T., Debus, J., Abdollahi, A., & Mairani, A. (2018). Fast robust dose calculation on GPU for high-precision 1H, 4He, 12C and 16O ion therapy: the FRoG platform. *Scientific Reports*, *8*(1), 1–12. https://doi.org/10.1038/s41598-018-33194-4

Mein, S., Kopp, B., Vela, A., Dutheil, P., Lesueur, P., Stefan, D., Debus, J., Haberer, T., Abdollahi, A., Mairani, A., & Tessonnier, T. (2022). How can we consider variable RBE and LETd prediction during clinical practice? A pediatric case report at the Normandy Proton Therapy Centre using an independent dose engine. *Radiation Oncology*, *17*(1), 1–16. https://doi.org/10.1186/s13014-021-01960-w

Mohan, R. (2022). A review of proton therapy – Current status and future directions. *Precision Radiation Oncology*, *6*(2), 164–176. https://doi.org/10.1002/pro6.1149

Newhauser, W. D., & Zhang, R. (2015). The physics of proton therapy. *Physics in Medicine and Biology*, *60*(8), R155–R209. https://doi.org/10.1088/0031-9155/60/8/R155

Niemierko, A. (1997). Reporting and analyzing dose distributions: A concept of equivalent uniform dose. *Medical Physics*, *24*(1), 103–110. https://doi.org/10.1118/1.598063

Niemierko, A., Schuemann, J., Niyazi, M., Giantsoudi, D., Maquilan, G., Shih, H. A., & Paganetti, H. (2021). Brain Necrosis in adult patients after proton therapy: Is there evidence for dependency on linear energy transfer? *International Journal of Radiation Oncology Biology Physics*, *109*(1), 109–119. https://doi.org/10.1016/j.ijrobp.2020.08.058

Nill, S., Bortfeld, T., & Oelfke, U. (2004). Inverse planning of intensity modulated proton therapy. *Zeitschrift fur Medizinische Physik*, *14*(1), 35–40. https://doi.org/10.1078/0939-3889-00198

Ödén, J. (2019). *Relative biological effectiveness in proton therapy: accounting for variability and uncertainties* (Dissertation). Stockholm University.

Ödén, J., Eriksson, K., & Toma-Dasu, I. (2017a). Inclusion of a variable RBE into proton and photon plan comparison for various fractionation schedules in prostate radiation therapy. *Medical Physics*, *44*(3), 810–822. https://doi.org/10.1002/mp.12117

Ödén, J., Eriksson, K., & Toma-Dasu, I. (2017b). Incorporation of relative biological effectiveness uncertainties into proton plan robustness evaluation. *Acta Oncologica*, *56*(6), 769–778. https://doi.org/10.1080/0284186X.2017.1290825

Ödén, J., Toma-Dasu, I., Witt Nyström, P., Traneus, E., & Dasu, A. (2020). Spatial correlation of linear energy transfer and relative biological effectiveness with suspected

treatment-related toxicities following proton therapy for intracranial tumors. *Medical Physics*, *47*(2), 342–351. https://doi.org/10.1002/mp.13911

Oelfke, U., & Bortfeld, T. (2001). Inverse planning for photon and proton beams. *Medical Dosimetry*, *26*(2), 113–124. https://doi.org/10.1016/S0958-3947(01)00057-7

Paganetti, H. (2002). Nuclear interactions in proton therapy: Dose and relative biological effect distributions originating from the primary and secondary particles. *Physics in Medicine and Biology*, *47*(5), 747–764. https://doi.org/10.1088/0031-9155/47/5/305

Paganetti, H. (2005). Interpretation of proton relative biological effectiveness using lesion induction, lesion repair, and cellular dose distribution. *Medical Physics*, *32*(8), 2548–2556. https://doi.org/10.1118/1.1949807

Paganetti, H. (2009). Dose to water versus dose to medium in proton beam therapy. *Physics in Medicine and Biology*, *54*(14), 4399–4421. https://doi.org/10.1088/0031-9155/54/14/004

Paganetti, H. (2011a). Monte Carlo simulations. In H. Paganetti (Ed.), *Proton therapy physics* (pp. 265–304). CRC Press.

Paganetti, H. (2011b). The physics of proton biology. In H. Paganetti (Ed.), *Proton therapy physics* (pp. 593–626). https://doi.org/10.1201/b22053-23

Paganetti, H. (2012). Range uncertainties in proton therapy and the role of Monte Carlo simulations. *Physics in Medicine and Biology*, *57*(11). https://doi.org/10.1088/0031-9155/57/11/R99

Paganetti, H. (2014). Relative biological effectiveness (RBE) values for proton beam therapy. Variations as a function of biological endpoint, dose, and linear energy transfer. *Physics in Medicine and Biology*, *59*(22), R419–R472. https://doi.org/10.1088/0031-9155/59/22/R419

Paganetti, H. (2022). Mechanisms and review of clinical evidence of variations in relative biological effectiveness in proton therapy. *International Journal of Radiation Oncology Biology Physics*, *112*(1), 222–236. https://doi.org/10.1016/j.ijrobp.2021.08.015

Paganetti, H., Beltran, C., Both, S., Dong, L., Flanz, J., Furutani, K., Grassberger, C., Grosshans, D. R., Knopf, A. C., Langendijk, J. A., Nystrom, H., Parodi, K., Raaymakers, B. W., Richter, C., Sawakuchi, G. O., Schippers, M., Shaitelman, S. F., Teo, B. K., Unkelbach, J., … Lomax, T. (2021). Roadmap: Proton therapy physics and biology. *Physics in Medicine and Biology*, *66*(5). https://doi.org/10.1088/1361-6560/abcd16

Paganetti, H., Blakely, E., Carabe-Fernandez, A., Carlson, D. J., Das, I. J., Dong, L., Grosshans, D., Held, K. D., Mohan, R., Moiseenko, V., Niemierko, A., Stewart, R. D., & Willers, H. (2019). Report of the AAPM TG-256 on the relative biological effectiveness of proton beams in radiation therapy. *Medical Physics*, *46*(3), e53–e78. https://doi.org/10.1002/mp.13390

Paganetti, H., & Giantsoudi, D. (2018). Relative biological effectiveness uncertainties and implications for beam arrangements and dose constraints in proton therapy. *Seminars in Radiation Oncology*, *28*(3), 256–263. https://doi.org/10.1016/j.semradonc.2018.02.010

Paganetti, H., Niemierko, A., Ancukiewicz, M., Gerweck, L. E., Goitein, M., Loeffler, J. S., & Suit, H. D. (2002). Relative biological effectiveness (RBE) values for proton beam therapy. *International Journal of Radiation Oncology Biology Physics*, *53*(2), 407–421. https://doi.org/10.1016/S0360-3016(02)02754-2

Park, P. C., Zhu, X. R., Lee, A. K., Sahoo, N., Melancon, A. D., Zhang, L., & Dong, L. (2012). A beam-specific planning target volume (PTV) design for proton therapy to account for setup and range uncertainties. *International Journal of Radiation Oncology Biology Physics*, *82*(2), e329–e336. https://doi.org/10.1016/j.ijrobp.2011.05.011

Particle Therapy Co-operatice Group. (2022). Particle Therapy Co-Operative Group. Retrieved November 30, 2022, from https://ptcog.ch/

Peeler, C. R., Mirkovic, D., Titt, U., Blanchard, P., Gunther, J. R., Mahajan, A., Mohan, R., & Grosshans, D. R. (2016). Clinical evidence of variable proton biological effectiveness in pediatric patients treated for ependymoma. *Radiotherapy and Oncology*, *121*(3), 395–401. https://doi.org/10.1016/j.radonc.2016.11.001

Pepin, M. D., Penoncello, G. P., Brom, K. M., Gustafson, J. M., Long, K. M., Rong, Y., Fong de los Santos, L. E., & Shiraishi, S. (2022). Assessment of dose-volume histogram precision for five clinical systems. *Medical Physics*, *49*(10), 6303–6318. https://doi.org/10.1002/mp.15916

Perl, J., Shin, J., Schümann, J., Faddegon, B., & Paganetti, H. (2012). TOPAS: An innovative proton Monte Carlo platform for research and clinical applications. *Medical Physics*, *39*(11), 6818–6837. https://doi.org/10.1118/1.4758060

Permatasari, F. F., Eulitz, J., Richter, C., Wohlfahrt, P., & Lühr, A. (2020). Material assignment for proton range prediction in Monte Carlo patient simulations using stopping-

power datasets. *Physics in Medicine and Biology*, *65*(18), 185004. https://doi.org/10.1088/1361-6560/ab9702

Peters, N. (2021). *Assessment and reduction of the clinical range prediction uncertainty in proton therapy* (Dissertation). Technische Universität Dresden.

Peters, N., Wohlfahrt, P., Hofmann, C., Möhler, C., Menkel, S., Tschiche, M., Krause, M., Troost, E. G., Enghardt, W., & Richter, C. (2022). Reduction of clinical safety margins in proton therapy enabled by the clinical implementation of dual-energy CT for direct stopping-power prediction. *Radiotherapy and Oncology*, *166*, 71–78. https://doi.org/10.1016/j.radonc.2021.11.002

Pflugfelder, D., Wilkens, J. J., & Oelfke, U. (2008). Worst case optimization: a method to account for uncertainties in the optimization of intensity modulated proton therapy. *Physics in Medicine and Biology*, *53*(6), 1689–1700. https://doi.org/10.1088/0031-9155/53/6/013

Pimblott, S. M., & LaVerne, J. A. (2007). Production of low-energy electrons by ionizing radiation. *Radiation Physics and Chemistry*, *76*(8-9), 1244–1247. https://doi.org/10.1016/j.radphyschem.2007.02.012

Qi, X. S., Schultz, C. J., & Li, X. A. (2006). An estimation of radiobiologic parameters from clinical outcomes for radiation treatment planning of brain tumor. *International Journal of Radiation Oncology Biology Physics*, *64*(5), 1570–1580. https://doi.org/10.1016/j.ijrobp.2005.12.022

Rana, S., Traneus, E., Jackson, M., Tran, L., & Rosenfeld, A. B. (2022). Quantitative analysis of dose-averaged linear energy transfer (LETd) robustness in pencil beam scanning proton lung plans. *Medical Physics*, *49*(5), 3444–3456. https://doi.org/10.1002/mp.15569

RaySearch Laboratories AB. (2016). *RayStation Reference Manual RSL-D-RS-6.0-REF-EN-1.0-2016-12-22*.

Resch, A., Heyes, P. D., Fuchs, H., Bassler, N., Georg, D., & Palmans, H. (2020). Dose- rather than fluence-averaged LET should be used as a single-parameter descriptor of proton beam quality for radiochromic film dosimetry. *Medical Physics*, *47*(5), 2289–2299. https://doi.org/10.1002/mp.14097

Resch, A., Landry, G., Kamp, F., Cabal, G., Belka, C., Wilkens, J., Parodi, K., & Dedes, G. (2017). Quantification of the uncertainties of a biological model and their impact

on variable RBE proton treatment plan optimization. *Physica Medica*, *36*, 91–102. https://doi.org/10.1016/j.ejmp.2017.03.013

Roberts, K. W., Wan Chan Tseung, H. S., Eckel, L. J., Harmsen, W. S., Beltran, C., & Laack, N. N. (2019). Biologic dose and imaging changes in pediatric brain tumor patients receiving spot scanning proton therapy. *International Journal of Radiation Oncology Biology Physics*, *105*(3), 664–673. https://doi.org/10.1016/j.ijrobp.2019.06.2534

Romano, F., Cirrone, G. A., Cuttone, G., Rosa, F. D., Mazzaglia, S. E., Petrovic, I., Fira, A. R., & Varisano, A. (2014). A Monte Carlo study for the calculation of the average linear energy transfer (LET) distributions for a clinical proton beam line and a radiobiological carbon ion beam line. *Physics in Medicine and Biology*, *59*(12), 2863–2882. https://doi.org/10.1088/0031-9155/59/12/2863

Rørvik, E., Fjæra, L. F., Dahle, T. J., Dale, J. E., Engeseth, G. M., Stokkevåg, C. H., Thörnqvist, S., & Ytre-Hauge, K. S. (2018). Exploration and application of phenomenological RBE models for proton therapy. *Physics in Medicine & Biology*, *63*(18), 185013. https://doi.org/10.1088/1361-6560/aad9db

Rørvik, E., Thörnqvist, S., Stokkevåg, C. H., Dahle, T. J., Fjaera, L. F., & Ytre-Hauge, K. S. (2017). A phenomenological biological dose model for proton therapy based on linear energy transfer spectra. *Medical Physics*, *44*(6), 2586–2594. https://doi.org/10.1002/mp.12216

Ruangchan, S., Knäusl, B., Fuchs, H., Georg, D., & Clausen, M. (2020). Experimental benchmarking of RayStation proton dose calculation algorithms inside and outside the target region in heterogeneous phantom geometries. *Physica Medica*, *76*(July), 182–193. https://doi.org/10.1016/j.ejmp.2020.07.010

Russo, G., Attili, A., Battistoni, G., Bertrand, D., Bourhaleb, F., Cappucci, F., Ciocca, M., Mairani, A., Milian, F. M., Molinelli, S., Morone, M. C., Muraro, S., Orts, T., Patera, V., Sala, P., Schmitt, E., Vivaldo, G., & Marchetto, F. (2015). A novel algorithm for the calculation of physical and biological irradiation quantities in scanned ion beam therapy: The beamlet superposition approach. *Physics in Medicine and Biology*, *61*(1), 183–214. https://doi.org/10.1088/0031-9155/61/1/183

Saager, M., Peschke, P., Brons, S., Debus, J., & Karger, C. P. (2018). Determination of the proton RBE in the rat spinal cord: Is there an increase towards the end of the spread-out Bragg peak? *Radiotherapy and Oncology*, *128*(1), 115–120. https://doi.org/10.1016/j.radonc.2018.03.002

Sánchez-Parcerisa, D., López-Aguirre, M., Dolcet Llerena, A., & Udías, J. M. (2019). MultiRBE: Treatment planning for protons with selective radiobiological effectiveness. *Medical Physics*, *46*(9), 4276–4284. https://doi.org/10.1002/mp.13718

Sarrut, D., Bardiès, M., Boussion, N., Freud, N., Jan, S., Létang, J.-M., Loudos, G., Maigne, L., Marcatili, S., Mauxion, T., Papadimitroulas, P., Perrot, Y., Pietrzyk, U., Robert, C., Schaart, D. R., Visvikis, D., & Buvat, I. (2014). A review of the use and potential of the GATE Monte Carlo simulation code for radiation therapy and dosimetry applications. *Medical Physics*, *41*(6Part1), 064301. https://doi.org/10.1118/1.4871617

Schellhammer, S. M. (2019). *Technical feasibilility of MR-integrated proton therapy: beam deflection and image quality* (Dissertation). Technische Universität Dresden.

Schneider, U., Pedroni, E., & Lomax, A. (1996). The calibration of CT Hounsfield units for radiotherapy treatment planning. *Physics in Medicine and Biology*, *41*(1), 111–124. https://doi.org/10.1088/0031-9155/41/1/009

Schneider, W., Bortfeld, T., & Schlegel, W. (2000). Correlation between CT numbers and tissue parameters needed for Monte Carlo simulations of clinical dose distributions. *Physics in Medicine and Biology*, *45*(2), 459–478. https://doi.org/10.1088/0031-9155/45/2/314

Scholz, M., Kellerer, A. M., Kraft-Weyrather, W., & Kraft, G. (1997). Computation of cell survival in heavy ion beams for therapy: The model and its approximation. *Radiation and Environmental Biophysics*, *36*(1), 59–66. https://doi.org/10.1007/s004110050055

Seltzer, S. M., Bartlett, D. T., Burns, D. T., Dietze, G., Menzel, H. G., & Wambersie, A. (2011). ICRU report 85: Fundamental quantities and units for ionizing radiation. *Journal of the ICRU*, *11*(1), 1–32. https://doi.org/10.1093/jicru/nd

Shin, J., Kooy, H. M., Paganetti, H., & Clasie, B. (2020). DICOM-RT Ion interface to utilize MC simulations in routine clinical workflow for proton pencil beam radiotherapy. *Physica Medica*, *74*(April), 1–10. https://doi.org/10.1016/j.ejmp.2020.04.018

Smith, E. A. K., Winterhalter, C., Underwood, T. S. A., Aitkenhead, A. H., Richardson, J. C., Merchant, M. J., Kirkby, N. F., Kirkby, K. J., & Mackay, R. I. (2021). A Monte Carlo study of different LET definitions and calculation parameters for proton beam therapy. *Biomedical Physics & Engineering Express*, *11*(20), 5035–5040. https://doi.org/10.1088/2057-1976/ac3f50

Sobolewski, J. (2021). *Calculating variable relative biological effectiveness for clinical treatment plans at the West German Proton Therapy Centre Essen* (Master Thesis). Technische Universität Dortmund.

Sørensen, B. S., Pawelke, J., Bauer, J., Burnet, N. G., Dasu, A., Høyer, M., Karger, C. P., Krause, M., Schwarz, M., Underwood, T. S., Wagenaar, D., Whitfield, G. A., & Lühr, A. (2021). Does the uncertainty in relative biological effectiveness affect patient treatment in proton therapy? *Radiotherapy and Oncology*, *163*, 177–184. https://doi.org/10.1016/j.radonc.2021.08.016

Stewart, R. D., Streitmatter, S. W., Argento, D. C., Kirkby, C., Goorley, J. T., Moffitt, G., Jevremovic, T., & Sandison, G. A. (2015). Rapid MCNP simulation of DNA double strand break (DSB) relative biological effectiveness (RBE) for photons, neutrons, and light ions. *Physics in Medicine and Biology*, *60*(21), 8249–8274. https://doi.org/10.1088/0031-9155/60/21/8249

Stuschke, M., & Thames, H. D. (1999). Fractionation sensitivities and dose-control relations of head and neck carcinomas: Analysis of the randomized hyperfractionation trials. *Radiotherapy and Oncology*, *51*(2), 113–121. https://doi.org/10.1016/S0167-8140(99)00042-0

Taasti, V. T., Bäumer, C., Dahlgren, C. V., Deisher, A. J., Ellerbrock, M., Free, J., Gora, J., Kozera, A., Lomax, A. J., De Marzi, L., Molinelli, S., Kevin Teo, B.-K., Wohlfahrt, P., Petersen, J. B., Muren, L. P., Hansen, D. C., & Richter, C. (2018). Inter-centre variability of CT-based stopping-power prediction in particle therapy: Survey-based evaluation. *Physics and Imaging in Radiation Oncology*, *6*, 25–30. https://doi.org/10.1016/j.phro.2018.04.006

Thomas, H., & Timmermann, B. (2020). Paediatric proton therapy. *The British Journal of Radiology*, *93*(1107), 20190601. https://doi.org/10.1259/bjr.20190601

Tian, L., Hahn, C., & Lühr, A. (2022). An ion-independent phenomenological relative biological effectiveness (RBE) model for proton therapy. *Radiotherapy and Oncology*, *174*, 69–76. https://doi.org/10.1016/j.radonc.2022.06.023

Toma-Dasu, I., Dasu, A., Vestergaard, A., Witt Nyström, P., & Nyström, H. (2020). RBE for proton radiation therapy–a Nordic view in the international perspective. *Acta Oncologica*, *59*(10), 1151–1156. https://doi.org/10.1080/0284186X.2020.1826573

Tommasino, F., & Durante, M. (2015). Proton Radiobiology. *Cancers*, *7*(1), 353–381. https://doi.org/10.3390/cancers7010353

Tran, L. T., Chartier, L., Bolst, D., Pogossov, A., Guatelli, S., Petasecca, M., Lerch, M. L., Prokopovich, D. A., Reinhard, M. I., Clasie, B., Depauw, N., Kooy, H., Flanz, J. B., McNamara, A., Paganetti, H., Beltran, C., Furutani, K., Perevertaylo, V. L., Jackson, M., & Rosenfeld, A. B. (2017). Characterization of proton pencil beam scanning and passive beam using a high spatial resolution solid-state microdosimeter. *Medical Physics*, *44*(11), 6085–6095. https://doi.org/10.1002/mp.12563

Traneus, E., & Ödén, J. (2019). Introducing proton track-end objectives in intensity modulated proton therapy optimization to reduce linear energy transfer and relative biological effectiveness in critical structures. *International Journal of Radiation Oncology Biology Physics*, *103*(3), 747–757. https://doi.org/10.1016/j.ijrobp.2018.10.031

Trofimov, A. (2011). Treatment-planning optimisation. In H. Paganetti (Ed.), *Proton therapy physics* (pp. 461–488). CRC Press. https://www.taylorfrancis.com/books/9781351855754/chapters/10.1201/b22053-3

Trofimov, A., Unkelbach, J., DeLaney, T. F., & Bortfeld, T. (2012). Visualization of a variety of possible dosimetric outcomes in radiation therapy using dose-volume histogram bands. *Practical Radiation Oncology*, *2*(3), 164–171. https://doi.org/10.1016/j.prro.2011.08.001

Uber, S. (2018). *Simulation der relativen biologischen Wirksamkeit der Protonentherapie bei Pencil Beam Scanning an der Universitäts Protonen Therapie Dresden* (Master Thesis). Technische Universität Dresden.

Underwood, T. S., Grassberger, C., Bass, R., MacDonald, S. M., Meyersohn, N. M., Yeap, B. Y., Jimenez, R. B., & Paganetti, H. (2018). Asymptomatic late-phase radiographic changes among chest-wall patients are associated with a proton RBE exceeding 1.1. *International Journal of Radiation Oncology Biology Physics*, *101*(4), 809–819. https://doi.org/10.1016/j.ijrobp.2018.03.037

Underwood, T. S., McNamara, A. L., Appelt, A., Haviland, J. S., Sørensen, B. S., & Troost, E. G. (2022). A systematic review of clinical studies on variable proton Relative Biological Effectiveness (RBE). *Radiotherapy and Oncology*, *175*, 79–92. https://doi.org/10.1016/j.radonc.2022.08.014

Unkelbach, J., Alber, M., Bangert, M., Bokrantz, R., Chan, T. C., Deasy, J. O., Fredriksson, A., Gorissen, B. L., Van Herk, M., Liu, W., Mahmoudzadeh, H., Nohadani, O., Siebers, J. V., Witte, M., & Xu, H. (2018). Robust radiotherapy planning. *Physics in Medicine and Biology*, *63*(22). https://doi.org/10.1088/1361-6560/aae659

Unkelbach, J., Bortfeld, T., Martin, B. C., & Soukup, M. (2009). Reducing the sensitivity of IMPT treatment plans to setup errors and range uncertainties via probabilistic treatment planning. *Medical Physics*, *36*(1), 149–163. https://doi.org/10.1118/1.3021139

Unkelbach, J., Botas, P., Giantsoudi, D., Gorissen, B. L., & Paganetti, H. (2016). Reoptimization of intensity modulated proton therapy plans based on linear energy transfer. *International Journal of Radiation Oncology Biology Physics*, *96*(5), 1097–1106. https://doi.org/10.1016/j.ijrobp.2016.08.038

Unkelbach, J., & Paganetti, H. (2018). Robust proton treatment planning: Physical and biological optimization. *Seminars in Radiation Oncology*, *28*(2), 88–96. https://doi.org/10.1016/j.semradonc.2017.11.005

Van Herk, M., Remeijer, P., Rasch, C., & Lebesque, J. V. (2000). The probability of correct target dosage: Dose-population histograms for deriving treatment margins in radiotherapy. *International Journal of Radiation Oncology Biology Physics*, *47*(4), 1121–1135. https://doi.org/10.1016/S0360-3016(00)00518-6

Wagenaar, D. (2022). *Advanced treatment planning: robust optimization and proton RBE* (Dissertation). University of Groningen. https://doi.org/10.33612/diss.203011060

Wagenaar, D., Tran, L. T., Meijers, A., Marmitt, G. G., Souris, K., Bolst, D., James, B., Biasi, G., Povoli, M., Kok, A., Traneus, E., van Goethem, M.-J., Langendijk, J. A., Rosenfeld, A. B., & Both, S. (2020). Validation of linear energy transfer computed in a Monte Carlo dose engine of a commercial treatment planning system. *Physics in Medicine and Biology*, *65*(2), 025006. https://doi.org/10.1088/1361-6560/ab5e97

Wang, W., Huang, Z., Sheng, Y., Zhao, J., Shahnazi, K., Zhang, Q., & Jiang, G. (2020). RBE-weighted dose conversions for carbon ionradiotherapy between microdosimetric kinetic model and local effect model for the targets and organs at risk in prostate carcinoma. *Radiotherapy and Oncology*, *144*, 30–36. https://doi.org/10.1016/j.radonc.2019.10.005

Wedenberg, M., Lind, B. K., & Hårdemark, B. (2013). A model for the relative biological effectiveness of protons: The tissue specific parameter α / β of photons is a predictor for the sensitivity to LET changes. *Acta Oncologica*, *52*(3), 580–588. https://doi.org/10.3109/0284186X.2012.705892

Wedenberg, M., & Toma-Dasu, I. (2014). Disregarding RBE variation in treatment plan comparison may lead to bias in favor of proton plans. *Medical Physics*, *41*(9), 091706. https://doi.org/10.1118/1.4892930

Wendling, M., Zijp, L. J., McDermott, L. N., Smit, E. J., Sonke, J. J., Mijnheer, B. J., & Van Herk, M. (2007). A fast algorithm for gamma evaluation in 3D. *Medical Physics*, *34*(5), 1647–1654. https://doi.org/10.1118/1.2721657

Wilkens, J. J., & Oelfke, U. (2003). Analytical linear energy transfer calculations for proton therapy. *Medical Physics*, *30*(5), 806–815. https://doi.org/10.1118/1.1567852

Wilson, L. J., Pirlepesov, F., Moskvin, V., Li, Z., Guo, Y., Li, Y., Merchant, T. E., & Faught, A. M. (2021). Proton therapy delivery method affects dose-averaged linear energy transfer in patients. *Physics in Medicine and Biology*, *66*(7). https://doi.org/10.1088/1361-6560/abe835

Wilson, R. R. (1946). Radiological use of fast protons. *Radiology*, *47*(5), 487–491. https://doi.org/10.1148/47.5.487

Wohlfahrt, P., Möhler, C., Enghardt, W., Krause, M., Kunath, D., Menkel, S., Troost, E. G., Greilich, S., & Richter, C. (2020). Refinement of the Hounsfield look-up table by retrospective application of patient-specific direct proton stopping-power prediction from dual-energy CT. *Medical Physics*, *0*(September 2019), 1–11. https://doi.org/10.1002/mp.14085

Wohlfahrt, P., Möhler, C., Richter, C., & Greilich, S. (2018). Evaluation of stopping-power prediction by dual- and single-energy computed tomography in an anthropomorphic ground-truth phantom. *International Journal of Radiation Oncology Biology Physics*, *100*(1), 244–253. https://doi.org/10.1016/j.ijrobp.2017.09.025

Wohlfahrt, P., Möhler, C., Stützer, K., Greilich, S., & Richter, C. (2017). Dual-energy CT based proton range prediction in head and pelvic tumor patients. *Radiotherapy and Oncology*, *125*(3), 526–533. https://doi.org/10.1016/j.radonc.2017.09.042

Wohlfahrt, P., & Richter, C. (2020). Proton therapy special feature: Review article status and innovations in pre-treatment CT imaging for proton therapy. *British Journal of Radiology*, *93*(July), 20190590.

Yang, Y., Vargas, C. E., Bhangoo, R. S., Wong, W. W., Schild, S. E., Daniels, T. B., Keole, S. R., Rwigema, J. C. M., Glass, J. L., Shen, J., DeWees, T. A., Liu, T., Bues, M., Fatyga, M., & Liu, W. (2021). Exploratory investigation of dose-linear energy transfer (LET) volume histogram (DLVH) for adverse events study in intensity modulated

proton therapy (IMPT). *International Journal of Radiation Oncology Biology Physics*, *110*(4), 1189–1199. https://doi.org/10.1016/j.ijrobp.2021.02.024

Zhang, Y. Y., Huo, W. L., Goldberg, S. I., Slater, J. M., Adams, J. A., Deng, X.-W., Sun, Y., Ma, J., Fullerton, B. C., Paganetti, H., Loeffler, J. S., Lu, H. M., & Chan, A. W. (2021). Brain-Specific Relative Biological Effectiveness of Protons Based on Long-term Outcome of Patients With Nasopharyngeal Carcinoma. *International Journal of Radiation Oncology Biology Physics*, *110*(4), 984–992. https://doi.org/10.1016/j.ijrobp.2021.02.018

Danksagung

Ich bin allen Beteiligten zutiefst dankbar, die direkt oder indirekt zum Gelingen dieser Arbeit beigetragen haben.

Ich danke Armin Lühr für die Bereitstellung des Promotionsthemas, die großartige Zusammenarbeit und die fachliche Betreuung über die vielen Jahre. Aber auch dafür, Themen außerhalb der Wissenschaft immer gemeinsam diskutieren zu können. Wolfgang Enghardt danke ich für die Übernahme des Erstgutachtens dieser Arbeit. Ebenso danke ich ihm für den Enthusiasmus, mit dem er auch mich für die Medizinphysik begeistert hat. Kristian Smeland Ytre-Hauge danke ich für die Bereitschaft, diese Dissertation zu begutachten.

Den Kollegen aus der Dresdner Protonentherapie bin ich zutiefst dankbar, dass sie mich in ihren Kreis aufgenommen und während der letzten Jahre unterstützt haben: Wolfgang Enghardt, Christian Richter, Daniela Kunath, Stefan Menkel, Maria Tschiche, Sebastian Makocki, Julia Hytry, Michalina Sleczek und Julia Thiele. Bei Steffen Appold und Tobias Hölscher bedanke ich mich außerdem für ihre kritischen Blicke auf die vielen Bestrahlungspläne. Mechthild Krause und Esther Troost danke ich für die Unterstützung und Förderung in klinischen und translationalen Fragen. Genauso wie ihrer Offenheit dafür, diese Arbeit aus der Ferne fortführen zu können. Genauso möchte ich mich bei allen (ehemaligen) Doktoranden und Postdocs am OncoRay für die schönen (virtuellen) Kaffeerunden bedanken.

Allen Kolleginnen und Kollegen an der TU Dortmund danke ich für die großartige Arbeitsatmosphäre. Lisa-Marie Meier danke ich, dass sie als Ansprechpartnerin immer ein offenes Ohr hat. Genauso Lena Heuchel, der ich auch für die tolle Zusammenarbeit in Lehre und Forschung danke. Julia Sobolewski und Jona Bensberg danke ich sehr für den regen Austausch zu allen Programmier- und RBW-Themen.

Ohne die Kolleginnen und Kollegen vom Westdeutschen Protonentherapiezentrum in Essen wäre ein wesentlicher Teil zur Planoptimierung in dieser Arbeit nicht möglich gewesen.

Mein Dank gilt besonders Christian Bäumer, Jörg Wulff und Sandija Plaude.

Für das sorgfältige Korrekturlesen einzelner Abschnitte dieser Arbeit bedanke ich mich bei Steffen Löck und Armin Lühr. Bei Almut Dutz bedanke ich mich für das Korrekturlesen und für ihre Hilfe in jeder Notsituation.

Für die Untersützung von meiner Familie und meinen Freunden während der gesamten Promotionszeit bin ich überaus glücklich und dankbar. Mein ganz besonderer Dank gebührt Anja Wölker für ihre unerschöpfliche Unterstützung in allen Lebenslagen.

Erklärungen zur Eröffnung des Promotionsverfahrens

1. Hiermit versichere ich, dass ich die vorliegende Arbeit ohne unzulässige Hilfe Dritter und ohne Benutzung anderer als der angegebenen Hilfsmittel angefertigt habe; die aus fremden Quellen direkt oder indirekt übernommenen Gedanken sind als solche kenntlich gemacht.
2. Bei der Auswahl und Auswertung des Materials sowie bei Erstellung des Manuskripts habe ich Unterstützungsleistungen von folgenden Personen erhalten:
   JProf. Dr. Armin Lühr, Jona Bensberg und Julia Sobolewski.
3. Weitere Personen waren an der geistigen Herstellung der vorliegenden Arbeit nicht beteiligt. Insbesondere habe ich nicht die Hilfe eines kommerziellen Promotionsberaters bzw. einer kommerziellen Promotionsberaterin in Anspruch genommen. Dritte haben von mir weder unmittelbar noch mittelbar geldwerte Leistungen für Arbeiten erhalten, die im Zusammenhang mit dem Inhalt der vorgelegten Dissertation stehen.
4. Die Arbeit wurde bisher weder im Inland noch im Ausland in gleicher oder ähnlicher Form einer anderen Prüfungsbehörde vorgelegt.
5. Die Inhalte dieser Dissertation wurden in folgender Form veröffentlicht:
   - Hahn, C., Eulitz, J., Peters, N., Wohlfahrt, P., Enghardt, W., Richter, C., & Lühr, A. (2020). Impact of range uncertainty on clinical distributions of linear energy transfer and biological effectiveness in proton therapy. *Medical Physics*, *47*(12), 6151–6162. https://doi.org/10.1002/mp.14560
   - Hahn, C., Ödén, J., Dasu, A., Vestergaard, A., Fuglsang Jensen, M., Sokol, O., Pardi, C., Bourhaleb, F., Leite, A., de Marzi, L., Smith, E., Aitkenhead, A., Rose, C., Merchant, M., Kirkby, K., Grzanka, L., Pawelke, J., & Lühr, A. (2022). Towards harmonizing clinical linear energy transfer (LET) reporting in proton radiotherapy: a European multi-centric study. *Acta Oncologica*, *61*(2), 206–214. https://doi.org/10.1080/0284186X.2021.1992007
   - Hahn, C., Heuchel, L., Ödén, J., Traneus, E., Wulff, J., Plaude, S., Timmermann, B., Bäumer, C., & Lühr, A. (2022). Comparing biological effectiveness guided plan optimization strategies for cranial proton therapy: potential and challenges. *Radiation Oncology*, *17*(1), 169. https://doi.org/10.1186/s13014-022-02143-x
6. Ich bestätige, dass es keine zurückliegenden erfolglosen Promotionsverfahren gab.
7. Ich bestätige, dass ich die Promotionsordnung der Medizinischen Fakultät Carl Gu-

stav Carus der Technischen Universität Dresden anerkenne.

8. Ich habe die Zitierrichtlinien für Dissertationen an der Medizinischen Fakultät der Technischen Universität Dresden zur Kenntnis genommen und befolgt.
9. Ich bin mit den ”Richtlinien zur Sicherung guter wissenschaftlicher Praxis, zur Vermeidung wissenschaftlichen Fehlverhaltens und für den Umgang mit Verstößen” der Technischen Universität Dresden einverstanden.

Dresden, 19.12.2022 _____

Erklärung über die Einhaltung der gesetzlichen Bestimmungen

Hiermit bestätige ich die Einhaltung der folgenden aktuellen gesetzlichen Vorgaben im Rahmen meiner Dissertation

- ☒ das zustimmende Votum der Ethikkommission bei Klinischen Studien, epidemiologischen Untersuchungen mit Personenbezug oder Sachverhalten, die das Medizinproduktegesetz betreffen
  EK365072019, DRKS00004384, DRKS00005363, EK601122019
- ☐ ~~die Einhaltung der Bestimmungen des Tierschutzgesetzes~~
  nicht zutreffend
- ☐ ~~die Einhaltung des Gentechnikgesetzes~~
  nicht zutreffend
- ☒ die Einhaltung von Datenschutzbestimmungen der Medizinischen Fakultät und des Universitätsklinikums Carl Gustav Carus.

Dresden, 19.12.2022 _____